

University of Alberta

Modelling a hydrocyclone for fine particle separation

by

Morteza Ghadirian

A thesis submitted to the Faculty of Graduate Studies and Research
in partial fulfillment of the requirements for the degree of

Doctor of Philosophy
in
Chemical Engineering

Department of Chemical and Materials Engineering

©Morteza Ghadirian
Spring 2014
Edmonton, Alberta

Permission is hereby granted to the University of Alberta Libraries to reproduce single copies of this thesis and to lend or sell such copies for private, scholarly or scientific research purposes only. Where the thesis is converted to, or otherwise made available in digital form, the University of Alberta will advise potential users of the thesis of these terms.

The author reserves all other publication and other rights in association with the copyright in the thesis and, except as herein before provided, neither the thesis nor any substantial portion thereof may be printed or otherwise reproduced in any material form whatsoever without the author's prior written permission.

Dedicated to

My lovely wife, parents and teachers

Abstract

In this study a complete solution methodology is developed for the simulation of hydrocyclones. A commercial software package, Ansys 12 Fluid Dynamics (Fluent), is used to solve the governing conservation equations. Turbulence is modelled using the large eddy simulation, and the discrete particle model is used to predict the particle separation. Two hydrocyclones of different geometries were studied, and the simulation results are compared with the experimental values. There are two key factors for obtaining a reliable result. The first is the domain discretization, and the second is the generation of a consistent initial value, including the establishment of a stable air core. Using the methodology developed, superior agreement is obtained between the predicted and experimental values of pressure, velocity distribution, air core profile and separation efficiency.

The developed and validated model is used to investigate the hydrocyclone performance for separation of light and heavy particles in slurry. The effect of overflow pressure, feed flow rate, particle size, vortex finder length, particle concentration and vortex finder diameter were investigated. The prediction of air core profiles demonstrated the accuracy of the simulation. In terms of design variables increasing the vortex finder length is shown to result in an increase in the recovery of light particles in the overflow. In the case of operating variables, the recovery of light particles in the overflow improved by increasing the size of light particles, feed flow rate and decreasing feed solid concentration. The ratio of

the vortex finder diameter to the apex diameter was found to be the most important design factor on the hydrocyclone performance.

Acknowledgements

I take this opportunity to thank all the people who have helped me during my Ph.D. at the University of Alberta.

I have had the pleasure of working with two excellent supervisors and would like to thank them both for their continued guidance, patience and encouragement.

My sincere gratitude to Dr. Hayes for the continuous support of my Ph.D. study and research, for his patience, motivation, enthusiasm, and immense knowledge. His guidance helped me in all the time of research and writing of this thesis. I could not have imagined having a better supervisor and mentor for my Ph.D. study.

I would like to express my gratitude to Dr. Xu for all his contributions of time, ideas and funding to make my Ph.D. experience productive. I also would like to thank him for providing me with enough academic freedom so as to enable me to be in control of the research project.

I am also very grateful to Artin Afacan for all his contributions, patience and motivation. His guidance helped me in all the time of research and writing the thesis. He has always answered my queries with patience from the very first day.

At last but not the least I would like to thank Dr. Mmbaga for his valuable time and help during my research. He has always provided encouragement, academic resources and feedback during my research.

Table of Contents

1	Introduction.....	1
1.1	Problem statement.....	4
1.2	Objectives.....	4
1.3	Outline.....	5
2	Background.....	7
2.1	Effect of operation and design parameters on hydrocyclone performance	
	10	
2.1.1	Feed solid concentration.....	10
2.1.2	Feed flow rate.....	12
2.1.3	Underflow split ratio.....	13
2.1.4	Particle size.....	14
2.1.5	Vortex finder length.....	15
2.1.6	Cylindrical section length.....	16
2.2	Hydrocyclone models.....	17
2.2.1	Empirical models.....	20
2.2.2	Conservation equations.....	27
2.2.3	Turbulence models.....	28
2.3	Air core calculations and multiphase modeling.....	42

2.4	Particle tracking and forces acting on the particles	45
3	Development and validation of a CFD model for the hydrocyclone	48
3.1	Model development.....	48
3.1.1	Governing equations	48
3.1.2	Turbulence closure models	50
3.1.3	Multiphase model.....	56
3.1.4	Particle classification	57
3.2	Complications.....	59
3.2.1	The proposed hydrocyclone design.....	60
3.2.2	Mesh generation.....	62
3.2.3	Inlet	73
3.2.4	Particle tracking	77
3.2.5	Air core	79
3.2.6	Multiphase model.....	81
3.2.7	Initialization	82
3.3	Model validation	87
3.3.1	Delgadillo's Geometry.....	87
3.3.2	Lim's geometry.....	100
4	Application of the developed model on the separation of binary particles in a hydrocyclone.....	104

4.1	Simulation methodology	110
4.1.1	Two phase simulation	113
4.1.2	Three phase simulation	115
5	Conclusions and future work	131
	References	134

List of Figures

Figure 2.1-A typical hydrocyclone geometry and associated flows	8
Figure 3-1-Hsieh's hydrocyclone geometry	61
Figure 3-2-Tetrahedral mesh used for hydrocyclone	63
Figure 3-3(a)-Grid size 1 shown on hydrocyclone	67
Figure 3-4-Air core produced from a low quality mesh	69
Figure 3-5-Volume mesh for hydrocyclone.....	71
Figure 3-6-High quality mesh produced for hydrocyclone.....	71
Figure 3-7-High quality hexahedral mesh	72
Figure 3-8-Axial velocity comparison at 60 mm from the top	73
Figure 3-9-Hydrocyclone geometry with and without the inlet section	74
Figure 3-10-Air core generated inside the hydrocyclone with no inlet section	75
Figure 3-11-Tangential inlet vs. involuted inlet.....	76
Figure 3-12-Light and heavy particle separation inside the hydrocyclone.....	77
Figure 3-13-Comparison of light particle recovery to the overflow between granular injection and experimental data.....	78
Figure 3-14-A fully developed vs. an undeveloped air core.....	80
Figure 3-15-Light particle separation efficiency comparison between Mixture model and experimental data	81
Figure 3-16-Pressure profile after initialization.....	83
Figure 3-17-Tangential velocity comparison between Rajamani's experiments and simulations and this work without initialization at 60 mm from the top	84

Figure 3-18-Axial velocity comparison between Rajamani's experiments and simulations and this work without initialization at 60 mm from the top	85
Figure 3-19-Air core development in a time span	89
Figure 3-20-Pressure field distribution inside the hydrocyclone	90
Figure 3-21-Radial pressure profile distribution at 80 mm from the top of the cylindrical section	91
Figure 3-22-Predicted tangential velocity from Rajamani and this study compared to experimental results at 60 mm from the top	94
Figure 3-23-Predicted axial velocity from Rajamani and this study compared to experimental results at 60 mm from the top	94
Figure 3-24-Predicted tangential velocity from Rajamani and this study compared to experimental results at 120 mm from the top	95
Figure 3-25-Predicted axial velocity from Rajamani and this study compared to experimental results at 120 mm from the top	96
Figure 3-26-Predicted tangential velocity from Rajamani and this study compared to experimental results at 170 mm from the top	97
Figure 3-27-Predicted axial velocity from Rajamani and this study compared to experimental results at 170 mm from the top	98
Figure 3-28-Hydrocyclone particle separation efficiency at 5% wt concentration of particles, collected at underflow	99
Figure 3-29-Axial velocity profile comparison at 3 cm from the top of Lim's hydrocyclone	102

Figure 4.1-Hydrocyclone geometry used for two phase and three phase simulation	107
Figure 4.2-Schematic of hydrocyclone experiment setup.....	109
Figure 4.3-Effect of overflow pressure on water mass split ratio.....	113
Figure 4.4-Effect of overflow pressure on air core diameter.....	114
Figure 4.5-Effect of feed flow rate on Light particles recovery in overflow $\alpha_{lf}=1.4\%$; $\alpha_{hf}=1.9\%$; $d_{50}=460\mu\text{m}$;	118
Figure 4.6-Effect of particle size on light particles recovery in overflow $Q_f=33$ l/min ; $\alpha_{lf}=1.4\%$; $\alpha_{hf}=1.9\%$;.....	119
Figure 4.7-Effect of vortex finder length on recovery of overflow product, $Q_f=33$ l/min ; $\alpha_{lf}=1.4\%$; $\alpha_{hf}=1.9\%$; $d_{50}=460\mu\text{m}$;	121
Figure 4.8-Effect of feed solid concentration on light particles recovery in over flow $\alpha_{lf}=1.4\%$; $\alpha_{hf}=1.9\%$; $d_{50}=460\mu\text{m}$;	124
Figure 4.9- Recovery of light particles to the overflow at different overflow to underflow diameter ratio.....	126
Figure 4.10-The air core location and LZVV for the hydrocyclone with a large vortex finder.....	127
Figure 4.11-The air core location and LZVV for the hydrocyclone with the small vortex finder.....	128

List of Tables

Table 3.1-Hsieh's hydrocyclone dimensions.....	60
Table 3.2-Diameter of air core structure at various axial positions measured by PIV and predicted by Lim et al. and this work	101
Table 4.1- Hydrocyclone dimensions for the experimental work done by Mahmood (2007)	106
Table 4.2- Physical properties of heavy and light particles	110

1 Introduction

A hydrocyclone is a static mechanical device which separates different species in a continuous medium by size and density under centrifugal forces. Because of their high capacity, hydrocyclones are widely used in the pulp and paper industry, different chemical and mineral processing industries for liquid clarification, degassing of liquids, solids washing, slurry thickening and classification of solids according to size, shape and density. Cyclones are also used for the separation of light oil droplets from the continuous medium or from oil, sand and water three-phase systems.

The oil sands industry deals with the separation of light bitumen droplets from heavy sand particles in an aqueous slurry. Different technologies based on the principles of gravitational, centrifugal and thermal sedimentations have been tested for this primary separation. All of the current technologies used are efficient, but they have drawbacks in terms of maintenance, initial capital cost and a large footprint to deal with excessive volumes. Many oil sands producers use Primary Separation Vessel/Cell, which is a gravity settler, for the primary separation of bitumen droplets from water and heavy solids. With this technique, the recoveries achieved are above 90%. However, the existing extraction plants are geographically fixed. Oil sands slurry is transported from long distances using pipeline to the extraction plant for bitumen recovery, and tailings are pipelined for disposal in tailings ponds. Such operation requires transportation of a large mass of solids, leading to excessive energy demand and severe erosion of pumps and

pipelines. With time, the transport distance between the mining and new tailing areas increases, which leads to ongoing investment with increased maintenance and energy costs. This process also leads to environmental impacts, such as global warming and greenhouse gas emission, disturbance of land for tailings ponds, and impacting wildlife and air/water quality.

The hydrocyclone has the advantage over the above mentioned separation processes because of its simple structure, low capital cost, large capacity, easy maintenance and low space requirement. Unlike other gravitational settlers, the separation rate in a hydrocyclone is higher because the centrifugal force is 1000 times more than normal gravity. An important feature of the hydrocyclone is that it can be built as a mobile unit, which reduces the operating and capital cost by dumping the sand on the mining site and avoiding the need to build large tailings ponds.

Owing to its industrial importance, the hydrocyclone has been intensively studied for many decades. Despite the simple design and operational aspects, the flow within the hydrocyclone is complicated by features such as turbulence, vorticity preservation, air core development and suspended particles. In common with other processes of industrial significance, researchers have developed empirical models to evaluate and design hydrocyclones. These empirical models, although simple and easy to use, are restricted to the experimental range and hydrocyclone design from which they were derived, only relate to steady state condition, and provide no insight into the underlying physical phenomena of fluid flows.

To gain such insight and to extend the model into the dynamic range requires a phenomenological model based on the solution of the governing conservation equations for mass and momentum. Such fundamental models, based on the underlying partial differential equations, can provide insight into velocity and pressure profiles, turbulence level, etc. within an operating cyclone. These models must be solved numerically, in a process often referred to as computational fluid dynamics (CFD). As in other fields, there have been increasingly sophisticated models developed for the hydrocyclone.

An extensive amount of research studies have been conducted on the modelling of flow in a hydrocyclone. The design and operating conditions are drastically different for different types of applications. It is very time and money consuming to build a pilot plant to test the characteristics of each design to improve the hydrocyclone performance. Hydrocyclone modelling and simulation provide valuable information on the development of the technology and a means to ensure that the design methods are efficient to improve the performance. The aim of modelling is to gain some insight of the phenomena occurring inside hydrocyclones and compare the simulation results with the experimental data to validate the model. The target factors to predict are all components of velocity (tangential, axial, and radial), pressure drop across the hydrocyclone, air core diameter, flow split ratio and particle separation efficiency.

1.1 Problem statement

In spite of the large body of work reported on the hydrocyclone, there remains some controversy concerning the optimal methodology for obtaining a reliable solution. Many different numerical solution methodologies have been suggested but none of them predict the particle separation efficiency, velocity profile, air core diameter and pressure to a satisfactory degree. The other concern is light particle separation in the presence of heavy particles in the aqueous phase to simulate the separation of oil from the oilsands tailings which contains water, oil droplets and sand.

1.2 Objectives

This study presents a comprehensive model development for the hydrocyclone using a new unstructured hexahedral mesh. The overall methodology for the meshing and establishment of initial conditions is designed to determine the final shape of the air core, velocity profiles and particle separation. The target is establishing a workflow that leads to stable solutions with well-developed air core and good agreement with experimental results for particle separation.

Another objective of this study is to examine the effects of operating and design variables on the separation of light and heavy particles in liquid slurry by a hydrocyclone. The operating parameters investigated include feed flow rate, underflow split ratio, light particle size and feed solid concentration, and vortex finder lengths. The light and heavy particles selected for the study were chosen to mimic aerated bitumen and solid (coarse and fine) particles as in the oil sands

extraction plants. A numerical model was used to simulate the hydrocyclone and the results were compared with the experimental values.

1.3 Outline

This thesis is organized as follows. After introduction and description of thesis outline Chapter 2 starts with the background study on the hydrocyclone. It includes the literature review on the modeling work of the hydrocyclone and the hydrocyclone description and design. The effect of design and operating parameters is briefly discussed in this chapter.

Chapter 3 provides details on the development and validation of a CFD model for the hydrocyclone. At the beginning of the chapter the CFD approaches that have been used are summarized. Later in this chapter the challenges that exist in using CFD and the solution to these challenges are discussed. The development of the model equations in complete detail is explained in the next part. The validation of the modelling strategy of this work was done using two different geometries from the literature.

Chapter 4 is concerned with the experimental and modelling study of particle separation. The experimental data are compared against the validated model for different operating and design conditions for a specially designed hydrocyclone. How a hydrocyclone model can be enhanced further is then discussed. It is concluded that the LES is the best turbulence closure model suited for this simulation. The important the geometry discretization and air core development in establishing a reliable model is demonstrated. Based on the

observations from experiments and modelling further modelling and simulation by also considering particle/particle interaction and shear stress is recommended to account for the particle concentration effect in the separation process.

2 Background

Many researchers have worked to understand the physics and design principles of the hydrocyclone using experiments and modeling. This chapter presents a review of hydrocyclone modeling and experimental investigation.

A typical hydrocyclone is shown in Figure 2.1. A hydrocyclone is characterized by a relatively long cyclone body length, from four to seven times the body diameter, and by angles of the cone of less than about 25° . Such cyclones are capable of operating at low cut size and are thus suitable for liquid clarification or thickening duties where high mass recoveries are desirable. They are also used for solids classification duties where low cut sizes are required. The above mentioned design characteristics are often followed by relatively small sizes of the inlet and overflow orifices, which is another feature of high efficiency hydrocyclone types. The hydrocyclone is made of a cylindrical chamber attached to a conical section at the bottom. There is an inlet attached to the cylindrical section for the feed entry and it has two exits at the top and the bottom. The top of the hydrocyclone is enclosed by a cover, through which a tube is extended to some distance down to the centre. As shown in Figure 2.1 this tube is called vortex finder and is responsible for collecting the overflow stream flows. It is worth mentioning that the vortex finder should be extended below the feed entry level to reduce the chances of short-circuiting of the feed and it also needs to be above the cylinder-cone intersection to avoid the turbulence. The section where the underflow stream flows is called apex or spigot. The body of a hydrocyclone consists of two parts: a

cylindrical section followed by a conical part. Slurry is tangentially fed to the cylindrical part of hydrocyclone. No moving part is needed for the formation of the vortex inside the hydrocyclone since the rotation is produced by tangential injection of the fluid into the hydrocyclone.

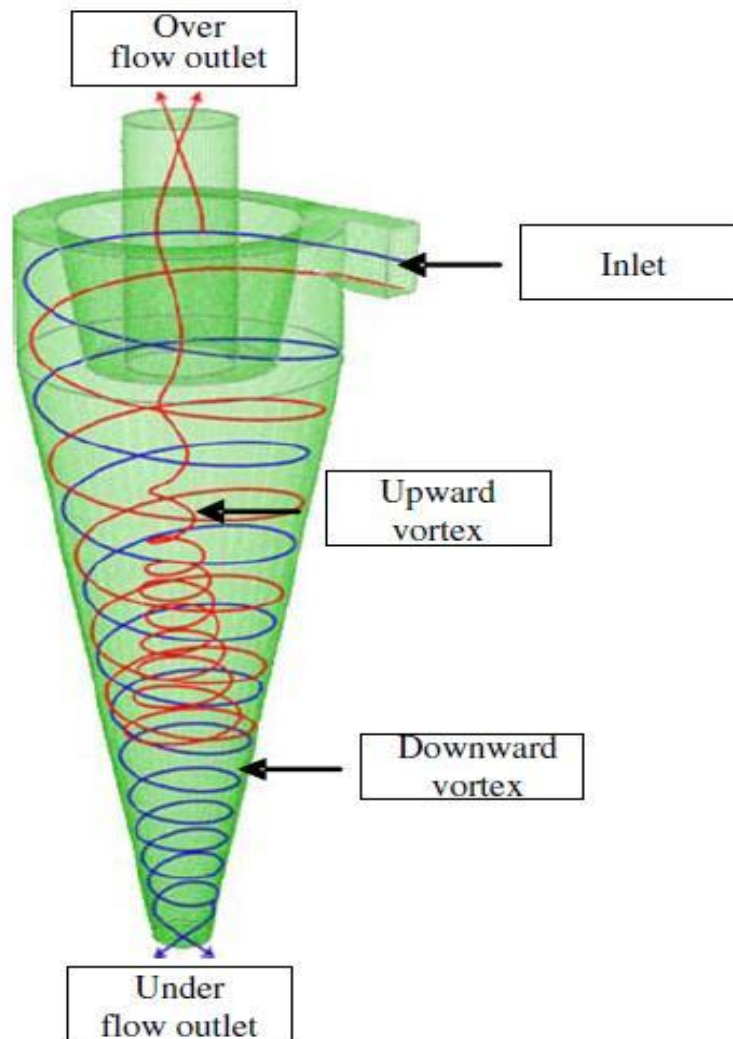


Figure 2.1-A typical hydrocyclone geometry and associated flows

Some hydrocyclones have two or even four symmetrical inlets. Hydrocyclones with more than one inlet are mainly used for liquid separation applications. In

those hydrocyclones for a specific feed flow rate a higher velocity profiles are recorded.

Hydrocyclone can have different design characteristics, depending on their application. For example, there are hydrocyclones with no vortex finder used for oil/water separation; or hydrocyclones with really long conical sections to separate finer particles from the liquid phase. The hydrocyclone shown in Figure 2.1 is the most typical type.

Hydrocyclones can separate, classify or sort multiphase systems based on its application in a specified technology. The separation phenomenon of a hydrocyclone is based on the effect of different forces acting on the phases to be separated. The fluid pressure energy turns into rotational motion of the slurry inside the cylindrical section of the hydrocyclone. Based on the density difference of phases rotational motion of each phase would be different from another one. This relative movement of phases sorts them throughout the hydrocyclone and they become separated by exiting from different exits.

Density difference of different phases forces the heavier phase to move towards the apex while the lighter phase is collected from the vortex finder. Pressure gradients inside the hydrocyclone create two vortices, one inside another and both spinning at the same radial direction but with opposite axial direction. The pressure difference inside sucks the air from the apex and causes the formation of an air core which leaves the cyclone from the top. A rotational motion has thus built into an inward radial motion. Particles suspended in the fluid have two

opposing forces acting on them, one in an outward radial direction due to the centrifugal acceleration, and the other one in an inward radial direction due to the drag forces of the inward moving fluid. The magnitude of these forces is dependent on the physical properties of both the fluid and the suspended particles. These properties are used to separate one material from another, or from the fluid.

2.1 Effect of operation and design parameters on hydrocyclone performance

Major operation and design parameters that affect the separation process in the hydrocyclone are discussed here.

2.1.1 Feed solid concentration

The feed or inlet slurry concentration affects the hydrocyclone performance in different ways. At higher concentrations, Stoke's law is not applicable because low concentration slurry is one of the assumptions of the theory. The other problem inherent in this law is the change in the pressure drop for the hydrocyclone. High solid concentration in rotating mass of fluid increases the viscosity, which affects the rotational movement. The higher viscosity consequently decreases the pressure drop for the same slurry inlet velocity. A further aspect of high solid concentration is the slurry behaviour at the underflow. Solid concentration is always higher at the apex. A higher feed concentration can even increase the underflow solid concentration to a limit that hydrocyclone efficiency would be impaired. In this case the underflow stream character changes and there is higher possibility of blocking the apex.

Dahlstorm (1954) studied the effect of high solid concentration in hydrocyclones. He concluded that the effects are negligible below a feed concentration which is equivalent to an 8:1 fluid to solid volume ratio; this corresponds to 11 % by volume of solid or 25 % by weight for a solid density 2.7g/cm^3 in water.

Svarovsky et al. (1980) investigated the solid concentration effect on hydrocyclone efficiency and proposed a correlation which relates the reduced cut size to the operating variables, including the solid concentration and the underflow mass ratio. They validated their correlation by comparison with results of tests performed with 125 mm and 50 mm diameter hydrocyclone at varying feed concentrations. They assumed the solid concentration has negligible effect under 8% by volume and claimed to be accurate for a wide range of 8% to 28% by volume. They developed their correlation using equations from Lynch (1975) and Bradley (1965).

It is also worth noting that the solid concentration effect depends on the design characteristics of the hydrocyclone as well. For smaller hydrocyclone this effect is noticeably bigger than for larger hydrocyclones. For particles lighter than water Young et al. (1994) stated that increasing the solid concentration in the feed flow results in an increase in overflow light particles recovery.

In general, at higher feed solid concentration it is expected to have higher particle/fluid and particle/particle interactions. The first changes the flow regime and slurry viscosity inside the hydrocyclone, and the latter increases the

turbulence all over the hydrocyclone, and more specifically in the regions closer to the apex.

2.1.2 Feed flow rate

The slurry flow in a hydrocyclone consists of an upward inner flow and outer downward flow spinning in the same tangential direction and opposite axial directions. As a result, the overflow and underflow streams are formed. Considering the continuum inside the hydrocyclone, a higher feed flow rate increases the velocity magnitude inside the hydrocyclone and the overflow and underflow stream velocities.

Bradley (1965) stated that efficiency increases linearly as feed flow rate increases. He added a direct relationship between pressure drop and flow rate inside the hydrocyclone. The higher flow rate results in a higher velocity profile, which increases the forces acting on the phases and a higher relative movement of the particles. The higher velocity of the particles results in higher efficiency and higher turbulence in the continuous medium which increases the pressure drop throughout the hydrocyclone.

Brookes et al. (1984) investigated the hydrocyclone performance related to the feed flow rate by using a 50 mm hydrocyclone unit for separating 100 micron particles with bulk particle density of 1.39 g/cm^3 . He showed that the effect of mean inlet water velocities upon the d_{50} . They found a reduction in cut size with increasing flow rate. Higher flow rates result in higher centrifugal forces, lower drag forces and smaller residence time while lower flow rates means greater drag

forces, smaller centrifugal forces and longer residence time based on Mukherjee et al. (2003) and King (2000).

Narasimha et al. (2006) also investigated the flow rate effect on other parameters inside hydrocyclone. He stated that a higher feed flow rate accelerates the flow inside the hydrocyclone by increasing the centrifugal forces on fluid elements and lowers the pressure along the central axis of the hydrocyclone. As a result it is easier for the central vortex to make the air core and air core diameter will be larger in this case.

2.1.3 Underflow split ratio

The underflow split ratio is mainly related to D_u/D_o ratio. By changing the feed flow rate the underflow split ratio changes as well, but the main factor still the outlet diameters' ratio. Dale and Charles (1994) investigated the effect of underflow split ratio on the purity of the underflow stream or percentage of particles going to the overflow on a 10 mm hydrocyclone. They concluded that by increasing the overflow split ratio (Q_o/Q_F) or decreasing the underflow split ratio (Q_u/Q_F) the number of particles leaving the hydrocyclone from the overflow increases and there is a higher separation efficiency for the hydrocyclone. Lynch (1975) claimed that the only design parameter which affects the performance of the hydrocyclone are the inlet and outlet diameters, which are in essence the factors that fix the underflow to overflow split ratio.

2.1.4 Particle size

The particle size has a strong effect on the separation efficiency. Stoke's law can be used to calculate the hydrocyclone performance based on particle size. Stokes law indicates that the settling velocity of the particles is directly proportional to the square of their size. Increasing the size of the light particles increases the radial centripetal forces acting on the particles and hence the axial velocity of the particles, resulting in a faster mobility of the larger sized light particles towards the central axis of the cyclone, where they are removed from the overflow stream. As a result, the recovery of the larger sized light particles is higher at all underflow split ratios compared to smaller light particles. For particles heavier than water, increasing the particle size also increases the centrifugal forces. This higher centrifugal force moves the particles to the downward flow, and heavy particles are collected in the underflow stream. So we observe opposite reactions from heavy and light particles by increasing the particle size.

Dale and Charles (1994) studied the effect of light particle size on purity of the underflow stream under different underflow split ratio for a 10 mm hydrocyclone. They showed that the underflow purity increases as the mean size of the light particle, kerosene, in the feed stream increases. Ali and Petty (1994) also observed the same phenomenon for 70 mm hydrocyclone processing a kerosene in water dispersion.

Some other researchers including Delgadillo and Rajamani(2005,2007), Schuetz et al.(2004), Lim et al. (2010), Ahmed et al. (2009) and Wang et al. (2006)

explored the effect of particle size on hydrocyclone performance for heavy particles. They concluded that particles heavier than water will have higher separation efficiency.

2.1.5 Vortex finder length

The vortex finder length has very little effect on the separation efficiency, but plays a major role in controlling the short circuit of flow. According to Bradley (1965), the vortex finder should not be parallel to the inlet opening or the joint of the cylindrical and conical sections. Otherwise, the short circuit flow and turbulence will affect the separation efficiency. When the vortex finder length is increased, the strength and length of the forced vortex inside the cyclone body are decreased. As a result, the separation efficiency is improved (Svarovsky, 1984). Extending the vortex finder's length into the conical section where the radial velocity increases from the wall to the centre of the hydrocyclone and higher radial velocity gradient is in the inner helical flow than outer vortex (Zhao and Xia, 2006). Higher radial velocity gradient in the inner helical flow helps the light particles to separate from the heavy ones, and recovery of the light particles in the overflow is increased. An increase in the vortex finder length increases the particle residence time of the particles. Particles with longer residence time have a better chance for collection in the overflow stream and the hydrocyclone separation efficiency increases. In the cylindrical section of the hydrocyclone, the outer vortex may swirl towards the cylinder top and then return down to the rim of the vortex finder where there is high chance of separation. By increasing the vortex finder length it becomes unlikelier for this phenomenon to happen and the

hydrocyclone performance decreases. Apparently the higher residence time effect on particle collection efficiency overshadows the shortcut phenomenon in our study.

Plitt (1976) defined residence time of particle in hydrocyclone as a function of vortex finder length. He claimed that the longer the residence time of a particle in a hydrocyclone, the greater the probability of that particle reporting to the correct flow stream.

2.1.6 Cylindrical section length

A longer cylindrical part results in a longer residence time and as mentioned before Plitt (1976) claims that a longer residence time results in particle falling to the correct stream. Svarovsky (1984) on the other hand stated that a longer residence time improves the hydrocyclone efficiency.

Martinez et al. (2007) analysed the influence of cylindrical section length on both pressure drop and turbulence inside the hydrocyclone. They concluded that a longer cylindrical section results in a lower turbulence and it decreases the pressure drop. According to Young et al. (1994) and Chu et al. (2002), increasing the cylindrical length increases the residence time, reduces the tangential velocity and angular momentum by dragging against the wall of the cylindrical section.

Chu et al. (2000) concluded that for slurry of heavy particles the reduced separation efficiency increases with the length of cylindrical part increasing,

which indicates that the centrifugal sedimentation in the cylindrical part makes a remarkable contribution to the separation process in the hydrocyclone.

Young et al. (1994) claimed that for the oil/water system shorter cylindrical lengths produce better separation. This is simply because the fluid in this section is not spinning fast enough to provide appreciable separation in comparison with the separation provided in other parts of the hydro-cyclone. At the same time the fluid is losing its angular momentum by the drag of the wall of the cylindrical section.

2.2 Hydrocyclone models

In one of the first efforts on using detailed modelling methodology for the hydrocyclone, Hsieh and Rajamani (1991) solved the turbulent transport equation for a two dimensional incompressible turbulent flow with constant properties and no body forces. A modified Prandtl mixing-length model was used. They utilized the vorticity-stream function approach to solve the governing Navier-Stokes equations and also balanced the centrifugal force against the radial drag force for particle trajectory calculations. They reported some level of agreement with experimental results for a number of hydrocyclone runs at various operational conditions. However, it should be noted that there was no attempt made to include the air core in their model. In a later work, He et al. (1999) compared the two dimensional axi-symmetric inlet hydrocyclone simulation with a three dimensional simulation. They concluded that the κ - ε model is inadequate, producing large errors and incorrect predictions for flow patterns for both cases. A

modified κ - ε model, however produced results in better agreement with experimental data for three-dimensional calculations, while the flow pattern predictions for a two dimensional hydrocyclone are approximate and inadequate for separation efficiency predictions.

Delgadillo and Rajamani (2005) pointed out that even with powerful computational resources, comprehensive and reliable hydrocyclone modelling remains a challenge owing to the presence of solid particles, liquid and gas. Hydrocyclones typically operate at very high velocities which makes the flow within the hydrocyclones highly turbulent. Moreover, the rotational motion and flow separation inside the hydrocyclone brings anisotropy and strains into the turbulence. The air core development and solids addition into the hydrocyclones introduce more turbulence anisotropy, which adds more complexity in solving the turbulence effects (Narasimha et al. 2006). Slack et al. (2000) found that the stress transport model gives acceptable predictions of velocity profiles in a hydrocyclone. Brennan (2006) compared the linear pressure strain modelling and quadratic pressure strain modelling in Differential Reynolds Stress Model (DRSM) and concluded that they are essentially the same but the linear DRSM can be calibrated by increasing the fast pressure strain constant. Turbulence and multiphase modeling are further discussed in the model development section.

A key phenomenon that strongly influences the performance of the hydrocyclone is the development of the air core. Many researchers have modelled the air core development in the hydrocyclone using different techniques. The simplest and

most common solution is to impose an air core of fixed diameter with a slip boundary condition at the gas/liquid interface. Theoretical models (Dyakowski and Williams, 1995) have been used as an aid in estimating the air core diameter. Neesse and Dueck (2007) predicted the air core diameter by assuming that the positive pressure gradient and the centrifugal force in the rotational flow field are balanced and concluded that this physical consideration indicates that the air core radius is primarily determined by the hydrocyclone geometry.

The accurate simulation of the particulate phases inside the hydrocyclone is also very important. There are two approaches in CFD to simulate these phases, the Eulerian and Lagrangian. Momentum and continuity equations are solved for both the dispersed and continuous phase in the Eulerian approach. Nowakowski et al. (2000), Suasnabar (2000) and Brennan et al. (2006) applied this approach in their simulations. The Lagrangian method simulates the paths of individual particles by balancing drag, buoyancy and other body forces on each particle. Hsieh (1988) used the Lagrangian approach to predict the classification of limestone in a 75 mm hydrocyclone with. It was an axisymmetric approach, which reduced the computational domain to two coordinates. As noted earlier, it requires a three dimensional model to predict the air core well, and consequently a better prediction for flow patterns and particle separation efficiency.

Wang and Yu (2006) studied hydrocyclone size and length effects using a Reynolds Stress Model for the turbulent flow. They applied the stochastic Lagrangian model to describe the particle flow and showed that hydrocyclone

performance depended on size. They concluded that smaller hydrocyclones had higher separation efficiencies.

In recent years, researchers such as Schuetz et al. (2004) and Cullivan et al. (2004) have made progress in performing comprehensive numerical studies for 3-D hydrocyclones using computational fluid dynamics and reported a need for further work and investigation in this field at higher concentration of particles and different hydrocyclones.

2.2.1 Empirical models

In the past 70 years a great deal of work has been done on developing and using empirical models for hydrocyclone. These models evaluate and predict the operational characteristics and hydrocyclone performance. Once they were developed for a specific hydrocyclone they were easy to use and comprehend for that specific operation. Some of them are more general and are applicable for a wider range of design and operating variables. Dahlstrom (1949, 1954) developed an equation for one type of cyclone which has been widely and usefully applied to many types:

$$d_{50} = \frac{81 \cdot (D_o \cdot D_i)^{0.68}}{Q^{0.53}} \cdot \left(\frac{1.73}{\sigma - \rho} \right)^{0.5} \quad (2.1)$$

where:

d_{50} is cut size in microns

D_o, D_i , are overflow and inlet diameter in inches

Q is the feed flow rate in gal/min

σ, ρ are solid and liquid density in g/cm^3

The constant 81 was determined for aqueous suspensions flowing in a 9 in., 20° cyclone. Application to other diameters was possible due to proportionate change in D_o and D_i . For small diameter cyclones (10 to 40 mm), Matschke and Dahlstrom (1959) modified the relationship to:

$$d_{50} = \frac{87.2 \cdot (D_o \cdot D_i)^{0.65}}{Q^{0.6}} \cdot \left(\frac{1}{\sigma - \rho} \right)^{0.5} \quad (2.2)$$

where the constant is given for the same units as the previous equation. Equation (2.1) was for cone angle of 20° . Equation (2.2) was obtained using a cone angle of 10° . According to Bradley (1965) application of these two equations for other angles was risky and application to media of different viscosity was impossible. The density term was obtained by assuming the validity of Stoke's law and using the density difference. Equation (2.1) was said to predict a low value for d_{50} .

Yoshioka and Hotta (1955) developed an equation based on the orbital concept and an equilibrium cone surface defined by the end of the vortex finder and the cone apex. The equation is:

$$d_{50} = 6.3 * 10^6 \cdot D_c^{0.1} \cdot D_i^{0.6} \cdot D_o^{0.8} \left(\frac{\eta}{Q(\sigma - \rho)} \right)^{0.5} \quad (2.3)$$

where

d_{50} is cut size in microns

D_c, D_o, D_i , are cyclone, overflow and inlet diameter in inches

Q is the feed flow rate in l/sec

σ, ρ are solid and liquid density in g/cm^3

η is the liquid viscosity in kg/m^3

The constant 6.3 was empirically obtained for aqueous suspensions in 6 in., 20° cyclone. Introduction of viscosity and density terms was done through Stoke's law.

Bradley (1965) theoretically compared the mentioned empirical equations and claimed that these equations reduce to the same form when applied to a cyclone of given proportions. The form is:

$$d_{50} \propto \left(\frac{D_c^3 \cdot \eta}{Q(\sigma - \rho)} \right)^{0.5} \quad (2.4)$$

He stated that the difference lies only in the proportionality constant. The form in relation to viscosity and density stems from the use of Stoke's law which has been applied by equation $C_D = 24/Re$.

Plitt (1976) developed a semi-empirical model. The original model was obtained by using a stepwise multiple linear regression programs. Plitt repeated the linear regression procedure with different functional forms

(linear, power and exponential and different variable combinations. He included in the model equations only those variables that were found significant at 99% level. He used 297 sets of data in proposing the equations for pressure drop, P and flow split,S, but only used 197 data sets for the cut size equation. Plitt's equation was dependant on the feed size so Flintoff et al. (1987) did some modification and revised it into a version that has no dependence on feed size characteristics and is given below:

$$d_{50c} = F_1 \frac{39.7 D_c^{0.46} D_i^{0.6} D_o^{1.21} \eta^{0.5} e^{0.063 C_V^P}}{D_u^{0.71} h^{0.38} Q^{0.45} \left[\frac{\rho_s - 1}{1.6} \right]^k} \quad (2.5)$$

$$m = F_2 1.94 \left(\frac{D_c^2 h}{Q} \right)^{0.15} e^{\frac{-1.58s}{1+s}} \quad (2.6)$$

$$P = F_3 \frac{1.88 Q^{1.8} e^{0.0055 C_V^P}}{D_c^{0.37} D_i^{0.94} h^{0.28} (D_o^2 + D_u^2)^{0.87}} \quad (2.7)$$

$$S = F_4 \frac{18.62 \rho_P^{0.24} \left(\frac{D_u}{D_o} \right)^{3.31} h^{0.54} (D_o^2 + D_u^2)^{0.36} e^{0.0054 C_V^P}}{D_c^{1.11} P^{0.24}} \quad (2.8)$$

where

F is a factor for calibration

D_c, D_i, D_o, D_u are diameters for cyclone, inlet, overflow and underflow

d_{50c} is corrected classification size, μm

h , the free vortex height

k , hydrodynamic exponent, to be estimated from data, 0.5 for laminar flow

m , classification index

P , cyclone feed pressure

S , volumetric flow split

C_v^p , percent solid in feed by volume

η , liquid viscosity

ρ_p, ρ_s , density of feed pulp and solid

Nageswararao et al. (2004) investigated this modified equation and stated that since Flintoff et al. (1987) did not include a specific feed size term, but provided F factors for calibration it is probably safe to assume that the model should be recalibrated whenever feed data are available, in preference of using the uncalibrated equations.

Nageswararao et al. (2004) also developed an empirical model and compared it with Plitt's empirical model. He claimed that the significance of his model is the appropriate choice of design and operating variables and the explicit assumptions made in binding them to the model equations. His empirical equation is:

$$\frac{Q}{D_c^2 \sqrt{P/\rho_P}} = K_{Q_o} \{D_c^{-0.10}\} \left(\frac{D_o}{D_c}\right)^{0.68} \left(\frac{D_i}{D_c}\right)^{0.45} \left(\frac{L_c}{D_c}\right)^{0.20} \theta^{-0.10} \quad (2.9)$$

$$\begin{aligned} \frac{d_{50c}}{D_c} &= K_{D_o} \{D_c^{-0.65}\} \left(\frac{D_o}{D_c}\right)^{0.52} \left(\frac{D_u}{D_c}\right)^{-0.50} \left(\frac{D_i}{D_c}\right)^{0.20} \\ &* \left(\frac{L_c}{D_c}\right)^{0.20} \theta^{0.15} \left(\frac{P}{\rho_P D_c g}\right)^{-0.53} \lambda^{0.27} \end{aligned} \quad (2.10)$$

Recovery of water to underflow:

$$\begin{aligned} R_f &= K_{W_o} \{D_c^{0.00}\} \left(\frac{D_o}{D_c}\right)^{-1.19} \left(\frac{D_u}{D_c}\right)^{2.40} \left(\frac{D_i}{D_c}\right)^{0.50} \\ &* \left(\frac{L_c}{D_c}\right)^{0.22} \theta^{-0.24} \left(\frac{P}{\rho_P D_c g}\right)^{-0.53} \lambda^{0.27} \end{aligned} \quad (2.11)$$

Volumetric recovery of feed slurry to underflow:

$$\begin{aligned} R_V &= K_{V_o} \{D_c^{0.00}\} \left(\frac{D_o}{D_c}\right)^{-0.94} \left(\frac{D_u}{D_c}\right)^{1.83} \\ &* \left(\frac{D_i}{D_c}\right)^{0.25} \left(\frac{L_c}{D_c}\right)^{0.22} \theta^{-0.24} \left(\frac{P}{\rho_P D_c g}\right)^{-0.31} \end{aligned} \quad (2.12)$$

where:

D_i, D_o, D_u, D_c are diameters of inlet, overflow, underflow and cyclone

Q , throughput of the cyclone, l/min

θ , full cone angle, degrees

λ , hindered settling factor $C_v/(1-C_v)^3$

K , common material dependant

L_c , length of the cylindrical section of the cyclone

Wang and Yu (2006) used the empirical model developed by Plitt (1976) and Flinthoff et al. (1987) for validation and comparison with their numerical model and their experimental data. They claimed that this model has a better accuracy than other empirical models such as the models developed by Chen et al (2000) and Nageswararao et al. (2004). They compared experimental results from Hseih (1988), the Plitt empirical model and their predicted values for cut size, pressure drop and split ratio reported to the underflow.

Lynch and Rao (1975) also constructed an empirical model to reflect correlations between performance criteria such as d_{50} and cyclone design and operating variables. The equation is:

$$\log d_{50} = K_1 D_o - K_2 D_u + K_3 D_i + K_4 C_w - K_5 Q_f - K_6 \quad (2.13)$$

where

$$Q_f = K D_o^{0.73} D_i^{0.86} P^{0.42} \quad (2.14)$$

2.2.2 Conservation equations

To provide more insight into phenomena such as velocity and pressure profiles, turbulence level, etc. inside the hydrocyclone it is necessary to solve the underlying partial differential equations. Mass and momentum conservation equations are the two important differential equations to solve. In the finite volume method (FVM), the entire domain is discretized into small control volumes, which are also known as computational cells. The flow field equations are discretized and solved for each computational cell (control volume) such that mass, momentum, and energy is conserved, not only for the whole domain, but also for each computational cell. The mass conservation equation can be represented as follows:

$$\frac{\partial \rho}{\partial t} + \frac{\partial(\rho u_i)}{\partial x_i} = 0 \quad (2.15)$$

For incompressible fluids it can be reduced to the following form:

$$\frac{\partial(u_i)}{\partial x_i} = 0 \quad (2.16)$$

The momentum conservation equations, which are also known as the Navier-Stokes equations, can be written as:

$$\frac{\partial}{\partial t}(\rho u_i) + \frac{\partial}{\partial x_j}(\rho u_i u_j) = -\frac{\partial P}{\partial x_i} + \mu \frac{\partial^2 u_i}{\partial x_j^2} + \rho g_i \quad (2.17)$$

It is extremely difficult to solve the Navier-Stokes equations for turbulent flow numerically. Such a fine mesh is required that the computational cost becomes significantly infeasible. To obviate this problem, different approaches must be used. Typically, time-averaged equations such as Reynolds-averaged Navier-Stokes equations (RANS) or time-varying flow computation models such as large eddy simulation (LES) are used.

2.2.3 Turbulence models

Turbulence is a complex phenomenon and one of the main challenges in hydrocyclone modelling. The level of turbulence is expected to increase as the ratio of inertia and viscous forces increases. This ratio is known as the Reynolds number. Depending upon flow, turbulence can occur over a range of length and time scales. If all the spatial and time scales can be resolved in a CFD simulation of the Navier-Stokes equations, then even the smallest feature of turbulence can be captured. Such simulations tend to provide accurate results. However, the associated computational cost limits the application of CFD for solving practical engineering problems. Hence, a balance between accuracy and productivity must be sought. Over the years, significant advances have been made in numerical methods and computational power; yet, the smallest length scale at which turbulence may occur remains much smaller than the smallest mesh size feasible to resolve by CFD today.

As it is not feasible to resolve turbulence or velocity fluctuations at all the length and time scales, turbulence models are required. The models can be categorized in

two main groups. One category of models modifies the original Navier-Stokes equations to the time-averaged form, also known as Reynolds Average Navier-Stokes (RANS) Equations. The other category of models is known as Large Eddy Simulation, which resolves eddies larger than the grid size, whereas smaller eddies are modelled using sub-grid scale turbulence models.

Prandtl mixing length model

Rhodes et al. (1987) solved the partial differential equations with a modified Prandtl mixing-length model and the symmetry assumption. Hsieh and Rajamani (1991) solved the turbulent transport equation to compute the velocity profiles of the fluid and the separation efficiency curve, also using a modified Prandtl mixing-length model. They utilized the vorticity-stream function approach to solve the governing Navier-Stokes equations, and also balanced the centrifugal force against the radial drag force for the particle trajectory calculations. They reported agreement with experimental results for a number of hydrocyclone runs at various operating conditions, which was their main advantage over the work of Rhodes et al. (1987). However, it should be noted that no attempt was made to include the air core in their model.

Monredon et al. (1990) adopted the Prandtl mixing length model using the symmetry assumption. They solved the Navier-Stokes equation in two dimensions and proposed that the mixing length varies both in the tangential and axial directions. They measured the velocity profiles inside the hydrocyclone using Laser Doppler Velocimetry (LDV). The model was for two-dimensional

incompressible turbulent flow with constant properties and no body forces. The dimensionless transport equations in conservative form relative to cylindrical coordinates are shown below:

Vorticity:

$$\frac{\partial \eta}{\partial t} = \frac{1}{r^3} \frac{\partial \Omega^2}{\partial z} - \frac{\partial u \eta}{\partial r} - \frac{\partial w \eta}{\partial z} + \frac{1}{Re} \left(\frac{\partial^2 \eta}{\partial r^2} + \frac{1}{r} \frac{\partial \eta}{\partial r} - \frac{\eta}{r^2} + \frac{\partial^2 \eta}{\partial z^2} \right) \quad (2.18)$$

Stream function:

$$\frac{\partial^2 \varphi}{\partial r^2} - \frac{1}{r} \frac{\partial \varphi}{\partial r} + \frac{\partial^2 \varphi}{\partial z^2} = -r \eta \quad (2.19)$$

Angular spin velocity:

$$\frac{\partial \Omega}{\partial t} = -\frac{\partial u \Omega}{\partial r} - \frac{u \Omega}{r} - \frac{\partial w \Omega}{\partial z} + \frac{1}{Re} \left(\frac{\partial^2 \Omega}{\partial r^2} - \frac{1}{r} \frac{\partial \Omega}{\partial r} + \frac{\partial^2 \Omega}{\partial z^2} \right) \quad (2.20)$$

And

$$\frac{1}{r} \frac{\partial \varphi}{\partial r} = w \quad (2.21)$$

$$\frac{1}{r} \frac{\partial \varphi}{\partial z} = u \quad (2.22)$$

$$\frac{\Omega}{r} = v \quad (2.23)$$

where Re is the Reynolds number defined as $R_c U_o / \nu$.

Then they used a modified prandtl mixing length model to compute the turbulent viscosity. The algebraic expression which includes the radial gradients of both tangential and axial velocities is:

$$\mu_t = \rho_m \lambda^2 \left(\left| \frac{\partial V}{\partial R} - \frac{V}{R} \right| + \left| \frac{\partial W}{\partial R} \right| \right) \quad (2.24)$$

The proposed mixing length for tangential and axial direction is:

$$\lambda_\eta = 0.010 R_c \left(\frac{\mu_m}{\mu_o} \right)^{1/5} \left(\frac{R_z}{R_c} \right)^{1/4} \left(\frac{R}{R_c} \right)^{1/2} \quad (2.25)$$

$$\lambda_\Omega = 0.015 R_c \left(\frac{\mu_m}{\mu_o} \right)^{1/5} \left(\frac{R_z}{R_c} \right)^{1/4} \left(\frac{R}{R_c} \right)^{1/2} \quad (2.26)$$

κ - ε model and modifications

Narasimha et al. (2005) applied the standard κ - ε model which is a semi-empirical model based on model transport equations for the turbulent kinetic energy (κ) and its dissipation rate (ε) and are shown below:

$$\frac{\partial}{\partial t} (\rho k) + \frac{\partial}{\partial x_i} (\rho k u_i) = \frac{\partial}{\partial x_j} \left[\left(\mu + \frac{\mu_i}{\sigma_k} \right) \frac{\partial k}{\partial x_j} \right] + G_k - \rho \varepsilon \quad (2.27)$$

$$\frac{\partial}{\partial t} (\rho \varepsilon) + \frac{\partial}{\partial x_i} (\rho \varepsilon u_i) = \frac{\partial}{\partial x_j} \left[\left(\mu + \frac{\mu_t}{\sigma_\varepsilon} \right) \frac{\partial \varepsilon}{\partial x_j} \right] + C_{1\varepsilon} \frac{\varepsilon}{k} (G_k) - C_{2\varepsilon} \rho \frac{\varepsilon^2}{k} \quad (2.28)$$

$$G_k = -\rho \overline{u_i u_j} \frac{\partial u_j}{\partial x_i} \quad (2.29)$$

In these equations, G_k represents the generation of turbulent kinetic energy due to the mean velocity gradients, $C_{1\varepsilon}$, $C_{2\varepsilon}$ and $C_{3\varepsilon}$ are constants. σ_k and σ_ε are the turbulent Prandtl numbers for k and ε , respectively. The ‘eddy’ or turbulent viscosity, μ_t can be computed by combining k and ε as follows:

$$\mu_t = \rho C_\mu \frac{k^2}{\varepsilon} \quad (2.30)$$

where C_μ is a constant.

The model constants $C_{1\varepsilon}$, $C_{2\varepsilon}$ and C_μ , σ_k and σ_ε were assumed to have the values of:

$$C_{1\varepsilon}=1.44, C_{2\varepsilon}=1.92, C_\mu=0.09, \sigma_k=1.0 \text{ and } \sigma_\varepsilon=1.3.$$

He compared his modelling results with experiments on a 101 mm hydrocyclone with two different spigot diameters. He investigates the effect of inlet flow rate and spigot diameter on hydrocyclone performance.

Stephens and Mohanarangam (2009) also used two equation models such as κ - ε and κ - ω for their simulation. They applied κ - ε turbulence model coupled with curvature correction and claimed it can accurately predict the mean flow behaviour. The same level of accuracy was only found with a SSG Reynolds stress model with a penalty of solving an additional five transport equations. A detailed mesh independency study was carried out to verify the model and in order to minimise any errors from mesh resolution. Experimental data of Monredon et

al. (1992) was used to validate our CFD models. They used tetrahedral and hexahedral mesh types with different mesh element sizes.

Bhaskar et al. (2007) made comparison of experimental and simulated results generated using different turbulence models i.e., standard κ - ε , Renormalization Group (RNG) κ - ε and Reynolds Stress Model (RSM) in terms of water throughput and split with the help of suitably designed experiments. The RNG κ - ε model they used is similar in form to the standard κ - ε model but includes additional terms for dissipation rate ε , a development that significantly improves the accuracy, especially for rapidly strained flows. The effect of swirl on turbulence is included in the RNG κ - ε model, enhancing accuracy for swirling flows. The RNG κ - ε model has a similar form to the standard κ - ε model:

$$\frac{\partial}{\partial t}(\rho k) + \frac{\partial}{\partial x_i}(\rho k u_i) = \frac{\partial}{\partial x_j} \left[\alpha_k \mu_{eff} \frac{\partial k}{\partial x_j} \right] + G_k + G_b - \rho \varepsilon - Y_M + S_K \quad (2.31)$$

$$\frac{\partial}{\partial t}(\rho \varepsilon) + \frac{\partial}{\partial x_i}(\rho \varepsilon u_i) = \frac{\partial}{\partial x_j} \left[\alpha_\varepsilon \mu_{eff} \frac{\partial \varepsilon}{\partial x_j} \right] + \quad (2.32)$$

$$C_{1\varepsilon} \frac{\varepsilon}{k} (G_k + C_{3\varepsilon} G_b) - C_{2\varepsilon} \rho \frac{\varepsilon^2}{k} - R_\varepsilon + S_\varepsilon$$

In these equations, G_k represents the generation of turbulence kinetic energy due to the mean velocity gradients. G_b is the generation of turbulence kinetic energy due to buoyancy, Y_M represents the contribution of the fluctuating dilatation in compressible turbulence to the overall dissipation rate. The quantities α_k and α_ε are

the inverse effective Prandtl numbers for k and ϵ , respectively. S_k and S_ϵ are user defined source terms. μ_{eff} is also calculated from the following equation:

$$\mu_{eff} = \mu + \mu_t \quad (2.33)$$

A three-dimensional simulation was performed by Yang et al. (2004) to predict the flow field and the separation efficiency for particles in a hydrocyclone for the sludge separation in water purifying plants. They applied Reynolds averaged Navier–Stokes and Reynolds averaged continuity equations by employing and solving RNG κ - ϵ model to calculate the turbulent flow field in a hydrocyclone.

They used the same form of RNG κ - ϵ as Bhaskar et al. (2007) applied in their studying and proposed some equations to evaluate G_k , S and R which are as follows:

$$G_k = \mu_t S^2 \quad (2.34)$$

where S is the modulus of the mean rate-of-strain tensor, defined as:

$$S = \sqrt{2S_{ij}S_{ij}} \quad (2.35)$$

with the mean strain rate S_{ij} is expressed as:

$$S_{ij} = \frac{1}{2} \left(\frac{\partial u_i}{\partial x_j} + \frac{\partial u_j}{\partial x_i} \right) \quad (2.36)$$

$$R = \frac{C_{\mu} \rho \eta^3 (1 - \eta/\eta_0) \varepsilon^2}{1 + \beta \eta^3} \frac{1}{k} \quad (2.37)$$

where $\eta = Sk/\varepsilon$, $\eta_0 = 4.38$, $\beta = 0.012$. The values of the model constants employed in their work were: $C_{1\varepsilon} = 1.42$, $C_{2\varepsilon} = 1.68$, $\sigma_k = \sigma_\varepsilon = 1.393$.

He et al. (1999) compared the two dimensional axi-symmetric inlet hydrocyclone simulation with a three dimensional simulation. They concluded that the $k-\varepsilon$ model is inadequate, producing large errors and incorrect predictions for flow patterns for both cases. A modified $k-\varepsilon$ model, however produced results in better agreement with experimental data for three-dimensional calculations, while the flow pattern predictions for a two dimensional hydrocyclone are approximate and inadequate for separation efficiency predictions.

Reynolds Stress Model

The turbulence inside the hydrocyclone is anisotropic, so the assumption of isotropic turbulence in the $\kappa-\varepsilon$ model makes it inappropriate as a tool for hydrocyclone simulation. Some researchers (e.g. Suasnabar, 2000) have modified the $\kappa-\varepsilon$ model and reported improved velocity profile predictions, but they also admitted that this approach was limited. Even with these modifications, their model produced large errors in the prediction of the air core and the flow pattern. This problem is somewhat alleviated by the use of the Reynolds Stress Models (RSM) which has the ability to model anisotropic turbulence and strained flows. Cullivan et al. (2004) showed that it is essential to use a high order turbulence model such as RSM to capture all of the fluctuations and to predict the

velocity profiles more accurately. They applied the RSM to a 50 mm hydrocyclone. The transport equation of Reynolds Stress in his work is shown below:

$$\begin{aligned}
\frac{\partial}{\partial t}(\rho\langle u_i u_j \rangle) + \frac{\partial}{\partial x_k}(\rho u_k \langle u_i u_j \rangle) &= \frac{\partial}{\partial x_k} \left(\frac{\mu_t}{\sigma_k} \frac{\partial \langle u_i u_j \rangle}{\partial x_k} \right) + \\
&\frac{\partial}{\partial x_k} \left(\mu_t \frac{\partial}{\partial x_k} (\langle u_i u_j \rangle) \right) \\
&- \rho \left(\langle u_i u_k \rangle \frac{\partial \langle u_j \rangle}{\partial x_k} + \langle u_i u_k \rangle \frac{\partial \langle u_i \rangle}{\partial x_k} \right) \\
&+ P \left\langle \left(\frac{\partial \langle u_i \rangle}{\partial x_k} + \frac{\partial \langle u_j \rangle}{\partial x_k} \right) \right\rangle - 2\mu \left\langle \frac{\partial \langle u_i \rangle}{\partial x_k} \frac{\partial \langle u_j \rangle}{\partial x_k} \right\rangle
\end{aligned} \tag{2.38}$$

Two models for the pressure strain which are termed as linear and quadratic pressure-strain models were compared. The quadratic model showed a better result in the prediction of the velocity profiles according to Cullivan et al. (2004).

Slack et al. (2000) found that the stress transport model gave acceptable predictions of velocity profiles in hydrocyclone due to its ability to model anisotropic turbulence and strained flows. Schuetz et al. (2004) used the Reynolds Stress Model (RSM) to predict the velocity and pressure distribution, and grade efficiency curve in a hydrocyclone. They compared their numerical simulation with experimental results and claimed a good agreement with experiment, especially for the pressure drop and separation efficiency. The drawback of their model was its limitation to very low solid concentration.

Bhaskar et al. (2007) compared the standard k-ε model with the RNG (Re-Normalisation Group) k-ε model and the RSM, and concluded that the best agreement to experimental results is given by the RSM, with errors between 4 and 8 %. The main problem with their model was the disregard of the air core, which is one of the key components in hydrocyclone simulation.

Wang et al. (2007) presented a numerical study of the gas-powder-liquid flow in a standard hydrocyclone. In their approach, the turbulent fluid flow is described by the Reynolds stress model. The flow features were examined in terms of flow field, pressure drop, volume split ratio reported to the underflow, particle trajectories, and separation efficiency. They claimed that RSM is the appropriate turbulence model for cyclone flow, although it is computationally more expensive than other unresolved-eddy turbulence models. The governing equations for an incompressible fluid can thus be written as:

$$\frac{\partial \rho}{\partial t} + \frac{\partial(\rho u_i)}{\partial x_i} = 0 \quad (2.39)$$

$$\frac{\partial}{\partial t}(\rho u_i) + \frac{\partial}{\partial x_i}(\rho u_i u_j) = -\frac{\partial p}{\partial x_i} + \frac{\partial}{\partial x_j} \left[\mu \left(\frac{\partial u_i}{\partial x_j} + \frac{\partial u_j}{\partial x_i} \right) \right] + \frac{\partial}{\partial x_j} (-\rho \overline{u_i' u_j'}) \quad (2.40)$$

where the velocity components were decomposed into the mean and fluctuating velocities which were related by:

$$u_i = \bar{u}_i + u_i' \quad (2.41)$$

where the Reynolds stress term includes the turbulence closure, which must be modeled. Transport equations for the transport of the Reynolds stresses in the RSM were written as:

$$\frac{\partial}{\partial t}(\rho \overline{u_i' u_j'}) + \frac{\partial}{\partial x_k}(\rho u_k \overline{u_i' u_j'}) = D_{T,ij} + P_{ij} + \varphi_{ij} + \epsilon_{ij} \quad (2.42)$$

where ρ , u_i , u_i' and x_i were respectively liquid density, velocity, velocity fluctuation, and positional length. The two terms on the left were the local time derivative of the stress and convective transport term, respectively. The four terms in the right are:

The turbulent diffusion term

$$D_{T,ij} = -\frac{\partial}{\partial x_k} [\rho \overline{u_i' u_j' u_k'} + \overline{p(\delta_{kj} u_i' + \delta_{ik} u_j')}] \quad (2.43)$$

The stress production term

$$P_{ij} = -\rho \left(\overline{u_i' u_k'} \frac{\partial u_j}{\partial x_k} + \overline{u_j' u_k'} \frac{\partial u_i}{\partial x_k} \right) \quad (2.44)$$

The pressure strain term

$$\varphi_{ij} = \overline{p \left(\frac{\partial u_i'}{\partial x_j} + \frac{\partial u_j'}{\partial x_i} \right)} \quad (2.45)$$

The dissipation term

$$\epsilon_{ij} = -2\mu \overline{\frac{\partial u_i}{\partial x_k} \frac{\partial u_j}{\partial x_k}} \quad (2.46)$$

where δ was the Kronecker factor and μ and p are respectively the molecular viscosity and pressure.

Large Eddy Simulation

Delgadillo and Rajamani (2005) pointed out that even with powerful computational resources; comprehensive and reliable hydrocyclone modelling remains a challenge owing to the presence of different phases. Hydrocyclones typically operate at very high velocities which makes the flow within the hydrocyclone highly turbulent. Moreover, the rotational motion and flow separation inside the hydrocyclone brings anisotropy and strains into the turbulence.

Slack et al. (2000, 2004) reported good agreement with experimental results using RSM, but also stated that simulations with LES could give a better prediction of velocity profiles and separation efficiency. The drawback of LES is that it is computationally more time consuming than RSM.

Large eddy simulation solves the large scale turbulent fluctuations and models the sub grid scale eddies. Therefore it can capture a time-dependent vortex oscillation, making it a useful tool to study the flow inside the hydrocyclone. Delgadillo and Rajamani (2005) modeled a 75 mm and a 250 mm hydrocyclone using LES and found that this model predicts velocity profile and specifically tangential velocity

more accurately than other turbulence closure models. The momentum balance equations with turbulence closure models are:

$$\frac{\partial \rho}{\partial t} + \frac{\partial}{\partial x_i}(\rho u_i) = 0 \quad (2.47)$$

$$\frac{\partial}{\partial t}(\rho(u_i)) + \frac{\partial}{\partial x_i}(\rho(u_i)(u_j)) = -\frac{\partial P}{\partial x_i} + \frac{\partial}{\partial x_j} \left[\mu \left(\frac{\partial u_i}{\partial x_j} \right) \right] + \frac{\partial}{\partial x_i}(-\rho(u_i u_j)) + \rho g_i \quad (2.48)$$

where u_i represents the mean velocity and the $-\rho(u_i u_j)$ is the Reynolds stress tensor. This stress tensor is obtained from an average over the random turbulent fluctuations in the fluid. The Reynolds stress is the term which brings the need of different turbulence closure models. Each turbulence model solves the turbulent fluctuations to some extent and models the rest. So the turbulence model is selected based on the complexity of the flow physics, the required accuracy, the expected simulation time and computational resources available.

Delgadillo and Rajamani (2005) compared three different turbulence closure models for hydrocyclone and concluded that LES results are clearly closer to the experimental results than RSM and RNG k- ϵ . In a later work Delgadillo and Rajamani (2007) studied different hydrocyclone designs. They investigated six designs and compared them with a standard design. The mass balance and the classification curve were used to evaluate the performance of each hydrocyclone.

The flow patterns within a hydrocyclone separator system have been studied experimentally by Lim et al. (2010) using particle image velocimetry (PIV) and computationally via large eddy simulations. Various aspects of the flow field such

as the process of air core structure formation, pressure and velocity distributions within the system have been characterized. They reported that LES is deemed to be an adequate methodology for modelling the air core structure and flow patterns of the surrounding liquid in a hydrocyclone separator system. They modeled a 45 mm hydrocyclone with 105 hexahedral mesh elements.

Brennan et al. (2007) used Hsieh (1988) experimental data for their modelling. According to them the model is capable of predicting velocity profiles, flow splits, air core position and efficiency curves in classifying hydrocyclones. Their model approach uses the Mixture model with the granular options and large eddy simulation (LES) to resolve the turbulent mixing of the particles. They stated that refining the grid and using a higher order discretization scheme improve predictions by reducing the simulated short circuiting of the larger sized limestone fractions.

Narasimha (2007) also did a similar work and simulated turbulent driven flow in a dense medium cyclone with magnetite medium and showed that the predicted air-core shape and diameter were close to experimental results measured by gamma ray tomography. Large eddy simulation was used as a turbulence model for multiphase simulations, together with viscosity corrections according to the feed particle loading factor to give a more accurate prediction of axial magnetite segregation.

2.3 Air core calculations and multiphase modeling

A key phenomenon that strongly influences the performance of the hydrocyclone is the development of the air core. Many researchers have modelled the air core development in the hydrocyclone using different techniques. The simplest and most common solution is to impose an air core of fixed diameter with a slip boundary condition at the gas/liquid interface. Theoretical models (Dyakowski and Williams, 1995) have been used as an aid in estimating the air core diameter. Neesse and Dueck (2007) predicted the air core diameter by assuming that the positive pressure gradient and the centrifugal force in the rotational flow field are balanced and concluded that this physical consideration indicates that the air core radius is primarily determined by the hydrocyclone geometry.

A stable flow field in a hydrocyclone is an important requirement for effective performance. The stability of the flow depends strongly on the air core generated inside the hydrocyclone. The unsteady behaviour of the air core and its relation to the surrounding unsteady liquid flow have been the subject of research in recent years. Gupta et al. (2008), and Neesse and Dueck (2007) studied the air core formation and effective parameters during the process. Nowakowski et al. (2004) stated that the air core occurs because of the low pressure region in the hydrocyclone drops below atmospheric pressure, which allows air to enter the hydrocyclone. It is really not known how the air core is developed, and Narasimha et al. (2006) suggested that air core formation is principally a transport effect rather than a pressure effect.

Ideally, the air core should develop naturally as a part of the CFD simulations, which requires an appropriate method to model the multiphase flow. Delgadillo and Rajamani (2007) used the volume of fluid (VOF) model coupled with LES for modelling the turbulence closure and reported satisfactory predictions of the air core. The key factor in modelling the air core is accurate prediction of the interface. The air core interface can be located by using the Volume of Fluid model. The transport equations for air/water interface are:

$$\frac{\partial \rho}{\partial t} + \frac{\partial}{\partial x_i}(\rho u_i) = 0 \quad (2.49)$$

$$\frac{\partial}{\partial t}(\rho u_i) + \frac{\partial}{\partial x_j}(\rho u_i u_j) = -\frac{\partial P}{\partial x_i} + \frac{\partial}{\partial x_j} \left[\mu \left(\frac{\partial u_i}{\partial x_j} + \frac{\partial u_j}{\partial x_i} \right) \right] + \rho g_i \quad (2.50)$$

where α_p is the fraction of fluid in each cell.

Narasimha et al. (2007) used Mixture model as a multiphase model, which solves the equations of motion for the slurry mixture and solves transport equations for the volume fraction of any additional phases p , which are assumed to be dispersed throughout a continuous fluid (water) phase c :

$$\frac{\partial}{\partial t} \alpha_p + \frac{\partial}{\partial x_i}(\alpha_p u_i) + \frac{\partial}{\partial x_i}(\alpha_p u_{pm,i}) = 0 \quad (2.51)$$

$$u_{pm,i} = u_{pi} - u_i \quad (2.52)$$

$u_{pm,i}$ is the drift velocity of the p relative to the mixture m . This is related to the slip velocity $u_{pc,i}$ which is the velocity of the p relative to the continuous water phase c by the formulation:

$$u_{pmi} = u_{pci} - \sum_{l=1}^n \frac{\alpha_l \rho_l}{\rho_m} u_{lci} \quad (2.53)$$

$$u_{pci} = u_{pi} - u_{ci} \quad (2.54)$$

The mixture model calculates a separate slip velocity for each modeled phase p and assumes that the phase has a unique density and particle size. The slip velocity u_{pci} was calculated by Manninen et al. (1996) which assume that the particles which make up the phase p accelerate rapidly in the presence of any forces on the phase and therefore can be assumed to be always moving at their terminal velocity relative to the mixture. Manninen et al. (1996) referred to this assumption as a local equilibrium assumption. In the basic formulation of the mixture model, the Schiller and Naumann (1935) drag law was used and the slip velocity for phase p was calculated by:

$$u_{pci} = \frac{d_p^2 (\rho_p - \rho_m)}{18 f_{rep} \mu_c} \left(g_i - \frac{\partial}{\partial t} u_{mi} - u_{mj} \frac{\partial}{\partial x_j} u_{mi} \right) \quad (2.55)$$

The term outside the brackets is called the particle relaxation time and if the relaxation time is small compared to the scale of the flow, then the assumption that the particles associated with phase p are always moving at their terminal relative velocity is considered to be valid. The terms inside the brackets in u_{pmi} are

accelerations associated with the forces to which the particles are subject, which in the basic model are gravity, and, the time rate of change and convective terms from the mixture momentum equation. In particular it is the convective term from the mixture momentum equation which induces the centripetal force on the phase p in a flow with streamline curvature and thus models the classification force arising from swirl in a cyclone simulation. In principle other forces such as lift forces and turbulent dispersion forces can also be accounted for by including the acceleration associated with that force in equation related to u_{pci} .

2.4 Particle tracking and forces acting on the particles

The accurate simulation of the particulate phases inside the hydrocyclone is also very important. There are two approaches in CFD to simulate these phases, the Eulerian and Lagrangian. Momentum and continuity equations are solved for both the dispersed and continuous phase in the Eulerian approach. Nowakowski et al. (2000), Suasnabar (2000) and Brennan et al. (2007) applied this approach in their simulations. The Lagrangian method simulates the paths of individual particles by balancing drag, buoyancy and other body forces on each particle. Hsieh (1988) used the Lagrangian approach to predict the classification of limestone in a 75 mm hydrocyclone. It was an axisymmetric approach, which reduced the computational domain to two coordinates. As noted earlier, it requires a three dimensional model to predict the air core well, and consequently a better prediction for flow patterns and particle separation efficiency.

The main challenges in the solids modelling are the handling of high volumetric concentration of solid particles and the subsequent tracking of particle trajectories. Most hydrocyclone simulations use low concentrations of particles to reduce the magnitude of the first problem. To predict the trajectories of particles, it is commonly assumed that particle/particle and particle/fluid interactions are negligible for low concentration of particles (typically below a value of 10% solid by weight (Svarovsky 1980, Braun and Bohnet (1990))). A standard method utilizes discrete phase modelling (DPM) to capture all of the drag forces acting on the particles and particle diffusion due to flow turbulence. DPM captures the trajectory of particles by Lagrangian method while Eulerian method is used for continuous phase.

The balance of forces on the particles in a Lagrangian reference form is obtained by integrating drag, gravity, buoyancy and centrifugal forces expressed as follows:

$$\frac{du_p}{dt} = F_D(u - u_p) + g_x \left(\frac{\rho_P - \rho_L}{\rho_P} \right) + F_X \quad (2.56)$$

This equation is a simple balance between the forces acting on any single particle and particle inertia where $F_D(u - u_p)$ the drag force per unit particle mass is defined as:

$$F_D = \left(\frac{18\mu D_P^2}{\rho_P} \right) \left(\frac{C_D Re}{24} \right) \quad (2.57)$$

$$Re = \frac{\rho u D_p}{\mu} \quad (2.58)$$

where F_D is the drag force, C_D the drag coefficient and D_p the particle diameter.

In the next chapter models applied through the simulation will be discussed further. The manner these models are used in the simulation is directly related to the characteristics of each model. The discussed literature models were used as a guide to find the best solution algorithm in the hydrocyclone simulation.

3 Development and validation of a CFD model for the hydrocyclone

A variety of CFD concepts are needed to solve the hydrocyclone modelling problem. The ANSYS FLUENT package, which was based on finite volume method is used in this study. To model the dynamics of the flow we need to choose the appropriate governing equations, turbulence closer model, multiphase model and particle tracking model. All of these equations are described in Cartesian coordinates system using the index notation form.

3.1 Model development

3.1.1 Governing equations

Governing equations are needed to model the dynamics of the flow. For each control volume, mass, momentum and energy need to be conserved. The mass balance and momentum balance are the main part of the governing equations. The energy balance is not required since we assume that we are working under isothermal condition. The mass conservation equation can be represented by the continuity equation:

$$\frac{\partial \rho}{\partial t} + \frac{\partial(\rho u_i)}{\partial x_i} = 0 \quad (3.1)$$

For incompressible fluids it can be reduced to the following form:

$$\frac{\partial(u_i)}{\partial x_i} = 0 \quad (3.2)$$

The momentum balance is described by the Navier-Stoke's equation which can be written as:

$$\frac{\partial}{\partial t}(\rho u_i) + \frac{\partial}{\partial x_j}(\rho u_i u_j) = -\frac{\partial P}{\partial x_i} + \mu \frac{\partial^2 u_i}{\partial x_j^2} + \rho g_i \quad (3.3)$$

The next step would be solving the governing equations numerically which requires domain discretization. The finer the mesh, the more accurate the solution will be, but increasing the number of mesh element increases the computational cost drastically. By decomposing the velocity into mean and fluctuating components we can reduce the computational time. This decomposition process brings an extra term to the governing equation that needs to be solved with turbulence closure models.

$$u_i = \bar{u}_i + u'_i \quad (3.4)$$

$$\frac{\partial \rho}{\partial t} + \frac{\partial(\rho \bar{u}_i)}{\partial x_i} = 0 \quad (3.5)$$

$$\frac{\partial}{\partial t}(\rho \bar{u}_i) + \frac{\partial}{\partial x_i}(\rho \bar{u}_i \bar{u}_j) = -\frac{\partial \bar{p}}{\partial x_i} + \frac{\partial}{\partial x_j} \left[\mu \left(\frac{\partial \bar{u}_i}{\partial x_j} \right) \right] + \frac{\partial}{\partial x_j}(-\rho u'_i u'_j) + \rho g_i \quad (3.6)$$

where \bar{u}_i represents the mean velocity and the $-\rho(u'_i u'_j)$ is the Reynolds stress tensor. This stress tensor is obtained from an average over the random turbulent fluctuations in the fluid. The Reynolds stress is the term which brings the need of different turbulence closure models. Each turbulence model solves the turbulent fluctuations to some extent and models the rest. So the turbulence model is

selected based on the complexity of the flow physics, the required accuracy, the expected simulation time and computational resources available.

3.1.2 Turbulence closure models

There are different turbulence closure models to model the Reynolds stress tensor. RNG κ - ε model, Reynolds stress model (RSM) and large eddy simulation (LES) have been used in this study. Each turbulence closure model has been investigated deep enough to observe the suitability of that model for hydrocyclone simulation. Flow streams inside hydrocyclone change drastically throughout the hydrocyclone and the best turbulence model is the one that capture the optimum amount of dissipations in the shortest time.

κ - ε Turbulence model

κ - ε model is one of the turbulence closure models based on eddy-viscosity theory. The RNG κ - ε model is similar in form to the standard κ - ε model but includes an additional terms for dissipation rate ε , a development that significantly improve the accuracy, especially for rapidly strained flows. The effect of swirl on turbulence is included in the RNG κ - ε model, enhancing accuracy for swirling flows. The RNG κ - ε model has a similar form to the standard κ - ε model. The RNG κ - ε model describes the Reynolds stress term as written below:

$$-\rho \overline{u_i u_j} = \mu_t \left(\frac{\partial \bar{u}_i}{\partial x_j} + \frac{\partial \bar{u}_j}{\partial x_i} \right) \quad (3.7)$$

where μ_t is the turbulent viscosity and is related directly to the turbulent kinetic energy, κ , and the viscous dissipation, ε , as is shown below:

$$\mu_t = \rho C_\mu \frac{k^2}{\varepsilon} \quad (3.8)$$

The kinetic energy and dissipation rate are obtained from the two following transport equations:

$$\frac{\partial}{\partial t}(\rho k) + \frac{\partial}{\partial x_i}(\rho k u_i) = \frac{\partial}{\partial x_j} \left[\alpha_k \mu_{eff} \frac{\partial k}{\partial x_j} \right] + 2\mu_t S_{ij} S_{ij} - \rho \varepsilon \quad (3.9)$$

$$\frac{\partial}{\partial t}(\rho \varepsilon) + \frac{\partial}{\partial x_i}(\rho \varepsilon u_i) = \frac{\partial}{\partial x_j} \left[\alpha_\varepsilon \mu_{eff} \frac{\partial \varepsilon}{\partial x_j} \right] \quad (3.10)$$

$$+ C_{1\varepsilon} \frac{\varepsilon}{k} (2\mu_t S_{ij} S_{ij}) - C_{2\varepsilon} \rho \frac{\varepsilon^2}{k} - \frac{C_\mu \rho \eta^3 (1 - \eta/\eta_0) \varepsilon^2}{1 + \beta \eta^3} \frac{1}{k}$$

where $C_\mu=0.0845$ is derived from renormalization group method. μ_{eff} is the effective viscosity defined as in the in the differential equation below:

$$d \left(\frac{\rho^2 \kappa}{\varepsilon \mu} \right) = 1.72 \frac{\bar{v}}{\sqrt{\bar{v}^3 - 1 + C}} d\bar{v} \quad (3.11)$$

α_k and α_ε are the inverse effective Prandtl numbers for k and ε , respectively. The mean strain rate S_{ij} is expressed as:

$$S_{ij} = \frac{1}{2} \left(\frac{\partial u_i}{\partial x_j} + \frac{\partial u_j}{\partial x_i} \right) \quad (3.12)$$

According to Delgadillo (2006) the last term in the dissipation rate equation is the main difference between the standard κ - ε model and RNG κ - ε . When the strain

rate, S_{ij} , is large this term makes a negative contribution. In comparison with the standard κ - ϵ , there is a smaller destruction of the ϵ that eventually reduces the effective viscosity. As the result, in rapidly strained flows, the RNG κ - ϵ model yields a lower turbulent viscosity than the standard κ - ϵ model. The RNG model is more responsive to the effects of rapid strain and streamlines curvature than the standard κ - ϵ model, which explains the superior performance of the RNG model for certain hydrocyclone flows. The use of μ_{eff} allows the model to better handle low Reynolds number and near wall flows.

Reynolds stress model

The Reynolds stress model is a higher level turbulence model which is usually called second order closure. The Reynolds stress turbulence closure model solves separate transport equations for each of the six Reynolds stresses:

$$\frac{\partial}{\partial t}(\rho \overline{u_i u_j}) + \frac{\partial}{\partial x_k}(\rho u_k \overline{u_i u_j}) = D_{T,ij} + P_{ij} + \varphi_{ij} + D_{L,ij} - \epsilon_{ij} + F_{ij} \quad (3.13)$$

where:

$D_{T,ij}$ Turbulent diffusion term

$D_{L,ij}$ Molecular diffusion term

P_{ij} Stress production term

φ_{ij} Pressure strain term

ϵ_{ij} Dissipation term

F_{ij} Production by system rotation

Brennan (2006) compared the linear pressure strain modelling and quadratic pressure strain modelling in Differential Reynolds Stress Model (DRSM) and concluded that they are essentially the same but the linear DRSM can be calibrated by increasing the fast pressure strain constant. Turbulence and multiphase modeling are further discussed in the model development section.

The transport equation for Reynolds stress model is written below:

$$\begin{aligned} \frac{\partial}{\partial t}(\rho \langle \dot{u}_i \dot{u}_j \rangle) + \frac{\partial}{\partial x_k}(\rho u_k \langle \dot{u}_i \dot{u}_j \rangle) &= \frac{\partial}{\partial x_k} \left(\frac{\mu_t}{\sigma_k} \frac{\partial \langle \dot{u}_i \dot{u}_j \rangle}{\partial x_k} \right) \\ &+ \frac{\partial}{\partial x_k} \left(\mu_t \frac{\partial}{\partial x_k} (\langle \dot{u}_i \dot{u}_j \rangle) \right) \\ &- \rho \left(\langle \dot{u}_i \dot{u}_k \rangle \frac{\partial \langle u_j \rangle}{\partial x_k} + \langle \dot{u}_i \dot{u}_k \rangle \frac{\partial \langle u_i \rangle}{\partial x_k} \right) \\ &+ P \left\langle \left(\frac{\partial \langle \dot{u}_i \rangle}{\partial x_k} + \frac{\partial \langle \dot{u}_j \rangle}{\partial x_k} \right) \right\rangle - 2\mu \left\langle \frac{\partial \langle \dot{u}_i \rangle}{\partial x_k} \frac{\partial \langle \dot{u}_j \rangle}{\partial x_k} \right\rangle \end{aligned} \quad (3.14)$$

Large eddy simulation

Large eddy simulation turbulence closure model uses a filtering function to solve the governing equations. The velocity components in LES are decomposed. The small scales variables are universal in nature so they can easily be modeled with a small error. Whereas the large scale variables is more geometry and flow

dependant so they should directly be resolved to minimize the solution error as it is done in LES model.

A flow variable φ can be defined as sum of filtered (large scale or resolved) and sub-grid (modeled) part, as shown by equation below:

$$\varphi = \bar{\varphi} + \phi \quad (3.15)$$

The large scale part is obtained by the volume averaging procedure:

$$\bar{\varphi}(x_i, t) = \int_{Vol} G(x_i, \acute{x}_i) \varphi(\acute{x}_i, t) d\acute{x}_i \quad (3.16)$$

where G is the filter function. The filtered Navier-Stoke's equation can be represented as:

$$\frac{\partial}{\partial t}(\rho \bar{u}_i) + \frac{\partial}{\partial x_i}(\rho \bar{u}_i \bar{u}_j) = -\frac{\partial \bar{p}}{\partial x_i} + \mu \frac{\partial^2 \bar{u}_i}{\partial x_j^2} \quad (3.17)$$

The filtered equation contains a non-linear term made of filtered velocities, meaning that it is not possible to directly compute it from the filtered variables.

The non-linear term can be expanded:

$$\overline{\bar{u}_i \bar{u}_j} = \overline{(\bar{u}_i + \acute{u}_i)(\bar{u}_i + \acute{u}_i)} = \overline{\bar{u}_i \bar{u}_j} + \overline{\bar{u}_i \acute{u}_j} + \overline{\acute{u}_i \bar{u}_j} + \overline{\acute{u}_i \acute{u}_j} \quad (3.18)$$

Unlike time averaging, neither of the second nor the third term in the above equation becomes zero. Moreover, the equation is still not free from the unfiltered velocities. To overcome this issue, the non-linear term is reformulated in terms of

a new stress tensor which is known as the sub-grid scale (SGS) stress and the filtered velocity components such that the filtered Navier-Stoke's equation becomes:

$$\frac{\partial}{\partial t}(\rho \bar{u}_i) + \frac{\partial}{\partial x_i}(\rho \bar{u}_i \bar{u}_j) = -\frac{\partial \bar{p}}{\partial x_i} + \mu \frac{\partial^2 \bar{u}_i}{\partial x_j^2} - \frac{\partial(\rho \tau_{ij})}{\partial x_j} \quad (3.19)$$

where:

$$\tau_{ij} = -\bar{u}_i \bar{u}_j + \overline{u_i u_j} = \underbrace{-\bar{u}_i \bar{u}_j}_{L_{ij}} + \underbrace{(\overline{u_i \bar{u}_j} + \overline{\bar{u}_i u_j} + \overline{u_i u_j})}_{C_{ij}} + \underbrace{\overline{u_i u_j}}_{R_{ij}} \quad (3.20)$$

L_{ij}, C_{ij}, R_{ij} are known as Leonard, cross-stress and Reynolds sub-grid tensors, respectively. They represent the interaction among the large scales, the large and small scales, and the sub-grid scales. This equation contains non-filtered velocities and thus requires modeling, using the filtered velocity components, the SGS stress tensor is modeled with the help of a mixing-length based eddy-viscosity approach, as shown in the following equation:

$$\tau_{ij} - \frac{1}{3} \tau_{kk} \delta_{ij} = -\frac{2\mu_t \overline{S_{ij}}}{\rho} \quad (3.21)$$

where μ_t is the sub-grid scale turbulent viscosity, which can be modeled using different sub-grid scale models such as WALE or Smagorinsky model. The strain-stress tensor S_{ij} of the filtered flow-field is defined by:

$$\overline{S_{ij}} = \frac{1}{2} \left(\frac{\partial \overline{u_i}}{\partial x_j} + \frac{\partial \overline{u_j}}{\partial x_i} \right) \quad (3.22)$$

3.1.3 Multiphase model

The volume of fluid (VOF) was used to compute the interaction between water and air phases. VOF tracks volume fractions for all phases throughout the domain. It is applicable to a system in which the fluids are not interpenetrating but rather characterized by a free surface between the fluids. Tracking is by the solution of a continuity equation shown below:

$$\frac{1}{\rho_q} \left[\frac{\partial}{\partial t} (\alpha_q \rho_q + \nabla \cdot (\alpha_q \rho_q \overline{v}_q)) \right] = S_{\alpha q} + \sum_{p=1}^n (\dot{m}_{pq} - \dot{m}_{qp}) \quad (3.23)$$

The volume fraction of phase q is represented by α_q . \dot{m}_{pq} is the mass transfer from phase q to p and the the opposite goes for \dot{m}_{qp} . $S_{\alpha q}$ symbolises a source term.

A single momentum equation is solved for the entire flow domain. By use of the overall density and viscosity, the equation is dependent on the volume fraction of each phase:

$$\frac{\partial}{\partial t} (\rho \overline{v}) + \nabla \cdot (\rho \overline{v} \overline{v}) = -\nabla p + \nabla \cdot [\mu (\nabla \overline{v} + \nabla \overline{v}^T)] + \rho \overline{g} + \overline{F} \quad (3.24)$$

Properties such as density are determined as a volume weighted average for a multiphase system written as below:

$$\rho = \sum \alpha_q \rho_q \quad (3.25)$$

The surface tension model employed by FLUENT is the continuum Surface Force (CSF) model. Using this model, results in the addition of a source term to the momentum equation.

$$F_{vol} = \sigma_{ij} \frac{\rho k_i \nabla \alpha_i}{\frac{1}{2}(\rho_i + \rho_j)} \quad (3.26)$$

The source term is also referred to the volume force and denoted by F_{vol} . Interfacial tension is represented by σ_{ij} while k symbolises the surface force curvature. This equation illustrates that the surface tension source term for a cell, is indirectly proportional to the average density of the cell.

3.1.4 Particle classification

The accurate simulation of the particulate phases inside the hydrocyclone is very critical. There are two approaches in CFD to simulate these phases, the Eulerian and Lagrangian. The Lagrangian method simulates the paths of individual particles by balancing drag, buoyancy and other body forces on each particle. The balance of forces on the particles in a Lagrangian reference form is obtained by integrating drag, gravity, buoyancy and centrifugal forces expressed as follows:

$$\underbrace{\frac{du_{pi}}{dt}} = \text{drag force} + \underbrace{\frac{g_i(\rho_p - \rho_l)}{\rho_p}} + \text{pressure gradient force} \quad (3.27)$$

Particle inertia force gravity and buoyancy

This equation is a simple balance between the forces acting on any single particle and particle inertia where $F_D(u - u_p)$ the drag force per unit particle mass defined as is:

$$F_D = \left(\frac{18\mu D_p^2}{\rho_p} \right) \left(\frac{C_D \text{Re}}{24} \right) \quad (3.28)$$

$$\text{Re} = \frac{\rho u D_p}{\mu} \quad (3.29)$$

where F_D is the drag force, C_D the drag coefficient and D_p the particle diameter. To reduce the computational cost, effects of particles on the continuous phase and other particles are ignored. In other words particle/particle interactions and particle/water interactions are assumed to be negligible.

The diffusion of particles due to turbulence is modeled with the stochastic particle tracking model. The turbulence causes an effect on particle dispersion that can be integrated into a time scale. FLUENT calculates an integral time scale to describe the time which a particle spends in turbulent motion along the particle path.

$$T = \int_0^\infty \frac{u_p'(t)u_p'(t+s)}{\overline{u_p'^2}} \quad (3.30)$$

The eddy life-time can be defined as a constant or a variable that includes random variation:

$$\tau_e = 2T_L \quad (3.31)$$

$$\tau_e = -T_L \log r \quad (3.32)$$

where T_L is the fluid Lagrangian integral time and in the case of LES it is taken equivalent to the LES time scales. The variable r is a random variable between 0 and 1. Time taken by a particle to cross the eddy is defines as:

$$t_{cross} = -\tau \ln \left[1 - \left(\frac{L_e}{\tau |u - u_p|} \right) \right] \quad (3.33)$$

where L_e is the eddy length scale.

Using the mentioned turbulence closure models, the appropriate multiphase model and the particle classification method leads us to a model that can be later validated with experimental and simulation data from the literature to measure the validity and accuracy of the model.

3.2 Complications

The science of Computational Fluid Dynamics is quite developed for single phase, laminar flows such that it can directly be used as one of the main tools to study. However, the physics of multiphase and turbulent flows is so complicated that it requires additional levels of modeling, for which CFD is still under the process of development. Hence, in the present scenario it is essential to demonstrate the applicability of different turbulence and multiphase models used for a specific case. This can be achieved by comparing results from experiments and the simulations.

To obtain a reasonable agreement with experimental data an appropriate turbulence, closure model, multiphase model, particle tracking method and a good stepwise plan is needed. If we lack any of the mentioned parameters there would be no hope for a good agreement with experimental trends.

3.2.1 The proposed hydrocyclone design

To validate the model a simulated hydrocyclone with the experimental results was selected. This hydrocyclone was a work of Hsieh (1988). We investigated this hydrocyclone to use a reliable set of experimental data to validate the modelling. Table 3.1 provides the dimensions of Hsieh's hydrocyclones.

Table 3.1-Hsieh's hydrocyclone dimensions

Dimensions	
Cyclone diameter, mm	75
Inlet entry, mm	25
Cylindrical length, mm	75
Vortex finder diameter, mm	25
Vortex finder length, mm	50
Spigot diameter, mm	12.5
Cone Angle, °	20

Delgadillo and Rajamani (2005, 2007) used the experimental results from Hsieh's (1988) work to validate their numerical work. Tangential and Axial velocity

profiles, air core diameter, pressure drop and particle separation efficiency for a range of particle size was compared against experimental data in this work. This hydrocyclone geometry was chosen because there was a reasonable agreement between their experimental data and simulation. Hsieh's hydrocyclone geometry is shown in Figure 3.1.

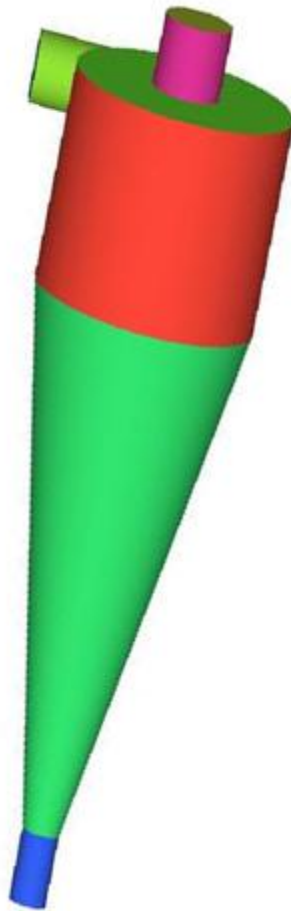


Figure 3-1-Hsieh's hydrocyclone geometry

As shown in Figure 3.1 Hsieh's hydrocyclone has a circular tangential inlet and it has only one conical section at the bottom.

3.2.2 Mesh generation

The 3D cells available in GAMBIT include hexahedral, tetrahedral, pyramid and wedge cells. Important aspects which were considered in the selection of the appropriate mesh cell type are the mesh quality, the amount of mesh cells and the associated computational expense.

The quality of simulation results obtained in ANSYS FLUENT package is highly dependent on suitable geometry and grid designs. Generation of hydrocyclone geometries and grids were performed in FLUENT pre-processing package, GAMBIT. The appropriate mesh type and an optimized mesh size play an important role in simulation convergence and better results.

Mesh type

The skewness and aspect ratio of a cell shape are two features that influence the accuracy of the solution. Cells that are highly skew tend to destabilise the solution and are almost intolerable in flows where strong gradients exist. The aspect ratio measures the extent to which the cell is stretched.

The first mesh type used in this study was tetrahedral. A volume mesh was used for the entire domain of the hydrocyclone as shown in Figure 3.2. Tetrahedral meshes are less tolerant to high aspect ratios while more cells are also required. Large aspect ratio cells in tetrahedral mesh cause inaccuracies. The noted

problems prevented a good prediction of the pressure and velocity profiles and even inhibit convergence due to the influence on the skewness of the cells. There are some chances of producing a closer agreement with experimental results with tetrahedral meshes by using a really good solution methodology but it was found that this mesh type is the best type for hydrocyclone simulation.

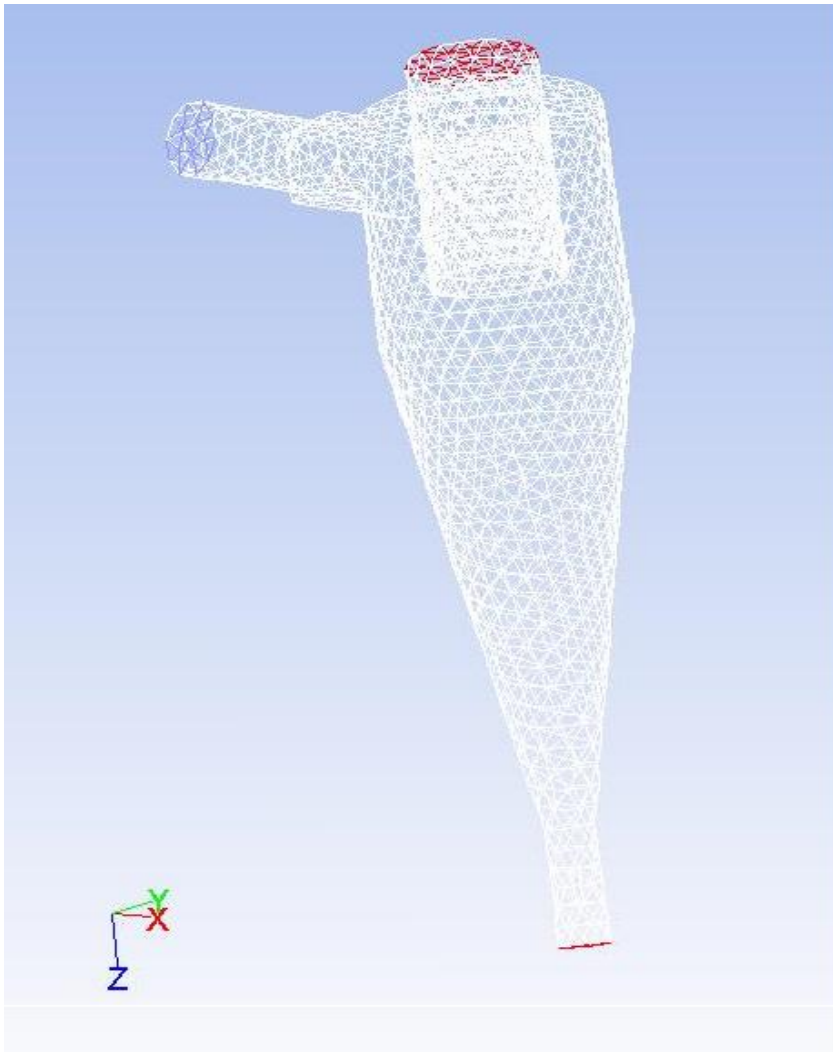


Figure 3-2-Tetrahedral mesh used for hydrocyclone

After much effort to trying to get the tetrahedral mesh working the mesh type was switched into hexahedral mesh type. The appropriate mesh type is an unstructured hexahedral mesh throughout the whole body, as this type of the mesh is more tolerant of high aspect ratios. Another advantage to this type of mesh type is hexahedral mesh elements are less diffusive than other types such as tetrahedral.

An advantage of hexahedral cells is that they allow a much larger aspect ratio than tetrahedral cells. Large aspect ratios in tetrahedral cells may cause inaccuracies and even inhibit convergence due to its influence on the skewness of the cells. For a simple geometry, the use of a hexahedral mesh can result in a solution of better quality than for tetrahedral cells, while fewer cells are also required. Unstructured hexahedral cells might prove even more advantageous as cells are not forced into place where not required, as often happens with a structured hexahedral mesh.

Mesh size

The solutions for turbulent flow systems are more easily influenced by the choice of mesh design due to the strong interactions involved. It is therefore suggested the mesh applied to a turbulent flow system should be sufficiently fine. Care should be taken not use a too fine mesh near the wall as the wall functions become invalid in the viscous sub layer (layer adjacent to the wall).

The grid resolution in complex 3D flows is constrained by the available computational resources and CPU time. With more computational cells, the accuracy will increase, but the computational requirements also increase.

Y^+ is a non-dimensional distance. It is critical in modeling turbulent flows to determine the proper size of the cells near the walls. Y^+ is often used to describe how coarse or fine a mesh is suitable for a particular flow pattern close to the domain walls. The turbulence model wall laws have restrictions on the y^+ value at the wall. A faster flow near the wall will produce higher values of y^+ , so the element size near the wall must be reduced. For the hexahedral meshes the y^+ values were typically between 3 and 400. Hence to capture the temporal turbulent fluctuations close to the wall, the maximum y^+ was kept between 30 and 300.

To study the grid independence initially a grid size of 5 mm was used to generate mesh density of about 120000 mesh elements. To ensure the validity of the results, furthermore grid refinement was applied to see at what point the difference between the results of different mesh sizes are small enough. For larger number of the grids, the accuracy will increase logarithmically to a point, but the computational requirements play a limiting role, and finally a grid size of 1 mm with mesh density of about 560,000 mesh elements was considered to be the optimum for the hydrocyclone geometry from Delgadillo and Rajamani (2005). A hydrocyclone with a 1 mm element size is shown in Figure 3.3(a).

The approach outlined above was used for the entire study and resulted closer agreement with the experimental data. The way the grid independence was carried out is fairly straight forward. The initial simulation was ran with the initial number of cells to ensure convergence with the residual error of 10^{-4} . Monitor points were steady and the maximum tangential velocity at 60 mm from the top of

the hydrocyclone was recorded. Once the convergence criteria was met for the first simulation the mesh was globally refined to have finer cells throughout the domain. The simulation was repeated with 420,000 cells until the convergence criteria was met with the same residual error. At this point the monitor points (Tangential velocity at 60 mm from the top) were compared against the first step to calculate the difference. The same procedure was followed until the difference was lower than the allowable tolerance. As it is shown in Figure 3.3(b) increasing the number of cells from 560,000 mesh elements to 700,000 does not improve the simulation results significantly and 560,000 grid cell was considered to be the optimum number of grid cells for this hydrocyclone geometry.

Numerical diffusion (or false diffusion) is another main contributor to error. This phenomenon has a similar effect as an increase in the diffusion coefficient. To minimise the presence of numerical diffusion it is best to refine the mesh or to align it in the direction of flow.

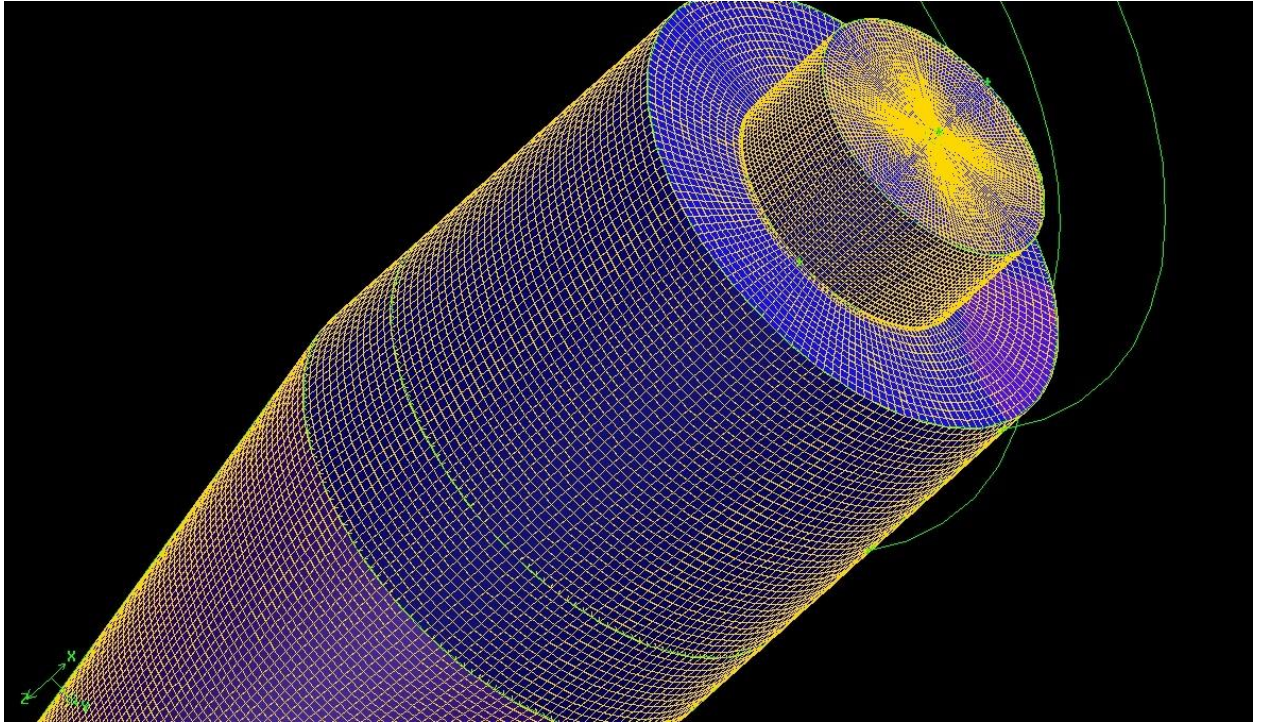


Figure 3-3(a)-Grid size 1 shown on hydrocyclone

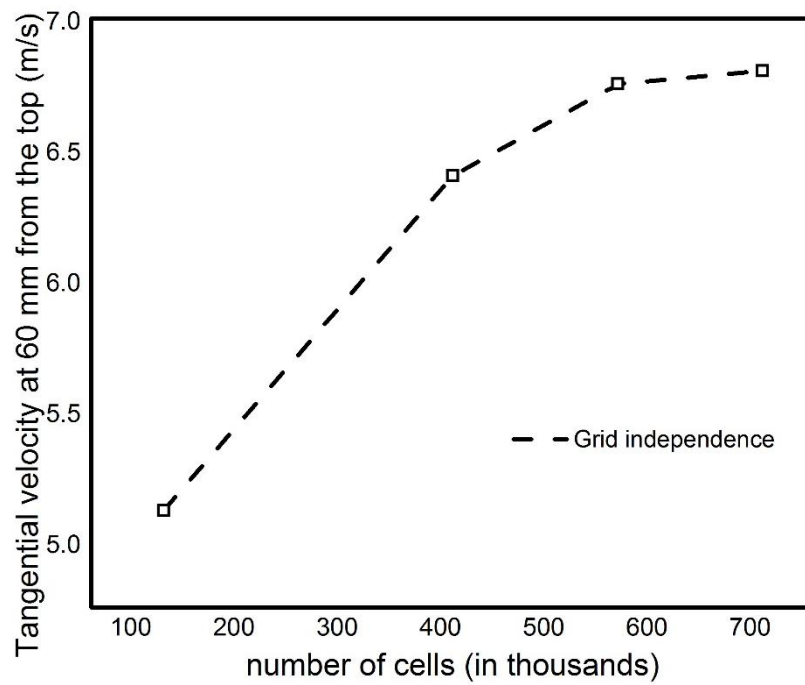


Figure 3-3 (b) - Maximum tangential velocity at 60 mm from the top of the hydrocyclone at different number of grid cells

As the number of mesh elements increase the computational power needed to solve the problem increases drastically, so the appropriate number of mesh elements depends on the desired accuracy, the available computer power and the time duration available to solve the problem.

Mesh quality

Even though mesh type and grid size are the main two aspects of the meshing process having them both in good condition is not necessarily enough. The mesh quality is another important factor to be considered.

A low quality mesh for the hydrocyclone body produces inconsistency and brings error into velocity profile prediction. The skewness and aspect ratio of a cell are two important aspects that influence the accuracy of a solution. Cells that are highly skewed tend to destabilize the solution and are intolerable in flows where steep gradients exist. In a low quality mesh, the numbers of cells with high aspect ratios or high skewness are higher than in a high quality mesh. Figure 3.4 shows an incomplete air core due to low quality mesh inside the body. Even though a good solution methodology was used for this simulation, the air core is not completely generated, showing the importance of mesh quality.

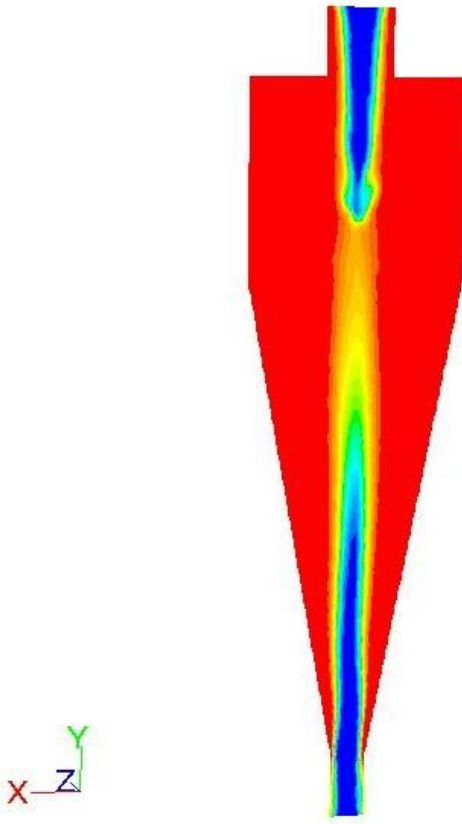


Figure 3-4-Air core produced from a low quality mesh

The best way to produce a high quality mesh is to use non-conformal hexahedral mesh by separating the hydrocyclone body into different volumes. The main body of the hydrocyclone was separated into seven simpler sub-geometries to facilitate the creation a high quality mesh. The cylindrical body was separated from the conical section and the inlet was also considered to be separate. Then the cylindrical section was divided into three incomplete cylindrical sections and one small cylinder to use appropriate hexahedral mesh schemes. Each part was meshed with a different scheme of the hexahedral mesh due to different shape of each section. The inlet section, the conical section and the vortex finder were

meshed with hexahedral cooper scheme while hexahedral map scheme along with cooper scheme were used to mesh the cylindrical part. Using this method ensures high quality volumes and a higher quality mesh for the entire body of the hydrocyclone at the end.

Figure 3.5 shows the conical section meshed along with the vortex finder. Then a mesh generation for the cylindrical chamber and the inlet was added to complete the meshing procedure, but it certainly was done volume by volume even though it was hard at some points to match the surface meshes at the volume intersections.

Mesh quality was assessed by examination of the equi-size skewness. Figure 3.6 shows the hydrocyclone, illustrating the equi-size skewness of cells. Blue cells have a low skewness and high quality, while purple and pink cells are more skew. A distribution of the equi-size skewness of the total cell population is provided in Figure 3.6 as well. As more than 95 % of the cells have skewness equal to or smaller than 0.2, the mesh structure is considered to be of high quality.

Because the majority of cells are of the hexahedral type, the mesh structure is more tolerable of high aspect ratios. Quick inspection of the aspect ratios revealed that more than 98% of the cells in the mesh lie in a range of 0 to 0.5. The mesh quality was therefore considered as high quality mesh.

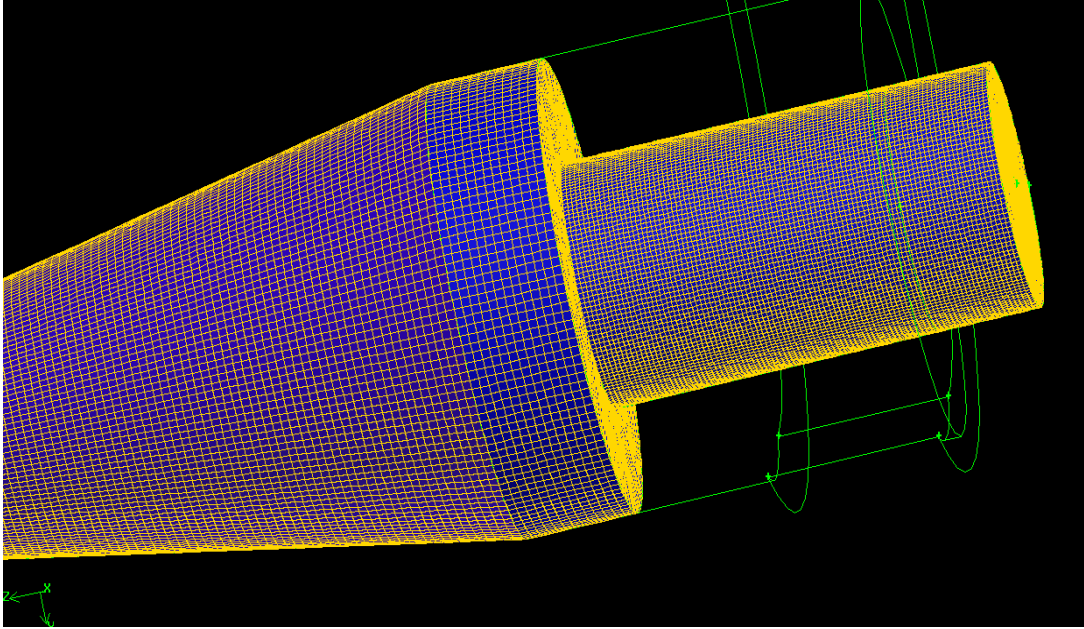


Figure 3-5-Volume mesh for hydrocyclone

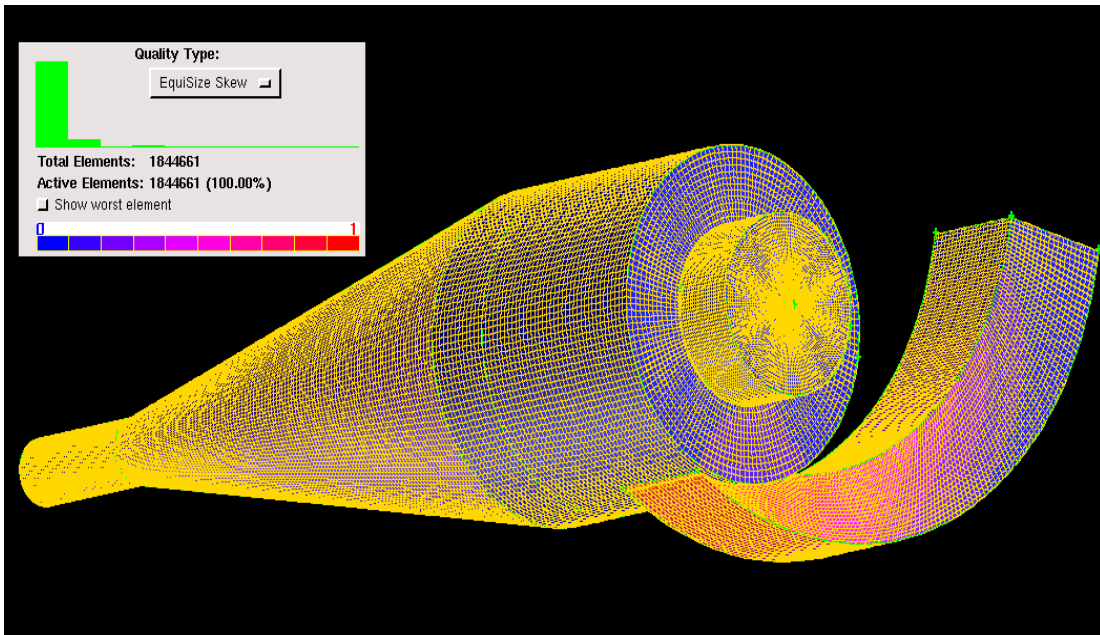


Figure 3-6-High quality mesh produced for hydrocyclone

High quality hexahedra mesh is shown in Figure 3.7 from the top and the side. Increasing the quality of the mesh is always a good option in providing a better solution. As mentioned earlier it also helps the simulation to run faster and reduces the computational cost.

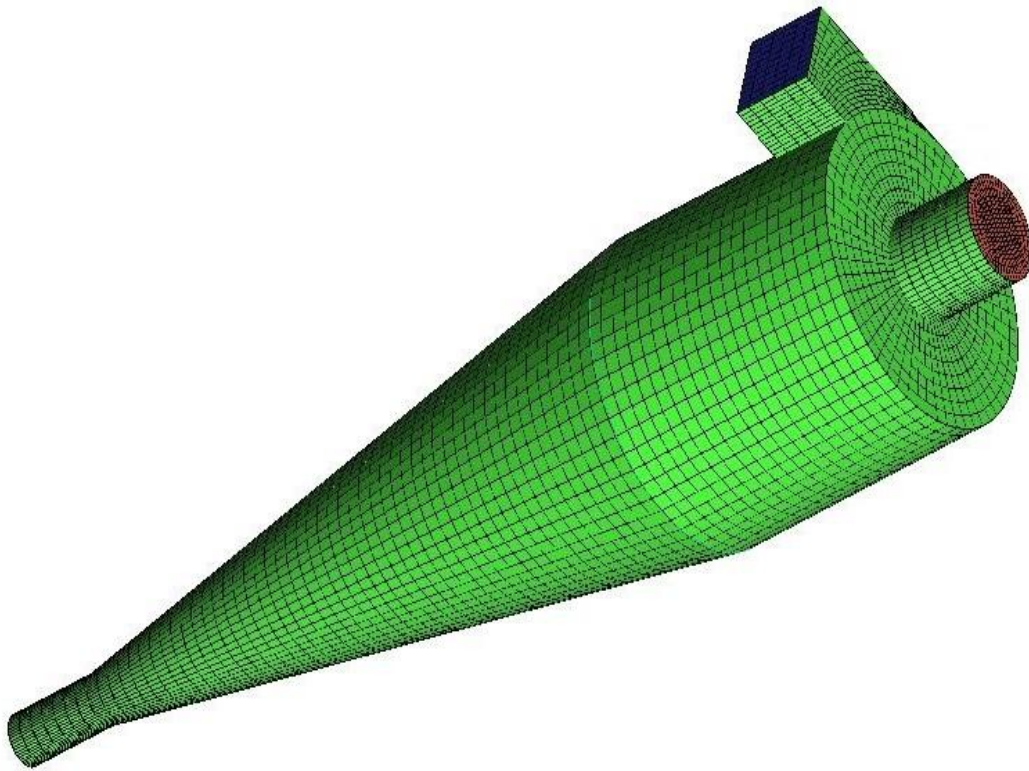


Figure 3-7-High quality hexahedral mesh

A high quality mesh and a low quality mesh are compared against experimental data in Figure 3.8. The axial velocity at 60 mm from the top of the cylindrical part from Hsieh's hydrocyclone (1988) experimental data is compared against our results from low and high quality mesh. It is evident that the high quality mesh predicts the velocity profile much better than the low quality mesh.

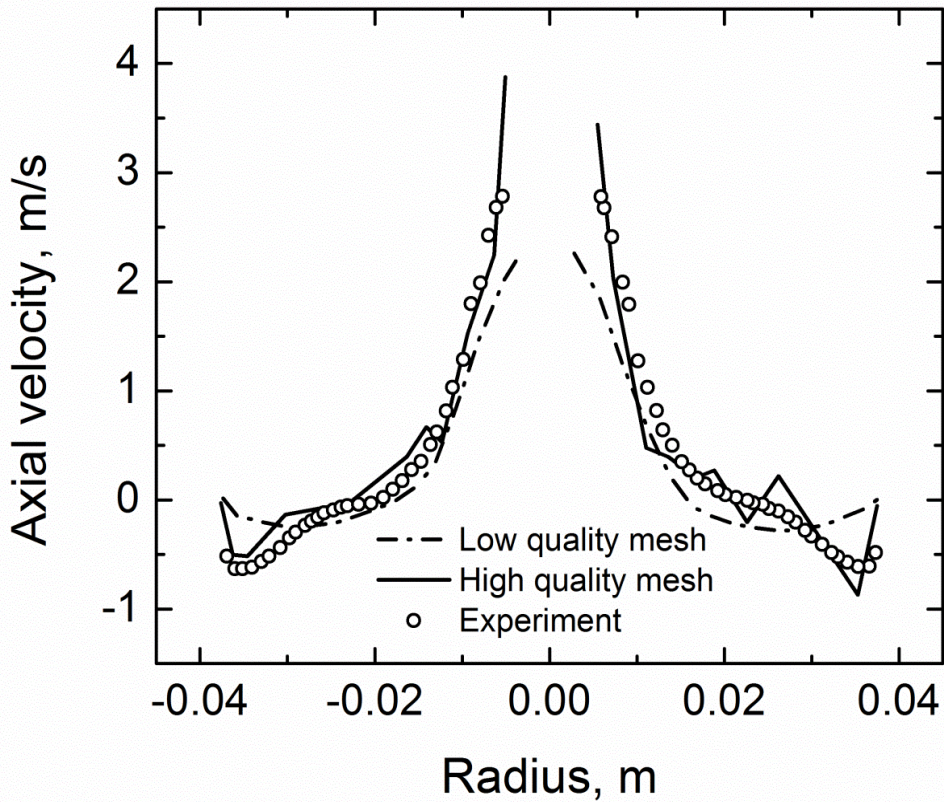


Figure 3-8-Axial velocity comparison at 60 mm from the top

3.2.3 Inlet

Inlet presence and its type also affect the accuracy and convergence of the solution in different ways. Inlet section is the place water phase and particles are injected to the hydrocyclone. It also gives the water phase enough time to fully develop and makes the simulation more realistic.

Hydrocyclone with inlet and no inlet

As shown in Figure 3.9 the presence of the inlet makes the simulation more realistic, but at the same time it makes it harder to generate mesh at the intersection of the inlet and the cylindrical section.

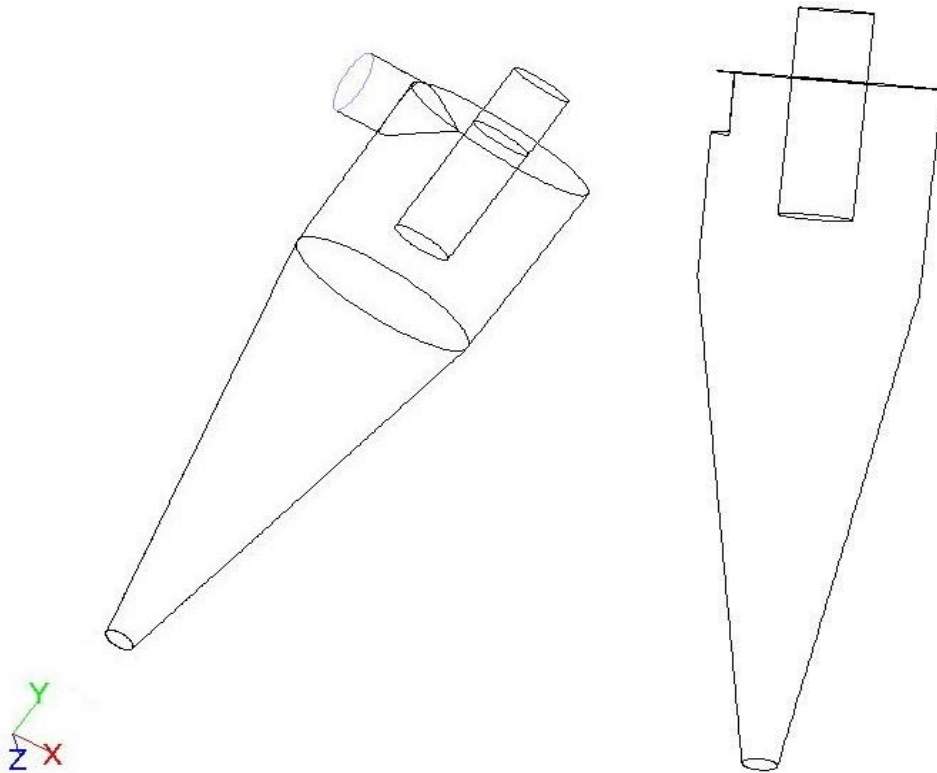


Figure 3-9-Hydrocyclone geometry with and without the inlet section

After choosing the appropriate mesh type and grid size it was observed that the mesh quality was noticeably lower at the inlet-cylinder intersection and the mesh elements were highly skewed so it was decided to remove the inlet and let the water and particle phase enter the hydrocyclone from inlet face only. Figure 3.9 shows the same hydrocyclone, with and without the inlet section.

The mesh quality was increased after removing the inlet and the simulation for water phase was accomplished faster and easier owing to high quality mesh. The air core was also generated for the water phase without the inlet section as shown in Figure 3.10.

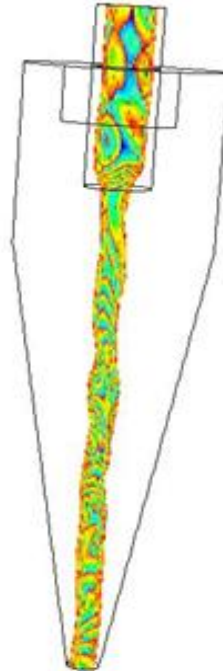


Figure 3-10-Air core generated inside the hydrocyclone with no inlet section

It was observed that the problem with inlet presence comes from the skewness of the mesh at the inlet-cylinder section so it was managed to increase the mesh quality inside the hydrocyclone domain and especially at the intersection by removing the skewed mesh cells.

Inlet type

There are three main inlet types for a hydrocyclone. Some hydrocyclones have involuted inlet which has a little curve before it attaches the cylinder contrary to the tangential inlet in Hsieh's hydrocyclone which is tangential. Figure 3.11 shows two hydrocyclones with tangential and involuted inlets. Inlets also can be circular or rectangular.

The challenge of the inlet type is regarding the mesh quality. Circular inlets are harder to mesh, so the mesh quality decreases if we tend to use a circular inlet rather than a tangential one. General speaking, any factor that causes the mesh element to skew more will decrease the mesh quality and reduces the solution accuracy.

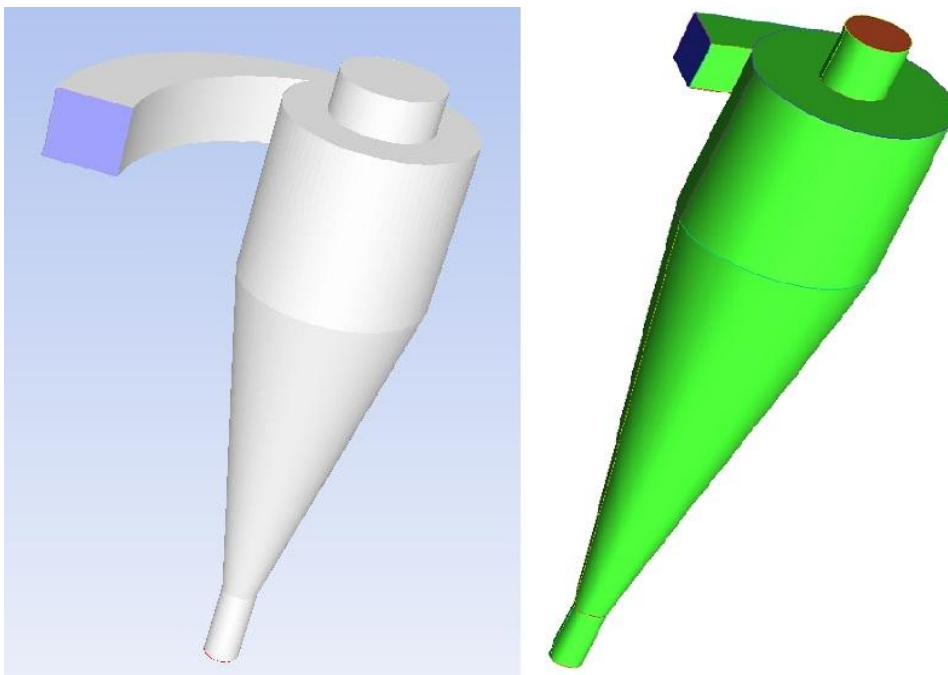


Figure 3-11-Tangential inlet vs. involuted inlet

It is easier to generate high quality mesh in a rectangular tangential inlet rather than other types of the inlet owing to the straight rectangular structure, but it is possible to make a good mesh up to a satisfactory level of quality by dividing the hydrocyclone into different parts and also probably dividing the inlet itself into smaller volumes that are easier to mesh.

3.2.4 Particle tracking

Light particles have a lower density than the water phase and heavy particles. Heavy particles were supposed to be collected in the underflow stream while light particles get collected in the overflow stream as shown in Figure 3.12(a) and 3.12(b) respectively.

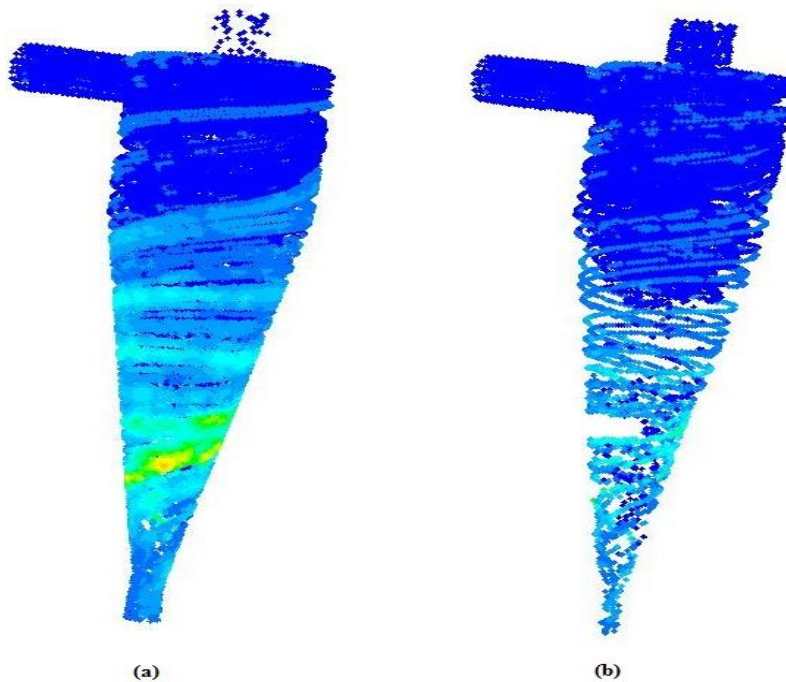


Figure 3-12-Light and heavy particle separation inside the hydrocyclone

In part (a) the majority of the particles go to the underflow stream and in part (b) the concentration of the particles is higher in the overflow stream. The first particle tracking method was granular particle injection for its simplicity, but it did not provide satisfactory results. As shown in Figure 3.13, granular injection method actually did predict the increasing trend for particle separation by increasing the underflow split ratio but the results were far from experimental data points.

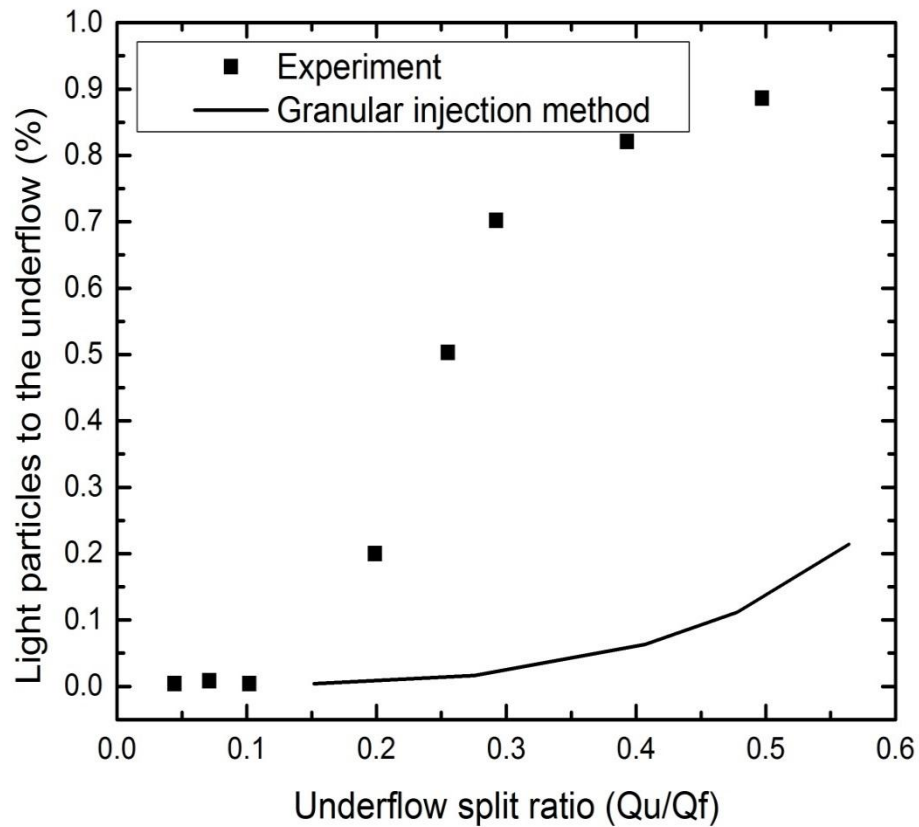


Figure 3-13-Comparison of light particle recovery to the overflow between granular injection and experimental data

Figure 3.13 shows that granular modelling is not an appropriate method to track the particle inside the hydrocyclone and later on we switched to discrete phase modelling which showed a better agreement with experimental data. The satisfactory results from discrete phase modeling are discussed later.

3.2.5 Air core

The development of a stable air core is crucial to achieving an accurate velocity distribution, and hence being able to predict separation processes to an acceptable degree. A number of factors contribute to the air core development, including the turbulence model, the mesh used and the initial conditions for the simulation.

A stable flow field with an air core is an important requirement for effective performance in a hydrocyclone. Most of the models used to predict the air core diameter are empirical calculations. To simplify the air core problem, Dyakowski and Williams (1995) modelled the air core with a fixed cylindrical surface to estimate the air core diameter. Delgadillo and Rajamani (2005) modelled the air core under different condition and concluded that a combination of Volume OF Fluid (VOF) and LES gave the best results. In a later work Ghadirian et al. (2012) showed a close agreement with air core diameter for two different hydrocyclone with the use of VOF and combination of RSM and LES.

There are many different factors that affect the full development of an air core which the most important one is the mesh quality. Other factors such as choosing the appropriate turbulence model and initialization process are important as well. The initialization process will be discussed later. Regarding the turbulence models

it should be noted that κ - ϵ model has a poor ability in producing the air core. The RSM model works better with air core prediction but not as well as LES model.

Figure 3.14 shows two different air cores. To generate a fully developed air core all the necessary requirements such as the high quality mesh, appropriate turbulence model and pre-established pressure field should be prepared. The air core must be established using a transient two phase simulation, with the results of the single phase runs as the starting point. The existence of a stable air core is absolutely critical for useful results to be obtained.

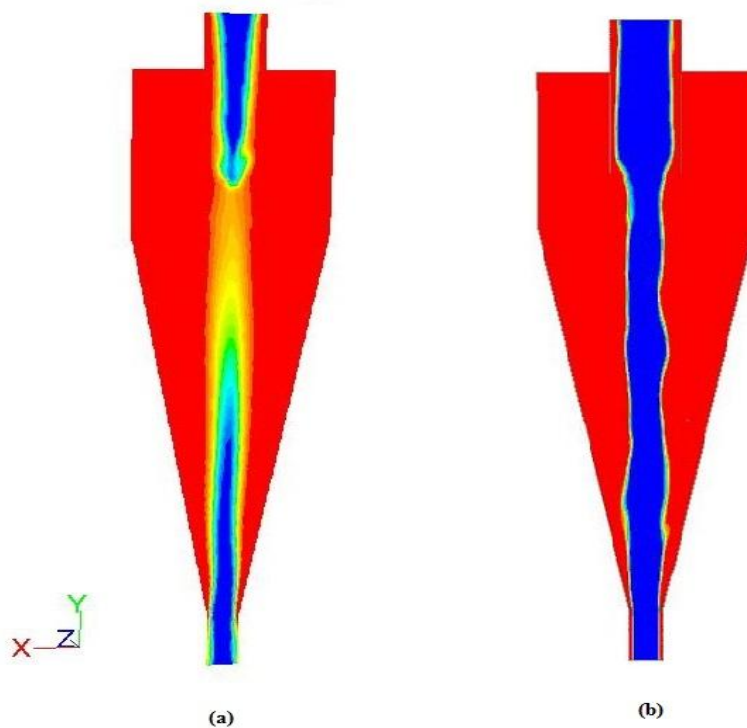


Figure 3-14-A fully developed vs. an undeveloped air core

3.2.6 Multiphase model

Different multiphase models have been tested in this work. Mixture model was one of the first ones that have been tried. The comparison between experimental data and simulation with Mixture multiphase model as shown in Figure 3.15 did not show a satisfactory level of agreement. An appropriate multiphase model is required to track the air/water interface and to numerically simulate the air core. As it has been discussed earlier without a fully developed air core the velocity profiles inside the hydrocyclone are not reliable. Hence the forces acting on the particles are not going to be well predicted which affects the performance hydrocyclone modelling.

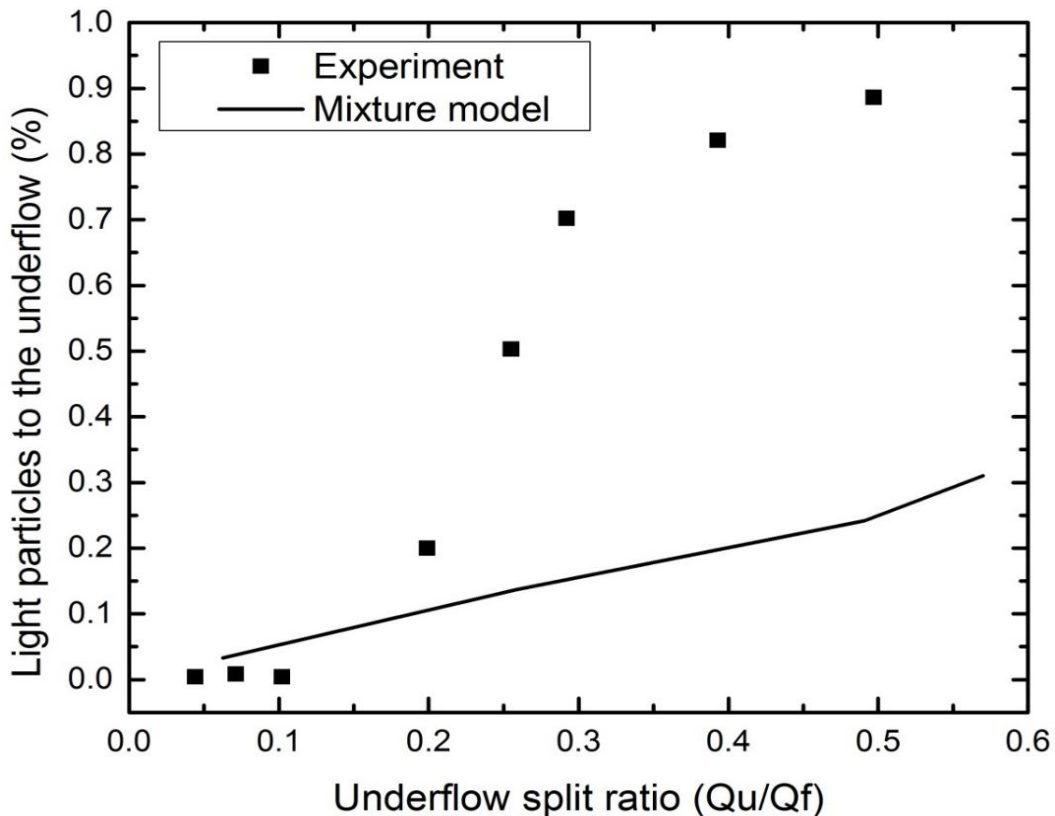


Figure 3-15-Light particle separation efficiency comparison between Mixture model and experimental data

Ghadirian et al. (2012) showed a reasonable agreement with air core diameter for two different hydrocyclone with the use of VOF and combination of RSM and LES. The volume of Fluid (VOF) ideally computes the interaction between the air/water phases in the hydrocyclone. The air core interface can be tracked by using the VOF.

3.2.7 Initialization

It was shown by Ghadirian et al. (2013), Delgadillo and Rajamani (2005), Brennan et al. (2006), and Leeuwner et al. (2008) that the initial condition is the key to having a good simulation, especially in the development of the air core, and thus the implementation of this initial solution should be carefully considered.

It was found that it is hard to achieve stable convergent solution without the establishment of the pressure profile and velocity profile inside the hydrocyclone. To pre-establish the pressure profile within the hydrocyclone it is needed to use water only system served as initializing condition for the multiphase system. No particle or gaseous phase is allowed inside and the hydrocyclone simulation runs until a negative core region is established at the central axis. These negative pressure region intakes the air inside when the outlets are open to the atmosphere and develops the air core.

Attempts were made to initialize air core formation without the establishment of a negative pressure zone. Unstable and divergent simulation was observed in those cases. This dependency of air core formation on established pressure fields supports the common understanding that air core formation is pressure driven.

Figure 3.16 shows the pressure profile within the hydrocyclone after establishing the negative pressure zone. The established profiles look more like the real profiles inside the hydrocyclone and are a better candidate for the initial solution of the simulation.

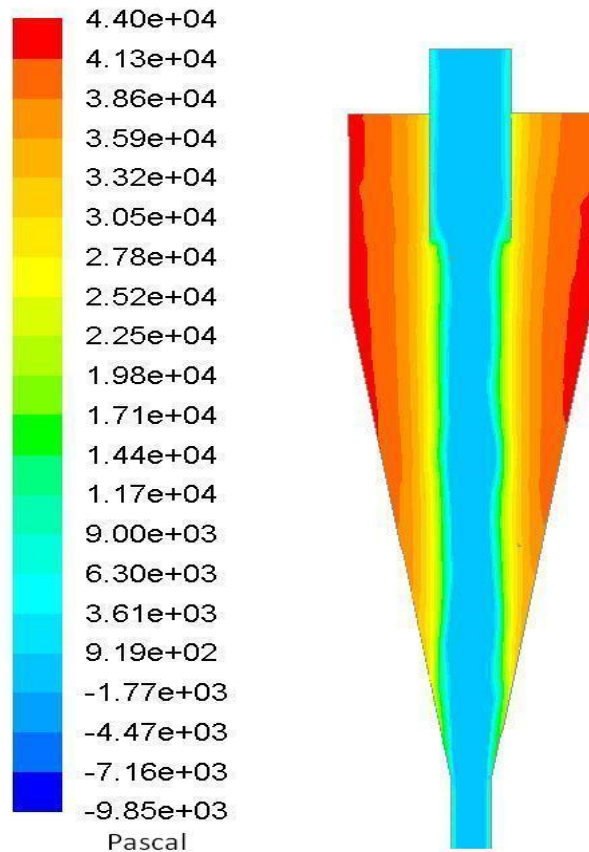


Figure 3-16-Pressure profile after initialization

Generation of a consistent initial value for velocity and pressure inside the hydrocyclone including the development of a stable air core is the key to obtain a close agreement with experimental results.

Figures 3.17 and 3.18 show the comparison between the experimental data and results from the simulation for axial and tangential velocity profiles at 60 mm from the top of the hydrocyclone. This work predicts the velocity profiles with a good agreement compared to Delgadillo and Rajamani's work (2005) but the level of agreement with experimental data is not satisfactory without the initialization process.

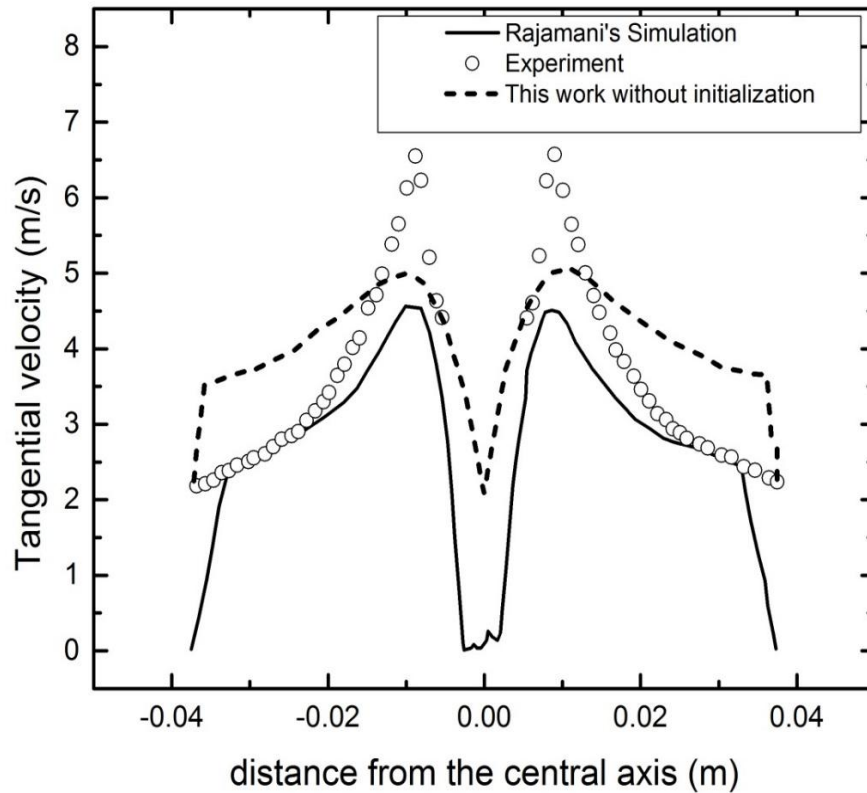


Figure 3-17-Tangential velocity comparison between Rajamani's experiments and simulations and this work without initialization at 60 mm from the top

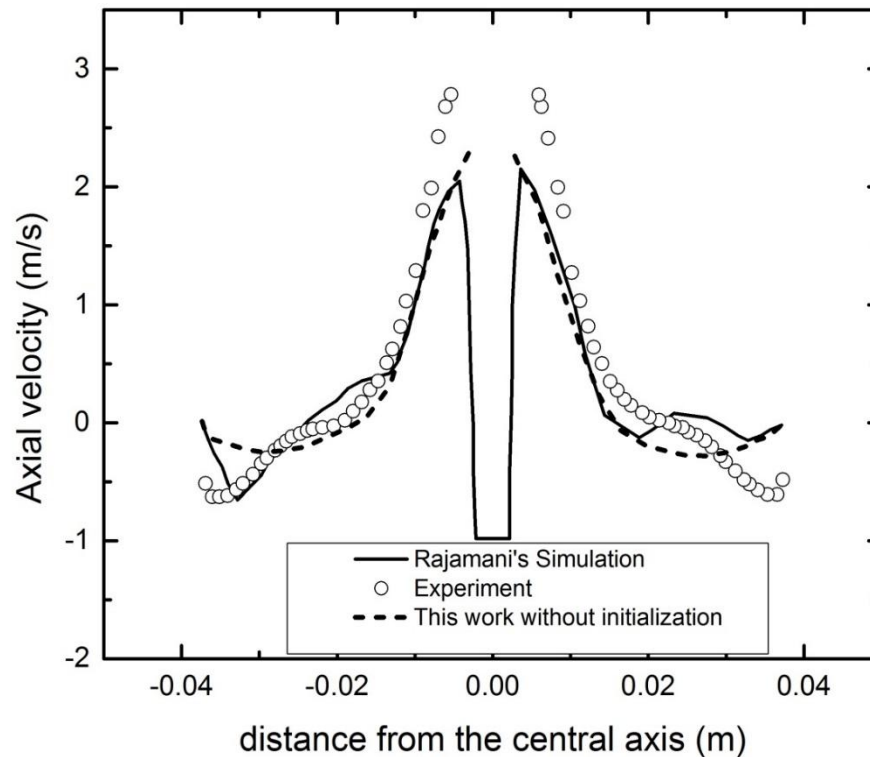


Figure 3-18-Axial velocity comparison between Rajamani's experiments and simulations and this work without initialization at 60 mm from the top

Two important factors were delineated as being critical for the accurate prediction of hydrocyclone performance. The first point relates to the domain discretization. It was found that not only the mesh size, but also the type used, strongly influenced the solution. Hexahedral elements aligned with the flow direction gave the best results, compared to experimental data and other literature simulations. The second point concerns the solution algorithm. The most stable solutions resulted when the pressure and velocity profiles were initialized correctly. This procedure required that a solution was first generated using single phase

simulations, starting with the steady state solution, and being followed by a period of transient operation. Secondly, the air core must be established using a transient two phase simulation, with the results of the single phase runs as the starting point. The existence of a stable air core is absolutely critical for useful results to be obtained. Finally, simulations involving particles could be performed. In addition to these two key aspects, we also note that the use of the LES turbulence model is essential.

In essence any of the mentioned challenges in the simulation process if remain unsolved will prevent the simulation prediction to be in reasonable agreement with the experimental data.

It is very likely that upon solving these challenges, parameters such as velocity components and global components will satisfy the experimental data automatically. Hence to build trust in a CFD model of a hydrocyclone, local velocity profiles must be validated against experimental data.

Validation of only global quantities like flow split or pressure drop does not necessarily ensure scale invariance of the turbulence models and the other transport properties that depend on turbulence intensity. Validation of detailed velocity distributions and turbulence quantities will ensure scale invariance of the model. Ultimately this will allow CFD to be an effective scale up tool, avoiding costly pilot studies. In the next chapter the model validation will be investigated against two different works from the literature to ensure the model validity and accuracy.

3.3 Model validation

3.3.1 Delgadillo's Geometry

A reliable and more cited work from the literature was selected to compare the simulation results of this work with their experimental data and simulation. Delgadillo and Rajamani studied a 75 mm hydrocyclone and compared the experimental axial and tangential components of the velocity profile at three different levels with their simulation.

As a boundary condition a constant velocity of 2.28 was imposed on the inlets of hydrocyclone. Both underflow and overflow outlets were set to specified pressures. The interior surfaces were set as no-slip conditions. As a result of the high swirl inside the hydrocyclone, a tangible radial pressure gradient is present, and therefore a radial pressure distribution was applied to the underflow and overflow outlets.

Air core development

A stable flow field in a hydrocyclone is an important requirement for effective performance. The stability of the flow depends strongly on the air core generated inside the hydrocyclone. The unsteady behaviour of the air core and its relation to the surrounding unsteady liquid flow has been the subject of research in recent years. Gupta et al. (2008), and Neesse and Dueck (2007) studied the air core formation and effective parameters during the process. Nowakowski et al. (2004) stated that the air core occurs because of the low pressure region in the hydrocyclone drops below atmospheric pressure, which allows air to enter the

hydrocyclone. It is really not known how the air core is developed, and Narasimha et al. (2006) suggested that air core formation is principally a transport effect rather than a pressure effect.

Ideally, the air core should develop naturally as a part of the CFD simulations, which requires an appropriate method to model the multiphase flow. Delgadillo and Rajamani (2007) used the volume of fluid (VOF) model coupled to LES for modelling the turbulence closure and reported satisfactory predictions of the air core. The key factor in modelling the air core is accurate prediction of the interface.

As discussed earlier, the development of a stable air core is crucial to achieving an accurate velocity distribution, and hence being able to predict separation processes to an acceptable degree. A number of factors contribute to the air core development, including the turbulence model, the mesh used and the initial conditions for the simulation. The methodology used to develop a good initial condition was described earlier. Also, as discussed earlier, the LES method is preferred for the accurate depiction of the air core. We now present the effects of mesh size on the air core development. To study the grid independence in the hydrocyclone initially a grid size of 2.5 was used to generate mesh density of about 160 000 mesh elements. To ensure the validity of the results, furthermore grid refinement was applied to see at what point the difference between the results of different mesh sizes are small enough. For larger number of the grids, the accuracy will increase logarithmically to a point, but the computational

requirements play a limiting role, and finally a grid size of 1.5 with mesh density of about 560 000 mesh elements was considered to be optimum. Figure 3.19 shows the air core development inside hydrocyclone as a function of time.

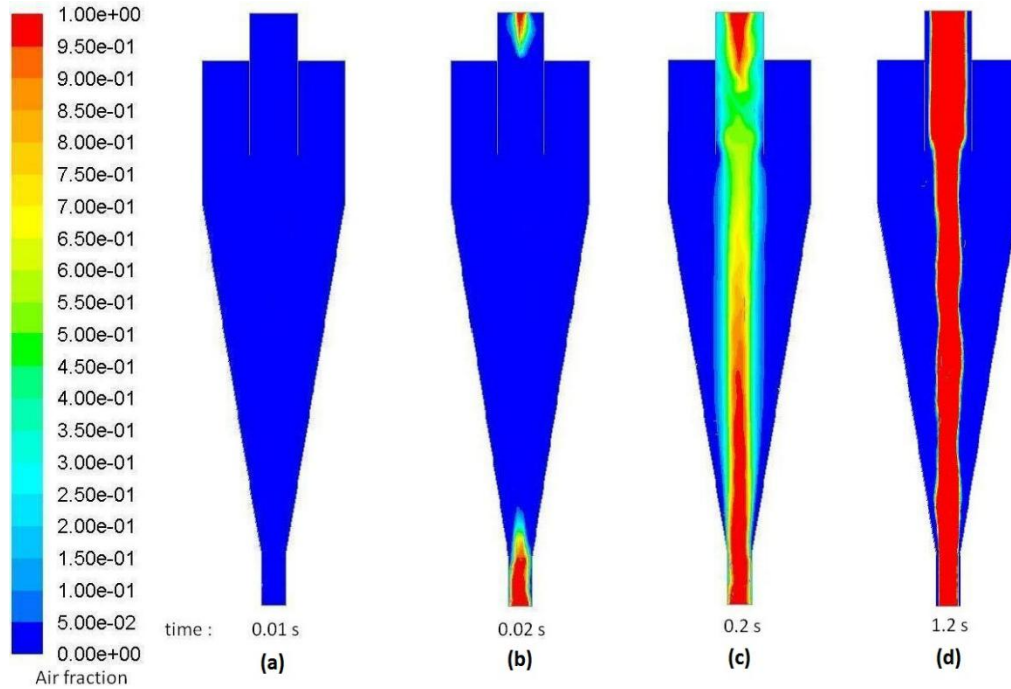


Figure 3-19-Air core development in a time span

Figure 3.19(a) shows the phase fraction distribution at the beginning of the simulation, when the initialized case has been used to start the simulation. Figures 3.19(b) and 3.19(c) show the propagation of the air core over time, where it grows from both the overflow and underflow. Finally Figure 3.19(d) shows the completed air core after 1.2 seconds. The negative pressure at the centre gives an inflow of air into the hydrocyclone, the air core develops and a mass balance is achieved. We emphasize that a stable air core was not achieved with either the unmodified $k-\epsilon$ model or the RSM.

Pressure profile

The pressure field distribution for hydrocyclone is shown in Figures 3.20 and 3.21. The minimum pressure area formed at the centre of the hydrocyclone is responsible for air intake into the body.

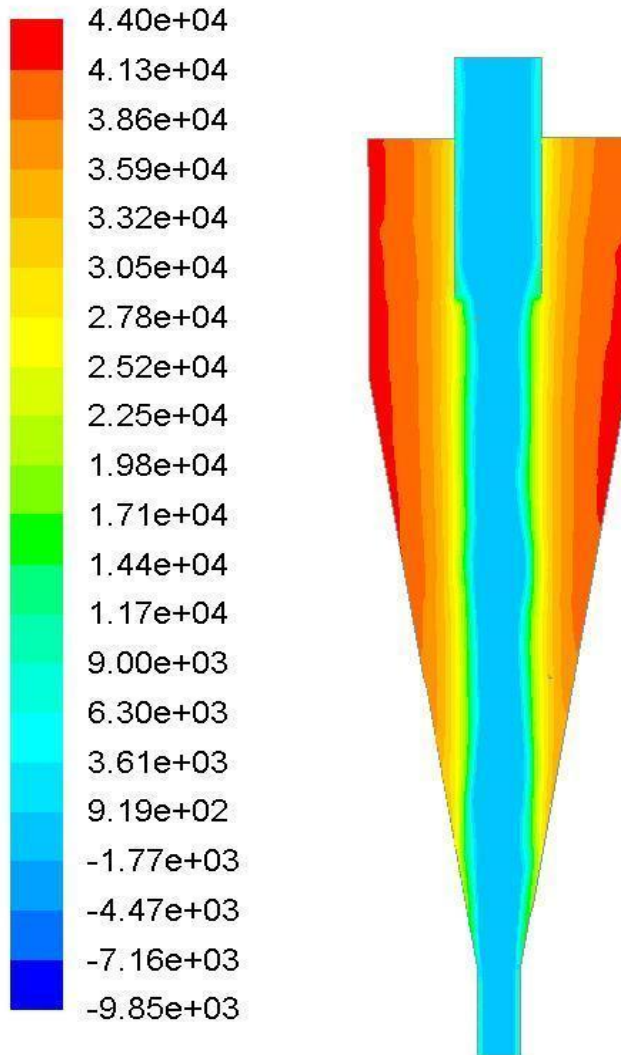


Figure 3-20-Pressure field distribution inside the hydrocyclone

The maximum pressure drop inside the hydrocyclone is 44000 Pa, which compares well with the 46700 Pa from the experimental results of Delgadillo and

Rajamani (2005), having 5.78 % error. As stated in the introduction, there are several empirical models extant for the hydrocyclone. The empirical model developed by Plitt (1976) is the most widely used to predict the pressure drop. For this case, the predicted pressure drop from this correlation was 43980 Pa, which is close to the prediction from the simulation.

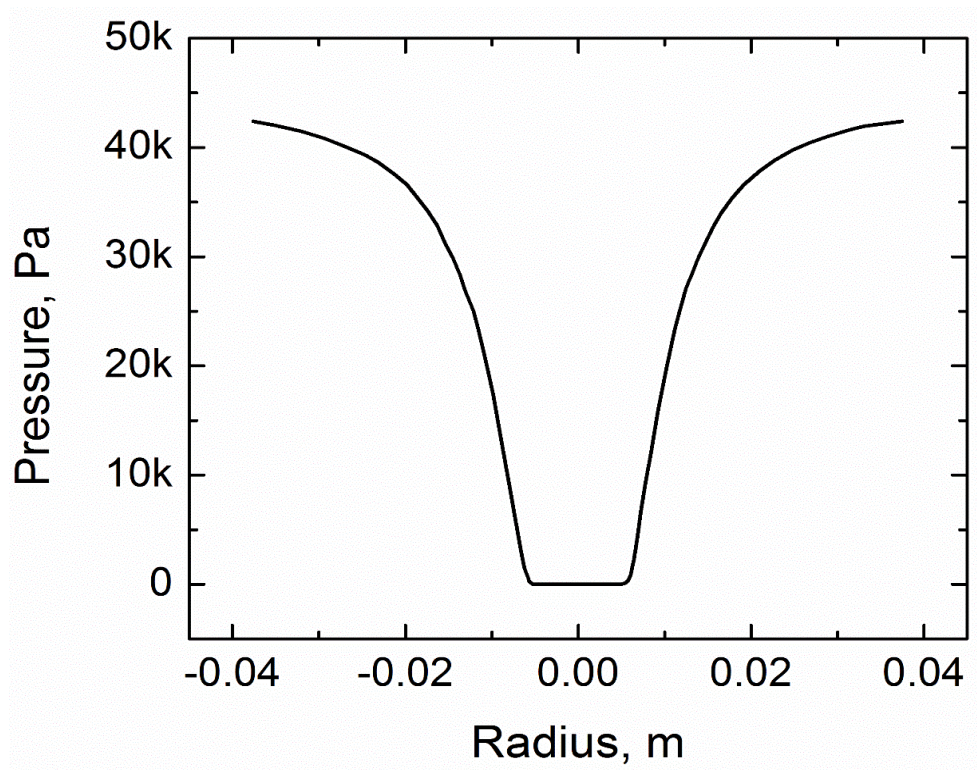


Figure 3-21-Radial pressure profile distribution at 80 mm from the top of the cylindrical section

Velocity profiles

Turning to velocity profile comparisons for the hydrocyclone, predicted and experimental tangential and axial velocity distributions are compared. Predicted velocity profiles were compared to experimental results from Hsieh (1988) and

the numerical simulation with LES turbulence closure model of Delgadillo and Rajamani (2005).

Figures 3.22 to 3.27 show the tangential and axial velocity profiles at different depths from the top of the hydrocyclone. Three different locations of the hydrocyclone are selected to make a comparison between experimental results and simulations. They show that the simulation results are in a good agreement with experimental ones. Tangential velocity distribution shows that it reaches its own maximum around the central axis and it decreases slightly near the walls. At the centre a higher tangential velocity compared to minimum tangential velocity in the air core can be seen. The comparison between the Delgadillo and Rajamani (2005) simulation and this work shows that the maximum tangential velocity reached in this study is much closer to the experimental results. From the fact that the tangential velocity is sensitive to the pressure field distribution inside the hydrocyclone it can be said that the reason of this difference between the two simulations is the better prediction of the pressure field inside the geometry. It is assumed that it is because of the way the mesh was generated inside the geometry in this study and the initialization process that prepared a good initialized case for the simulation. More certainly, it is known that both of these reasons helped the simulation to generate a better pressure profile to achieve better velocity profiles.

Turning to the axial velocity distribution, it is seen that the expected flow reversal inside the hydrocyclone is predicted, and the locus of zero vertical velocity (LZVV) is also captured. The comparison between simulations and the

experimental results shows that both the simulations from this work and the simulation from the work of Delgadillo and Rajamani (2005) are in a good agreement with the experimental results of Hsieh (1998). The difference between the two simulations is not considerable; however this work is closer to the experimental results. It is suspected that the reason of this phenomenon is less sensitivity of axial velocity distribution to the pressure profile inside the hydrocyclone.

At 60 mm from the top of the hydrocyclone there is lower turbulence compared to 120 mm and 170 mm from the top and the model predicts the velocity trend with more accuracy. At this distance from the top the model reports an over prediction for tangential velocity and keeps this trend for the entire level.

Figure 3.23 shows the axial velocity comparison at 60 mm from the top of the hydrocyclone. Axial velocity comparisons are much closer than tangential velocity profiles since both models have a good agreement for air core size prediction. The middle part that has no axial velocity represents the air core diameter.

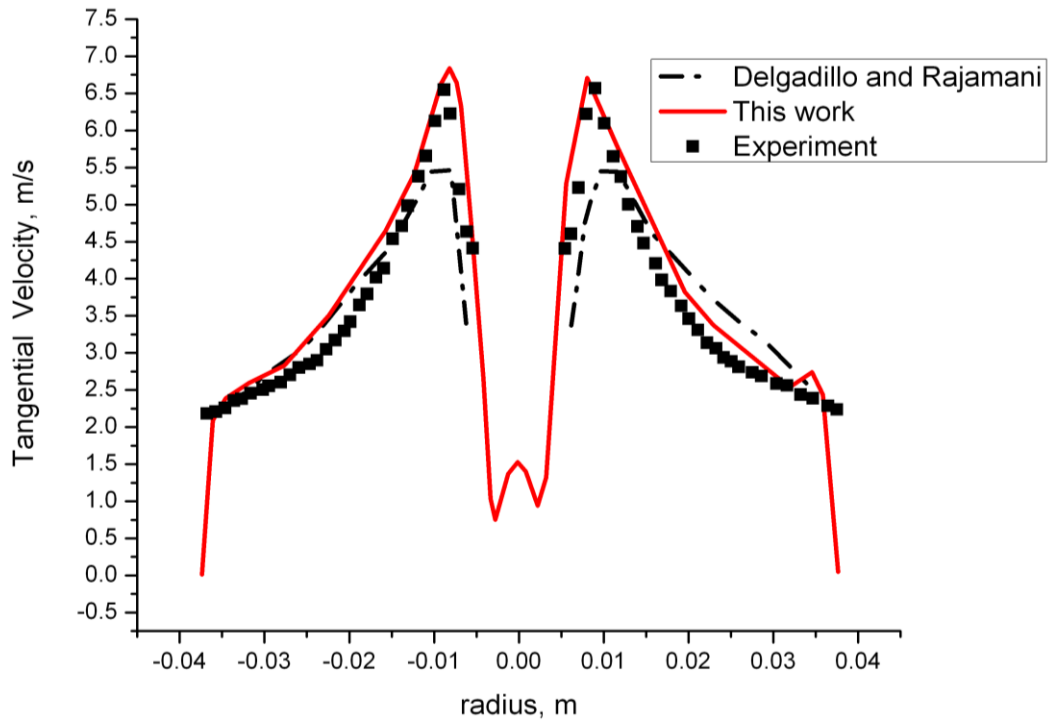


Figure 3-22-Predicted tangential velocity from Rajamani and this study compared to experimental results at 60 mm from the top

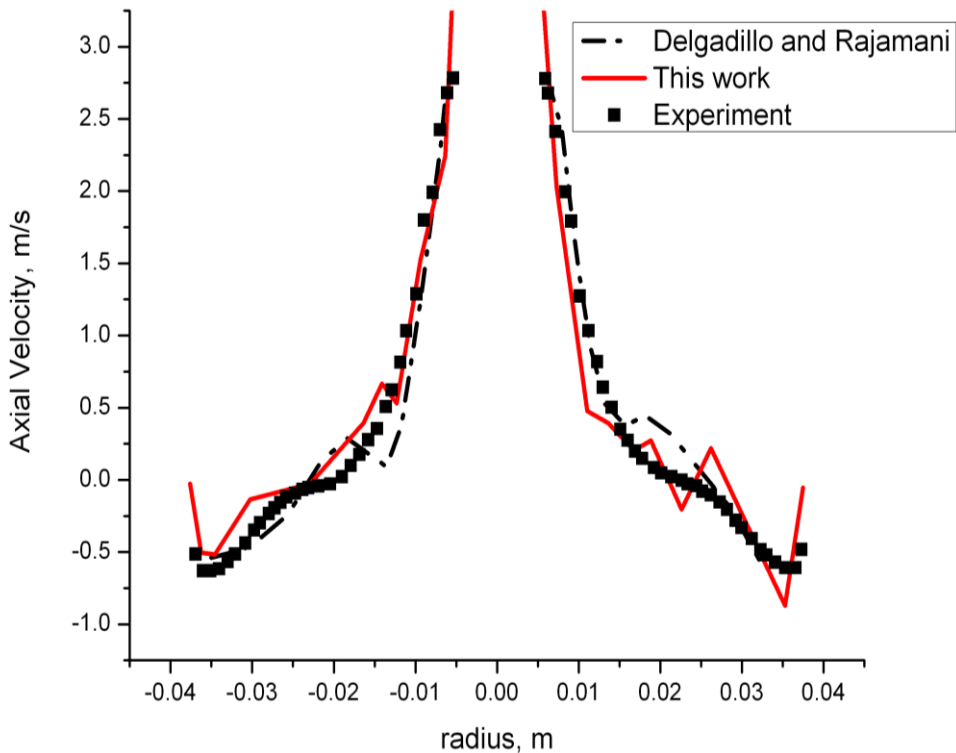


Figure 3-23-Predicted axial velocity from Rajamani and this study compared to experimental results at 60 mm from the top

Tangential velocity profile at 120 mm from the top of the hydrocyclone also reports an over prediction for velocity values and reports velocity of zero at the wall. Predicting the maximum and minimum velocity values at each level is hard task that this model did it at a satisfactory level. Axial velocity profile comparisons are shown in Figure 3.25. The air core diameter is well predicted at 120 mm from the top as well and axial velocity at wall is shown to be zero. The locus of zero vertical velocity can also be seen in this graph at point that the axial velocity reaches zero. Compared to axial velocity at 60 mm there is more turbulence at this level and the predictions are not as good.

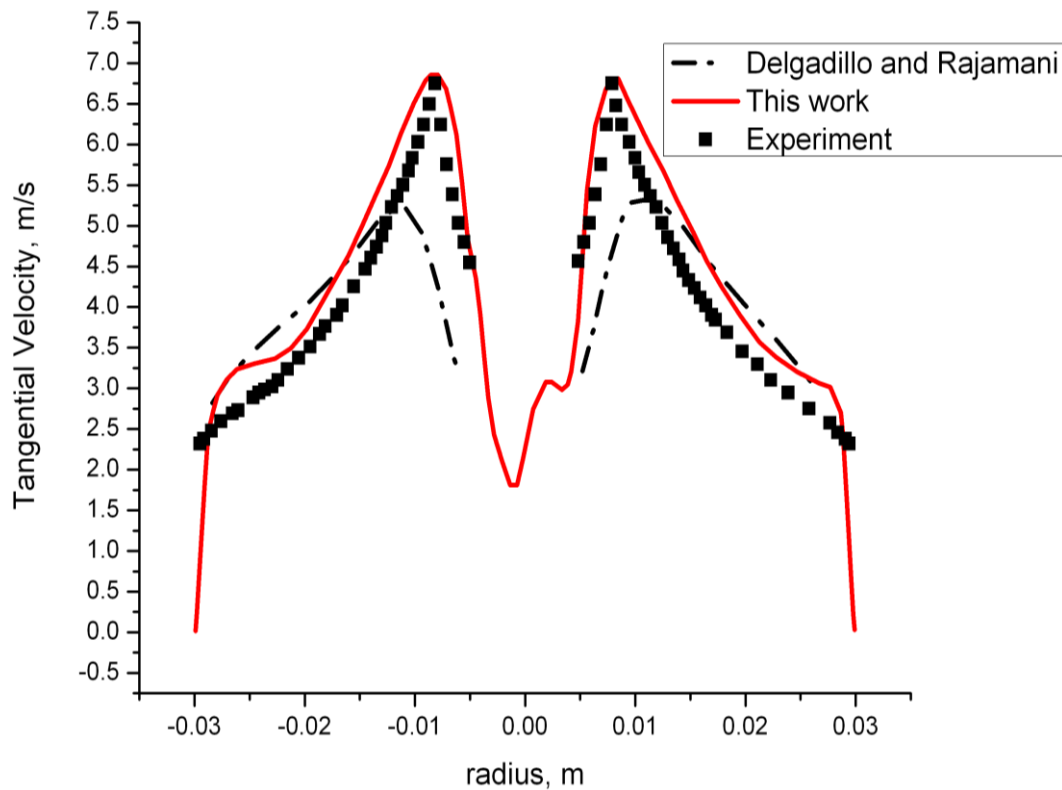


Figure 3-24-Predicted tangential velocity from Rajamani and this study compared to experimental results at 120 mm from the top

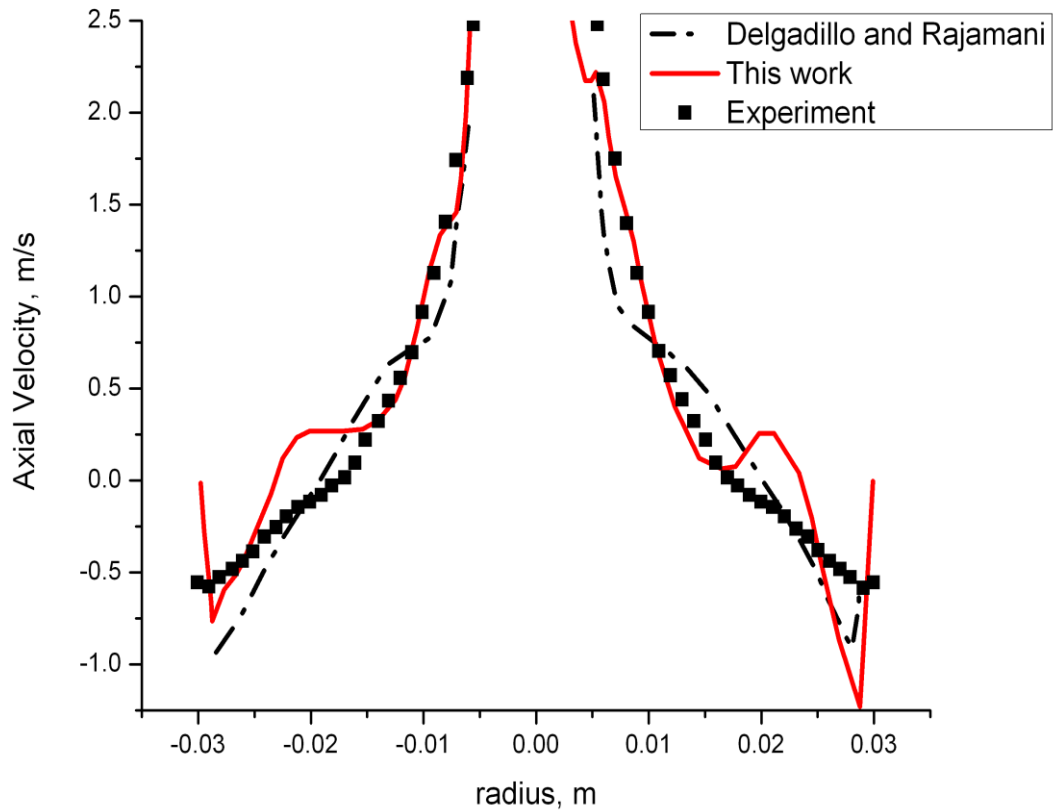


Figure 3-25-Predicted axial velocity from Rajamani and this study compared to experimental results at 120 mm from the top

Figure 3.26 shows the tangential velocity profile comparisons at 170 mm from the top. There is a high turbulence region at this level which makes it really hard to predict the tangential and axial velocity profiles. Despite the turbulence the model has a good prediction of the maximum and minimum tangential velocity at 170 mm as well.

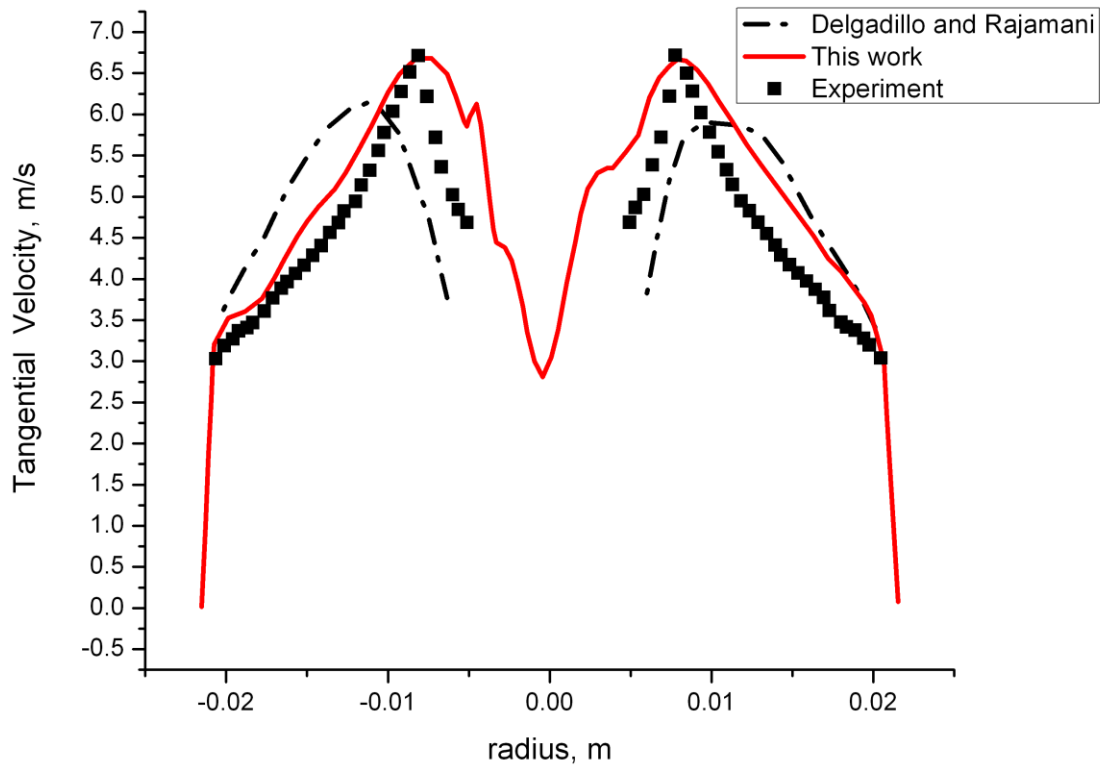


Figure 3-26-Predicted tangential velocity from Rajamani and this study compared to experimental results at 170 mm from the top

Axial velocity profile comparisons are shown in Figure 3.27. The locus of zero vertical velocity can be seen in this graph at points which the axial velocity value is zero. At those points the axial velocity direction of the water changes from upward to downward and vice versa. The turbulence inside the hydrocyclone at this level has a strong effect on the simulations.

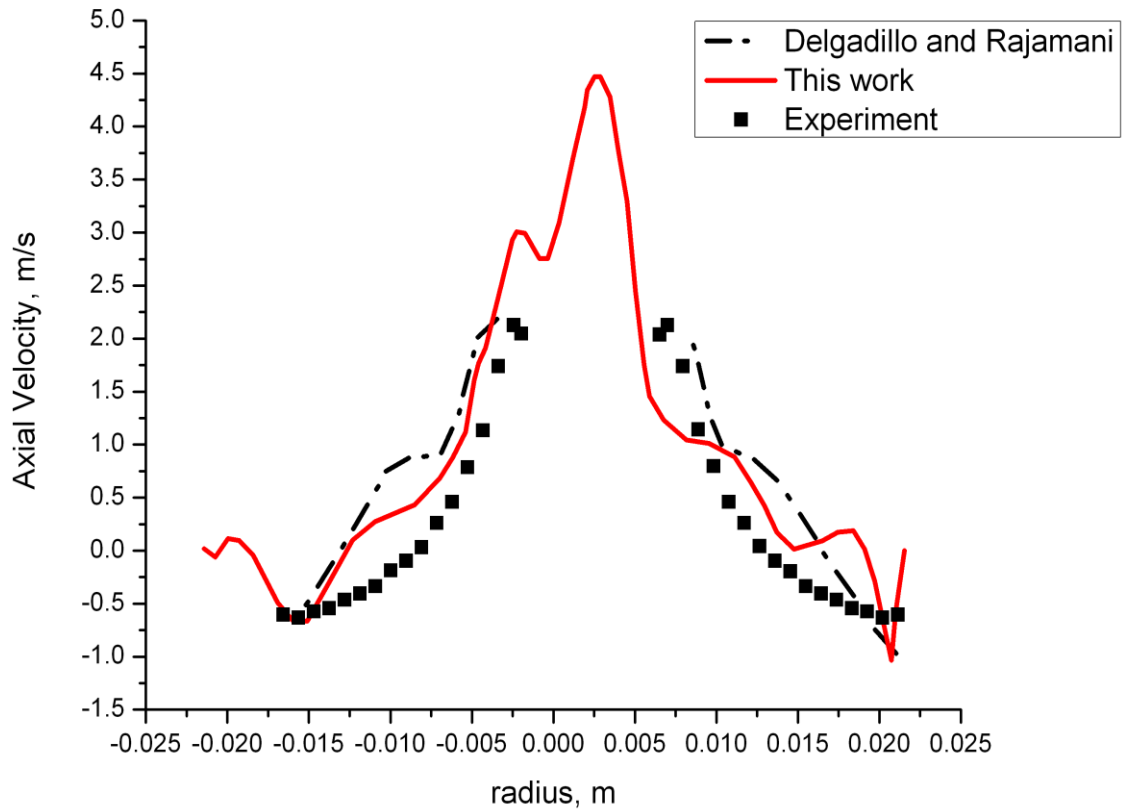


Figure 3-27-Predicted axial velocity from Rajamani and this study compared to experimental results at 170 mm from the top

Solid removal

The final goal of the hydrocyclone simulation is to calculate the separation efficiency. Hydrocyclone efficiency is usually referred to the number of particles collected at the underflow to the total number of particles injected through the inlet. To calculate the efficiency a number of particles were released at the inlet face and their trajectories were tracked until they were collected at the outlets. So

the percentage of each particle size leaving the hydrocyclone from the underflow was considered to be hydrocyclone separation efficiency.

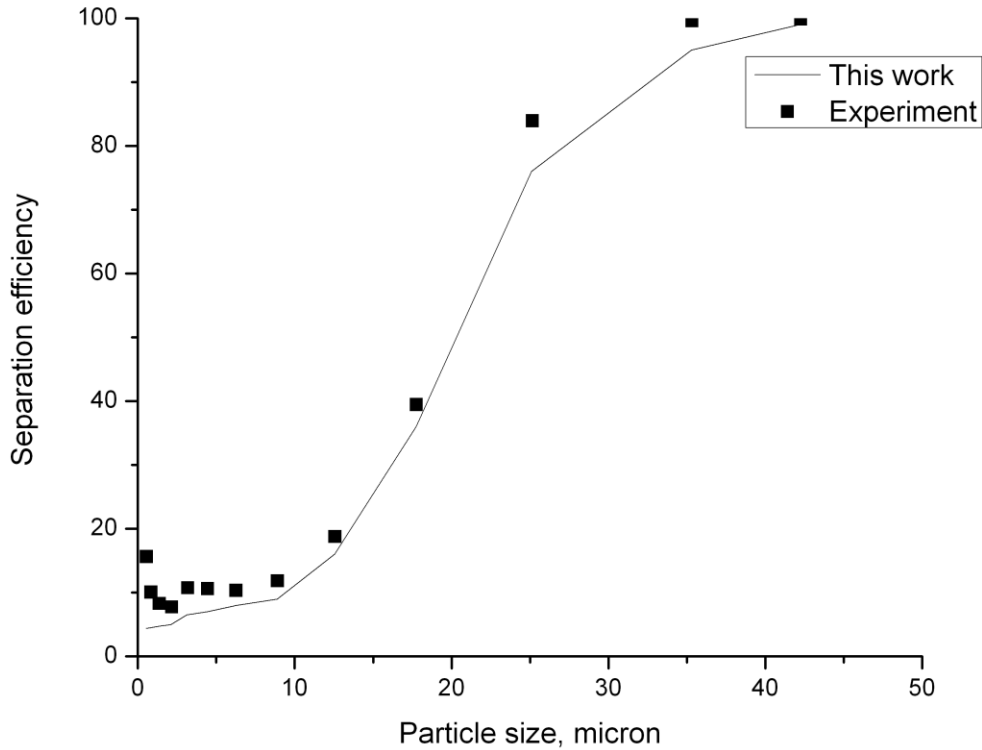


Figure 3-28-Hydrocyclone particle separation efficiency at 5% wt concentration of particles, collected at underflow

The velocity field calculations are not considered in particle separation efficiency calculations and because the particle concentration is less than 5% wt there was no need for solid/liquid phase momentum coupling. Figure 3.28 shows the predicted hydrocyclone efficiency curve. The range of particles sizes and particle density is based on the experiments conducted by Hsieh (1988). Fraction of each particle size reporting to the underflow is plotted as a function of particle size. As

shown in Figure 3.28 large particles are collected mainly due to their mass and the consequent centrifugal force pulling them to the outer wall for separation while smaller particles do not feel the same force and some of them escape from the overflow. The comparison between the results in Figure 3.28 shows that the simulation results correctly predict the separation trend and are in a good agreement with experimental data. To predict the best separation efficiency for hydrocyclone better velocity profile predictions are needed. The assumption of no particle/particle interactions and particle/fluid interactions also affect the predictions but the agreement between the results shows that the dilute inlet assumption is almost correct for this concentration of particles.

3.3.2 Lim's geometry

The last selected hydrocyclone geometry was the work from Lim et al. (2010). Lim studied axial velocity profiles in hydrocyclone for only water phase and measured the air core size at different locations inside the hydrocyclone. A comparison for axial velocity and air core size has been done between this model and Lim's work for further verification of accuracy and applicability of this model.

Air core

For Lim's hydrocyclone, air core sizes from this work are compared against various axial positions measured from particle image velocimetry (PIV), and the predicted diameter from the work of Lim et al. (2010). Air core structure diameter comparisons are presented in Table 3.2.

Table 3.2-Diameter of air core structure at various axial positions measured by PIV and predicted by Lim et al. and this work

Axial positions (mm)	D_{PIV}(mm)	D_{Lim et al.}(mm)	D_{This work}(mm)
40	2.46	3.12	2.66
45	2.15	2.98	1.86
50	1.92	2.87	1.68
55	1.74	1.76	1.33
60	1.54	1.33	1.33
65	1.47	1.31	1.06
70	2.08	1.29	1.51
75	2.15	1.42	1.68
80	2.15	1.45	2.04
85	1.74	2.35	2.22
90	1.85	2.62	2.31
95	1.90	2.09	2.57
Average (mm)	1.93		
Error%		7%	4%

It is seen that the air core diameter prediction is at a satisfactory level, and generally superior to the work of Lim et al. (2010). This observation supports the claim that the LES method with appropriate mesh is able to capture this important feature of the hydrocyclone.

Velocity profile

Figure 3.29 shows comparisons between particle image velocimetry (PIV) measurements, CFD simulations by Lim et al. (2010) and this study for Lim's hydrocyclone.

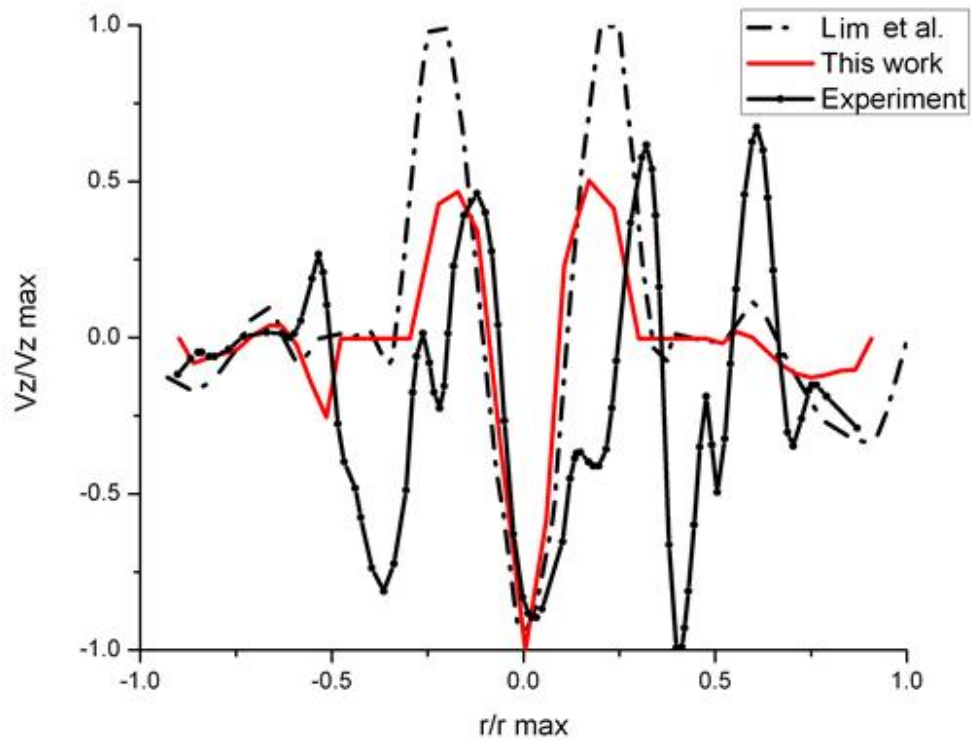


Figure 3-29-Axial velocity profile comparison at 3 cm from the top of Lim's hydrocyclone

Axial velocity profiles are compared at 30 mm from the top of the cylindrical part. The highly fluctuating nature of the air core can be seen. Steep changes in axial velocity can be seen at the centre where the air core is formed. The large downward velocity at the centre is surrounded by upward velocities right at air core edge. Both simulations predict the same trend for axial velocity comparisons, however, this work shows a better agreement with the PIV measurements.

It is concluded that the developed model well describes the velocity profiles along the axial and tangential direction for both mentioned geometries in this chapter.

The air core is an important parameter that must be fully developed and correctly predicted since flow split is key to size classification of particles. It is demonstrated that once the velocity field is accurately described the particle classification can be estimated from the computed split ratio for a small sample of particle of each size class.

In the following chapter the developed model that has passed all the challenges in the hydrocyclone simulation will be employed to predict the particle separation efficiency and air core diameter for the experiments done in this work and some other experimental data from a similar work.

4 Application of the developed model on the separation of binary particles in a hydrocyclone

In spite of all the literature on the hydrocyclone, there is a paucity of studies on the separation of binary (i.e. light and heavy) particles. The objectives of this work in this chapter are to apply the methodology, which was developed for separation single particle to the literature data obtained by Mahmood (2007) for the recovery of light and heavy particles in liquid slurry and to validate and discuss his experimental data using the developed model.

In Chapter 3, the model was developed based on Delgadillo and Rajamani's work (2005). Their hydrocyclone geometry is different from Mahmood's work (2007). Therefore, to apply the developed model to binary particle slurry, a methodology is needed to obtain a stable air core, including the turbulence model, the mesh to be used and proper initial conditions for the simulation.

The experiments from Mahmood (2007) included the effect of feed flow rate, underflow split ratio, and light particles size and feed solid concentration and vortex finder length on hydrocyclone performance. Since all of those experiments included water, particle and air as a three phase experiment it was not feasible to investigate the air core shape and size. As discussed in details earlier in chapter 3 air core plays an important role in hydrocyclone performance. Hence another set of experiments was needed to study this phenomenon. To investigate the air core

dimensions and mass split ratio under different operating conditions another series of experiments has been done solely for the two phase system of water-air.

In this study a series of experiments were performed using a two phase system (i.e. water-air) to investigate the effect of outlet pressure and mass split ratio on the air core diameter. Another set of experiments were performed in the work done by Mahmood (2007) for separation of light and heavy particles from the continuous phase in a liquid slurry. The two phase experiments done in this study and the three phase work done by Mahmood (2007) shared the same equipment and experimental procedure. The effect of different design and operating variables on the recovery of particles in the product stream was examined. The design parameters investigated include hydrocyclone overflow to underflow diameter ratio, cylindrical chamber length, vortex finder length, while operating variables include feed flow rate, underflow split ratio, light particle size and feed solid concentration.

The first series of experiments performed using the continuous phase (water), without particles. The purpose was to determine the range of potentially useful operating conditions (i.e. flow rate of water), which is governed to a large extent by the presence of an air core. The development of a stable air core is crucial to achieving an appropriate velocity distribution for separating the particles. Water was made to flow through the system, and the mass split ratio was adjusted by changing the overflow pressure using the manual diaphragm valve. The size of the air core at different overflow pressures and mass split ratio was recorded using

photography techniques. As stated earlier the second series of experiments are the experiments done by Mahmood (2007) in a Master’s program in the Chemical and Materials Engineering department at University of Alberta. The hydrocyclone separation efficiency was tested in his work using a three phase system including water, air and different particles.

The hydrocyclone geometry used for the current study is shown in Figure 4.1 and the dimensions are listed in Table 4.1. It is made of transparent Plexiglas to visualize the flow field and vortex formation inside the body. It consists of two sections: a cylindrical chamber and a conical section, which are interchangeable.

Table 4.1- Hydrocyclone dimensions for the experimental work done by Mahmood (2007)

Dimensions	
Cyclone diameter, mm	51
Inlet entry, mm	25
Cylindrical length, mm	51
Vortex finder diameter, mm	27
Vortex finder length, mm	38
Spigot diameter, mm	10
Cone Angle, °	20

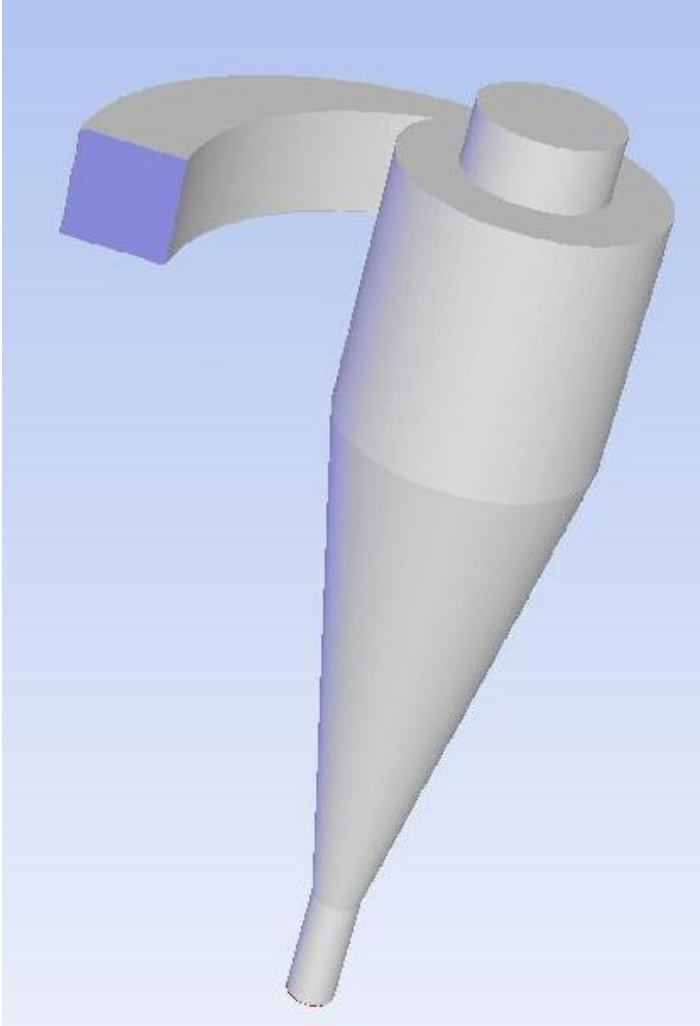


Figure 4.1-Hydrocyclone geometry used for two phase and three phase simulation

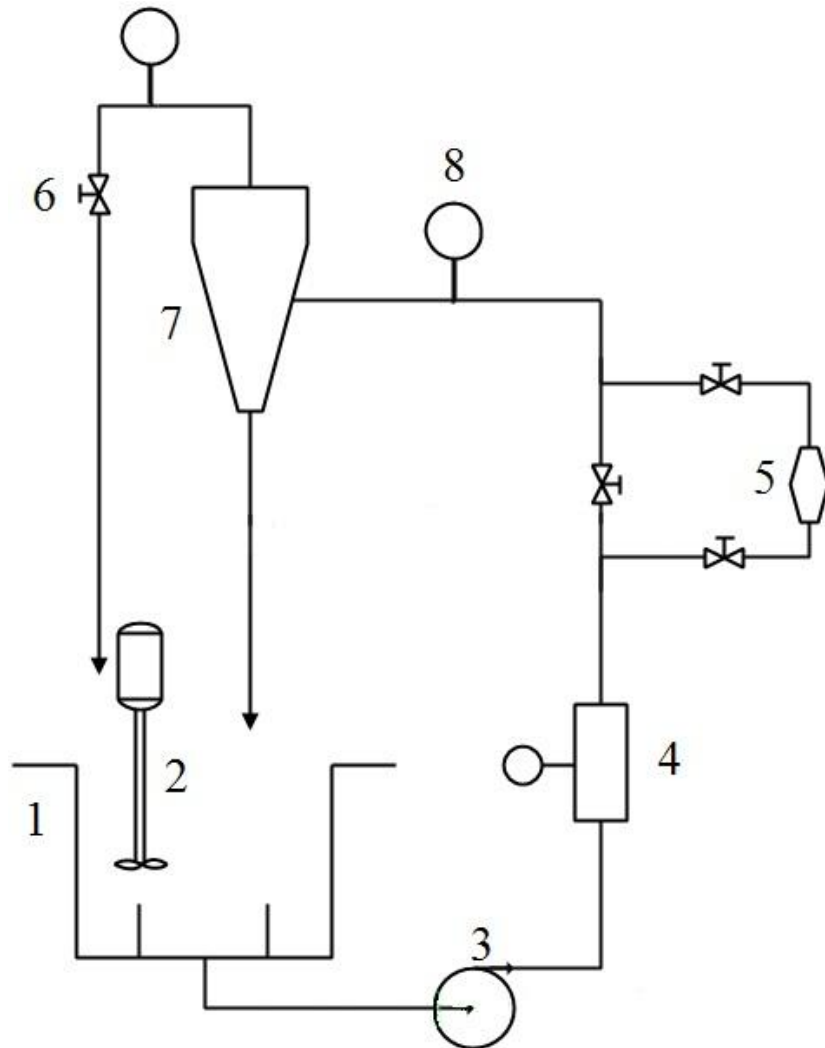
The hydrocyclone has an involuted feed entry, which begins as a circular opening but becomes a slit entry into the upper swirl chamber. This swirl chamber is called cylindrical section and is connected to the conical section. Additional cylindrical lengths can be connected to the swirl chamber. In the swirl chamber a tube protrudes axially from the top of the hydrocyclone body down to the lower edge of the feed entry. This tube is called the vortex finder.

Vortex finder's length is adjusted by moving it up and down inside the cap. The vortex finder diameter is greater than the underflow spigot diameter. Such type of hydrocyclone is called Forward Flow Hydrocyclone. This type of hydrocyclone has the characteristics of separating the higher specific gravity reject material from the underflow of the hydrocyclone, and the overflow is in the diluted form of the valuable product. This is convenient when the objective is to separate the valuables in the overflow, which can be concentrated in the next step by using another hydrocyclone for the overflow stream or by using a flotation column or a centrifuge. The other type of hydrocyclone is called Reverse Flow Hydrocyclone. The vortex finder diameter in this type is smaller than the underflow spigot diameter.

A schematic of the closed loop used for the current study is shown in Figure 4.2. The slurry was circulated and flow was controlled using a monyo pump with a variable speed drive. A coriolis meter was used to measure the water flow rates up to 100 L/min. The overflow to underflow split ratio was controlled manually using a diaphragm valve located on overflow line. The inlet and overflow pressures were measured using a pressure gauge with a range of 0-30 psig.

The slurry holding tank was filled with 150-liters of water. The pump was turned on and water was circulated through the closed loop during which the density and temperature of water were recorded from the calibrated coriolis meter as shown in the Figure 4.2. A hand operated control valve at the overflow stream was used to adjust the flow rate split ratio. The water was kept circulating for a few minutes at

constant feed flow rate. Overflow and underflow samples were taken at the same time to determine the solids concentration in the feed line. The particles characteristics used in his work are listed in Table 4.2.



- | | | |
|-----------------------|------------------------|--------------------------|
| 1-Slurry Holding Tank | 2-Mixer | 3-Monyo Pump |
| 4- Coriolis Meter | 5- Magnetic Flow Meter | 6-Overflow Control Valve |
| 7-Hydrocyclone | 8-Pressure Gauge | |

Figure 4.2-Schematic of hydrocyclone experiment setup

Three samples were taken for consistency purposes. At steady state, the feed rate in the feed line was constant. At a constant feed flow rate overflow pressure was changed by adjusting the top control valve. The overflow pressure controlled the underflow split ratio. The overflow valve controlled the overflow stream and since there was no accumulation inside the hydrocyclone the underflow feed rate to feed flow rate changed. Any change in mass split ratio changed the air core diameter.

Table 4.2- Physical properties of heavy and light particles

Material	Density (kg/m ³)	Mean particle size (µm)
Polyethylene	920	460
Cenosphere A	600-950	360
Cenosphere B	600-950	80
Sand	2650	62

4.1 Simulation methodology

Different hydrocyclone geometries were selected for the modelling purposes in Chapter 3 to investigate the accuracy and applicability of the model. Even though the model was developed and validated it was not tested for separating different

particles with different densities in a hydrocyclone. The binary system of two different particles and the study of different design and operational parameters in the work done by Mahmood (2007) made it worthwhile to model his hydrocyclone and compare the experimental data with the modelling values.

GAMBIT was used to obtain the hydrocyclone geometry. Using different cylindrical volumes and a frustum the hydrocyclone was broken down into several simpler geometries to ease the use of a non-conformal mesh. The main available mesh types in GAMBIT are hexahedral, tetrahedral and pyramid. The mesh type used in this study was selected based on results described in an earlier study (Ghadirian et al. 2013), and used a non-conformal hexahedral mesh throughout the body. Hexahedral meshes are more tolerant to the high aspect ratios that are common in this type of simulation. They are also less diffusive than other mesh types such as tetrahedral mesh.

The need for high quality mesh necessitated the breakdown of basic hydrocyclone geometry into simpler geometries to implement higher qualities of mesh in each one. Also to avoid the numerical diffusion mesh cells were aligned to the flow direction.

Ansys 13 dynamic package (Fluent) was used for the simulations. The use of volume of fluid (VOF) as the tool to model the air/water interface necessitated the application of an unsteady segregated solver. To improve the precision, the 3-D double precision mode was selected. Pressure staggered option (PRESTO) was used as the pressure interpolation scheme and semi implicit pressure linked

equation (SIMPLE) was used for pressure-velocity coupling. A higher order spatial discretization scheme, QUICK (Quadratic Upwind Interpolation), was also used to improve the convergence.

It was shown by Ghadirian et al. (2013) and other researchers that initializing a sub-atmospheric pressure zone is necessary to achieve a stable convergent solution. Development of the air core depends strongly on the initialization process. Steady state simulations were started using a modified k - ϵ model with water as the only phase present. Both outlets allow only water to be the back flow phase at this step. After a steady state condition was reached, the turbulence model was switched to RSM solver and the simulations were carried out for more iterations. Then the solver was changed to the unsteady solver, and the simulation was continued until a region of negative pressure (sub-atmospheric zone) completely formed at the centre. At this point the turbulence model was switched to LES and air was specified to be the only back flow phase. This result was the initialized case used as a starting point in the simulations. By establishing a sub-atmospheric pressure zone within the hydrocyclone and opening the outlets to the air the fluid pattern starts to generate and the air core develops.

A constant velocity was imposed on the inlet of hydrocyclone. Both underflow and overflow outlets were set to specified pressures. The interior surfaces were set as no-slip conditions. As a result of the high swirl inside the hydrocyclone, a tangible radial pressure gradient is present, and therefore a radial pressure distribution was applied to the underflow and overflow outlets.

4.1.1 Two phase simulation

The development of a stable air core is crucial to achieving an appropriate velocity distribution for separating the particles. As explained earlier in order to study the operating variables on the air core diameter a series of experiments were done on the binary system of air-water.

The comparison between experimental and modelling results for the effect of overflow pressure on the underflow mass split ratio is shown in Figure 4.3. At higher overflow pressure more mass leaves through the underflow and thus the mass split ratio increases. The increased underflow mass split ratio directly affects the hydrocyclone performance and the air core size. The modelling values predict the experimental data with a reasonable agreement.

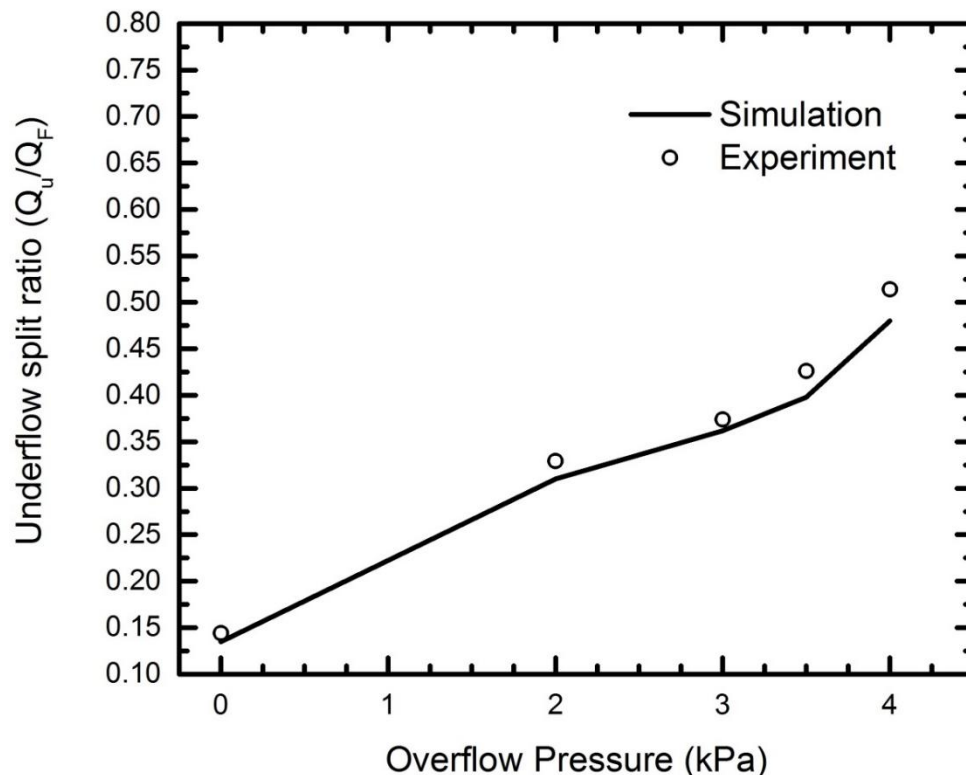


Figure 4.3-Effect of overflow pressure on water mass split ratio

Figure 4.4 shows that the diameter of the air core is decreased as the mass split ratio increases. The size of the air core was experimentally determined using photography techniques. At a critical underflow split ratio, the air core starts to show instability and fades away. At high underflow split ratio air cannot enter the hydrocyclone from the top, and an incomplete air core unattached to the top will exist. As shown in Figure 4.4 the smallest air core diameter is formed at underflow split ratio of 0.5. This quantity of underflow split ratio is a result of 4 kPa overflow pressure.

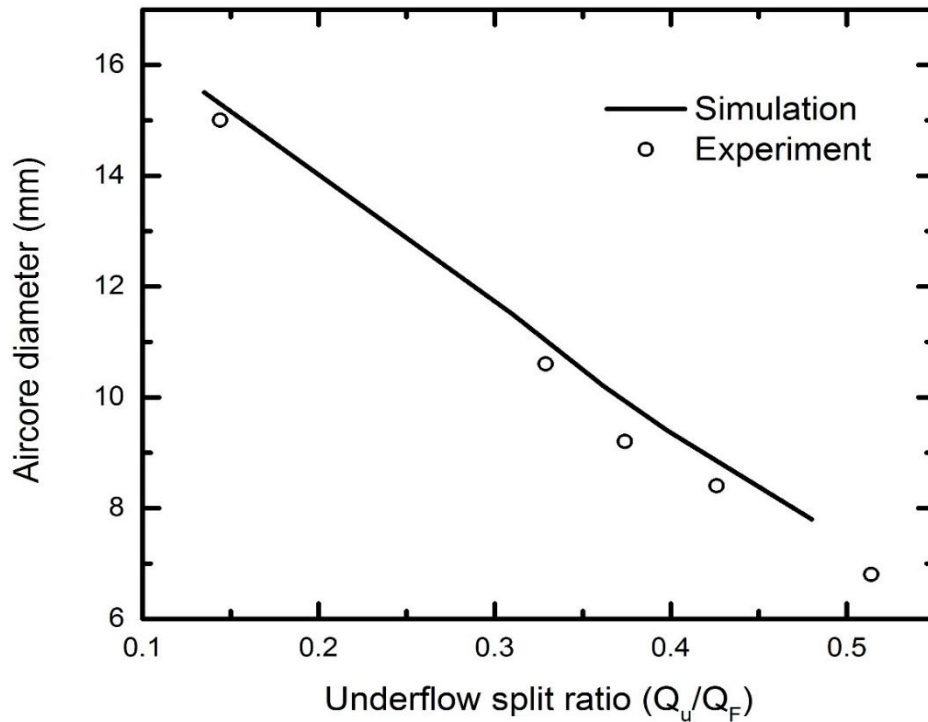


Figure 4.4-Effect of overflow pressure on air core diameter

At higher underflow split ratio (i.e. more than 0.5) the air core shows instability and fades away. Both experiment and simulation predict the high end for underflow split ratio to be around 0.5 for a stable air core production. Figure 4.4

show a reasonable agreement between the experimental and the simulation results. The stable air core zone is important for achieving particle separation. As shown in Figure 4.4 at underflow mass split ratio of 0.15 to 0.5 a developed air core exists inside the hydrocyclone and this is the region that the particle separation takes place in a hydrocyclone. In other words the hydrocyclone performance outside this zone is noticeably lower than the separation efficiency inside this zone.

4.1.2 Three phase simulation

Following these preliminary tests with two-phase flow done in this study, experiments with particles in the feed from the work done by Mahmood (2007) were investigated. In the following sections, the effects of feed flow rate, size of the light particles, vortex finder length and total solids concentration on hydrocyclone performance are discussed.

Inlet flow rate

In the first set of experiments with particles, the feed flow rate was changed over a wide range. For each set, the overflow pressure was adjusted to give the desired underflow split ratio, defined as the ratio of underflow rate divided by the feed flow rate. The light and heavy particles used were polyethylene and sand, respectively. The concentrations of the light and heavy particles in the feed were 1.4 % and 1.9 % by weight, respectively. Figure 4.5 shows the effect of the feed flow rate on the recovery of the light particles in the overflow streams as a

function of underflow split ratio. The recovery of the light particles in the overflow, R_{lo} was calculated using Equation (4.1).

$$R_{lo} = \frac{M_o \alpha_{lo}}{M_f \alpha_{lf}} \quad (4.1)$$

It is seen that the recovery of the light particles in the overflow increased as the underflow split ratio decreased from 0.7 to 0.1 for all feed flow rates. The light particles, due to the strong radial centripetal forces ($F_C < F_B + F_D$), are moved towards the central air core and are removed through the overflow stream, resulting in a higher recovery of the light particles in the overflow stream. As the underflow split ratio increases, the pressure differential inside the cyclone body becomes negligible, and the air core diminishes and ultimately disappeared, as shown in Figure 4.4. Under this condition, the light particles are pushed back along with the heavy ones to the underflow stream, leading to very low recovery of the light particles in the overflow.

$$F_C = \frac{\pi d_s \rho_s \omega^2 r}{6} \quad (4.2)$$

$$F_B = \frac{\pi d_s \rho_f \omega^2 r}{6} \quad (4.3)$$

$$F_D = \frac{C_D \pi d_s \rho_f v_r^2}{8} \quad (4.4)$$

Figure 4.5 also shows that the recovery of the light particles in the overflow decreased as the feed flow rate was increased from 17 to 46 L/min. At a high feed flow rate, the centrifugal force as given in Equation (4.2) acting on the feed particles increases due to the strong tangential motion of feed, but the centripetal buoyancy and drag forces as given in Equations (4.3) and (4.4) do not increase significantly. At low centripetal forces, the particles move towards the wall of the hydrocyclone ($F_C > F_B + F_D$). In addition, at high feed flow rates the light particles have a short residence time within the hydrocyclone body, and cannot migrate quickly to the centre axis, which also reduces the recovery of the light particles in the overflow stream. Figure 4.5 shows the comparison of experimental data for the recovery of the light particles in the over flow and predictions made using the model. At lower feed flow rates there is a closer agreement due to lower turbulence in the system. As the feed flow rate is increased, the difference between the experimental and simulated values increases. This higher turbulence is due to higher velocity profiles for both phases at higher flow rates. As the velocities are increased forces acting on both phases specifically the discrete phase becomes stronger and more particles leave the hydrocyclone through the overflow. It was found that the recovery of the heavy particles in the underflow was not affected by either increasing the feed flow rate or the underflow split ratio. This was due to the greater density differential between the heavy particles and the carrier fluid than that between the light particles and the carrier fluid.

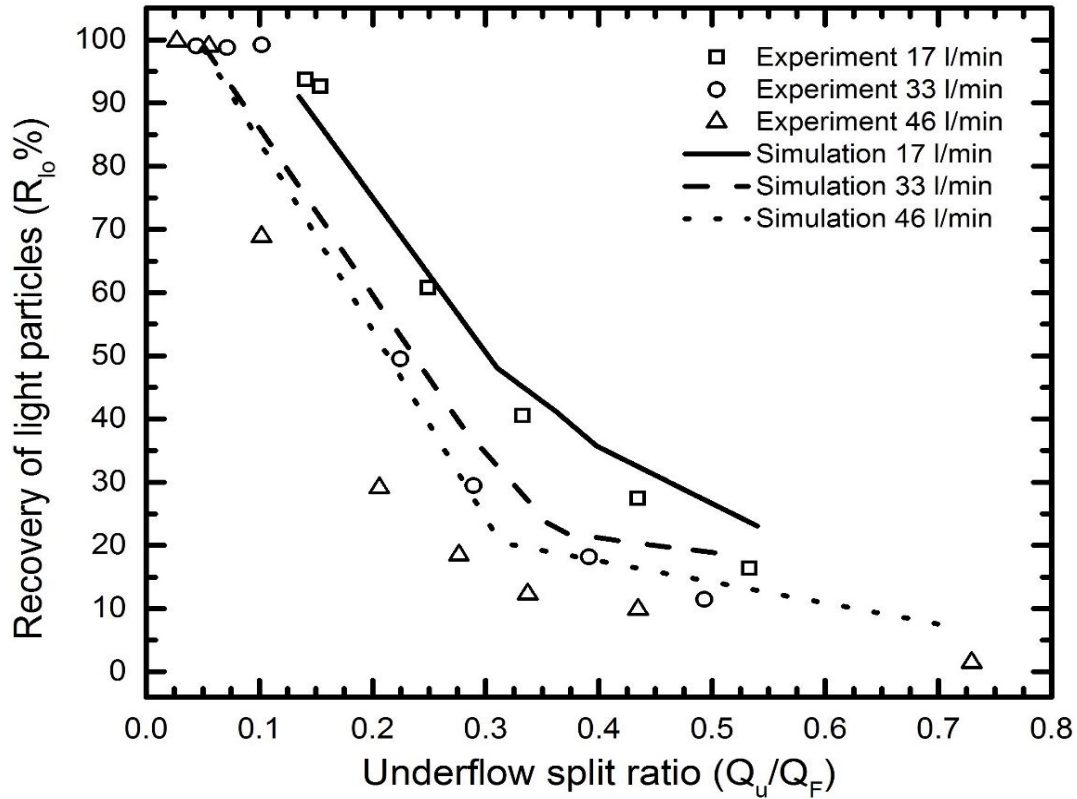


Figure 4.5-Effect of feed flow rate on Light particles recovery in overflow $\alpha_{lf}=1.4\%$; $\alpha_{hf}=1.9\%$; $d_{50}=460\mu\text{m}$;

In other words the condition of $d_h^2(\rho_h - \rho_f) > d_l^2(\rho_l - \rho_f)$ leads to stronger outward centrifugal forces than the inward centripetal buoyancy and drag forces. Eventually, the majority of the heavy particles reported to the underflow stream. According to Delgadillo and Rajamani (2005) most of the particles bigger than 44 micron are going to the underflow and since in this set of experiments particle sizes were 62 micron the expected recovery of heavy particles was almost 100%. The recovery of heavy particles in the underflow was nearly 99 % at all feed flow rates and underflow split ratios.

Particle size

The particle size has a strong effect on the separation efficiency. Figure 4.6 shows the effect of the size of the light particles on their recovery in the overflow streams at different underflow split ratio. In this set of tests, two light particles with similar densities, cenosphere A and cenosphere B, were used in combination with the heavy particles. The d_{50} of cenosphere A and cenosphere B were 360 and 80 μm , respectively. The concentration of the light and heavy particles in the feed was 1.4 and 1.9 % by weight, respectively. It is seen from Figure 4.6 that the recovery of the larger light particles in the overflow were improved at all underflow split ratios. Stokes law indicates that the settling velocity of the particles is directly proportional to the square of their sizes.

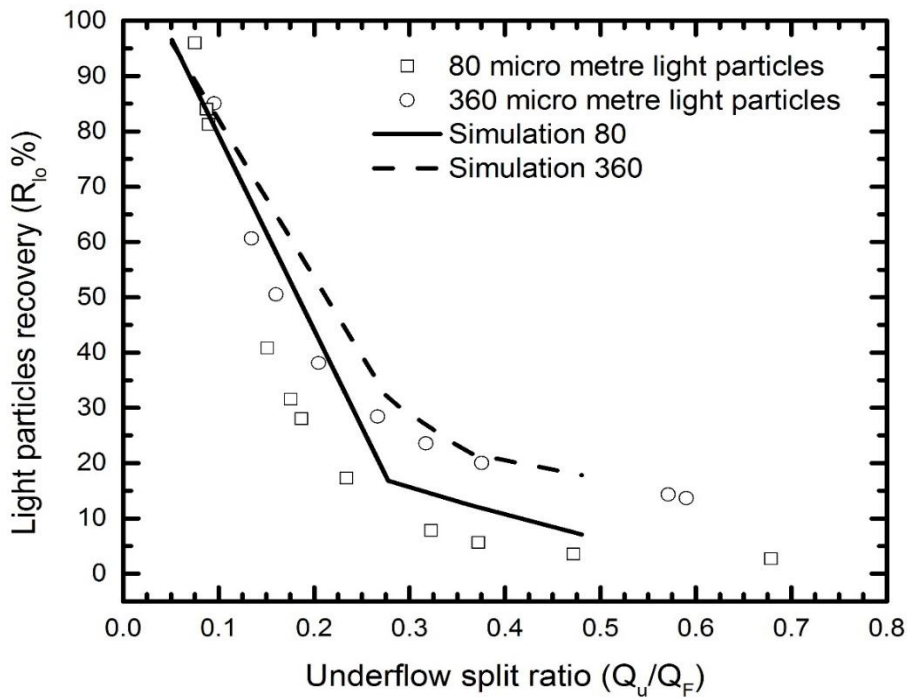


Figure 4.6-Effect of particle size on light particles recovery in overflow $Q_f=33$ l/min; $\alpha_{lf}=1.4\%$; $\alpha_{hf}=1.9\%$;

Increasing the size of the light particles increases the radial centripetal forces acting on the particles and hence the axial velocity of the particles, resulting in a faster mobility of the larger sized light particles towards the central axis of the cyclone, where they are removed from the overflow stream. As a result, the recovery of the larger sized light particles increased at all underflow split ratios. Figure 4.6 also shows that the simulation results are in a good agreement with the experimental trends. By increasing the diameter of the particles, the number of particles in the overflow consequently increases. The reason behind this phenomenon is the increase in the forces acting on the particles. Equations (4.5) and (4.6) show how an increase in the particle diameter directly affects the velocity of the particles. Faster particles move towards the central air core and tend to be collected in the upward flow.

$$F_D = \frac{C_D \pi d_s \rho_f v_r^2}{8} \quad (4.5)$$

$$v_o = \left[\frac{d_s^2 (\rho_s - \rho_f) \omega^2 r}{18\mu} \right] \quad (4.6)$$

Vortex finder length

Although, many earlier studies have focused on the effect of the diameter of the vortex finder, this study focuses on investigating the vortex finder insertion length. The vortex finder length has very little effect on the separation efficiency, but plays a major role in controlling the short circuit of flow. According to Bradley (1965), the vortex finder should not be parallel to the inlet opening or the

joint of the cylindrical and conical sections. Otherwise, the short circuit flow and turbulence will affect the separation efficiency. When the vortex finder length is increased, the strength and length of the forced vortex inside the cyclone body is decreased. As a result, the separation efficiency is improved (Svarovsky, 1984).

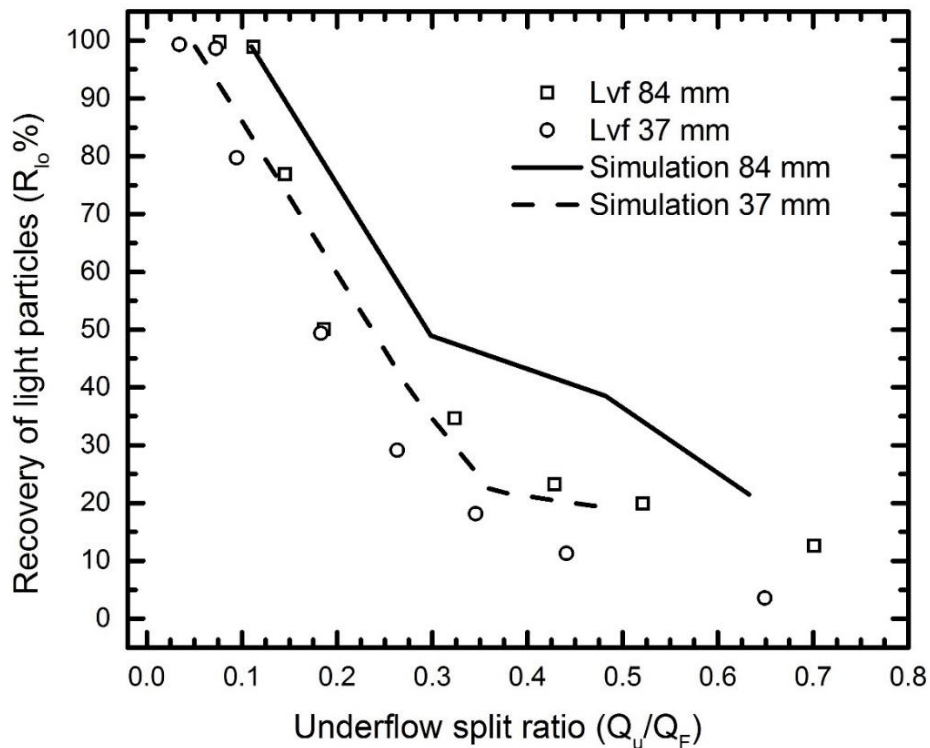


Figure 4.7-Effect of vortex finder length on recovery of overflow product, $Q_f=33$ l/min; $\alpha_{lf}=1.4\%$; $\alpha_{hf}=1.9\%$; $d_{50}=460\mu\text{m}$;

The effect of vortex finders length on the recovery of the light particles is shown in Figure 4.7. In these set of runs, two vortex finder lengths of 37 and 84 mm were used. The light and heavy particles used were polyethylene and sand having mean particles size of 460 and 62 μm , respectively. The concentration of the light

and heavy particles in the feed was 1.4 and 1.9% by weight, respectively. The feed flow rate was kept constant at 33 L/min. Figure 4.7 shows that the measured recovery was increased slightly by increasing the vortex finder length from 37 to 84 mm. Extending the vortex finder's length into the conical section ($L_{vf1}=84$ mm) the radial velocity increases from the wall to the centre of the hydrocyclone and higher radial velocity gradient is in the inner helical flow than outer vortex (Zhao and Xia, 2006). Higher radial velocity gradient in the inner helical flow helps the light particles to separate from the heavy ones, and recovery of the light particles in the overflow is increased. Figure 4.7 also shows the numerical simulation results of the influence of vortex finder length parameter on the separation efficiency. It can be seen that the simulation results are close agreement with the experimental trends. The dimension of vortex finder is closely related to the hydrocyclone performance, as it is important in defining the flow behaviour in a tangential flow hydrocyclone. An increase in the vortex finder length increases the residence time of the particles. Particles with higher residence time have a better chance for collection in the overflow stream and the hydrocyclone separation efficiency increases.

The other phenomenon is the lower chance of particles to shortcut to the overflow. In the cylindrical section of the hydrocyclone, the outer vortex may swirl towards the cylinder top and then return down to the rim of the vortex finder where there is high chance of separation. By increasing the vortex finder length it becomes less likely for this phenomenon to happen and the hydrocyclone

performance decreases. Apparently the higher residence time effect on particle collection efficiency overshadows the shortcut phenomenon in our study.

Solid concentration

The feed solids concentration is the most critical variable, and significantly affects the hydrocyclone separation efficiency, which directly depends on the particle settling velocity. Figure 4.8 shows the effect of feed solids concentration on the recovery of the light particles in the overflow stream as a function of the underflow split ratio. The total of the light and heavy solids concentration in the feed was 3.3 and 7.5 % by weight. It can be seen that by changing the feed total solids concentration from 3.3 to 7.5 % by weight, the recovery of the light particles in the overflow decreased over a 0.09 to 0.5 underflow split ratio. At high solid concentrations, the rising (in-ward migration) velocity of light particles was hindered due to the moving cloud of heavy particles towards the wall of the hydrocyclone. As a result, the recovery of the light particles in overflow decreased. Some researchers (e.g. Savrovsky, 1984; Delgadillo and Rajamani, 2005) suggested that feed solid concentration has no or negligible effect under 10 wt % concentrations, because there is only a small amount of particle/particle interactions. They also considered the particle/fluid interactions negligible at these concentration levels. As shown in Figure 4.8 there is a slight change in particle separation efficiency curves between 3.3 wt % and 7.5 wt %, which indicates an effect of particle separation. Figure 4.8 also shows that at 3.3 wt % concentration of particles the assumption of having low concentration slurry may be valid but for a 7.5 wt % concentration this assumption is not valid anymore. So for any

concentration above 3.3 wt. % the application of low concentration assumption should be used with caution. But at lower concentrations than 3.3 wt. % it is possibly acceptable to consider the slurry at a low concentration with a negligible particle/particle and particle/fluid interactions. For any specific hydrocyclone this low concentration limit is different and is based different factors such as type of the particles, particles density, particles average size, continuous phase density, hydrocyclone configuration and sizes and operating conditions.

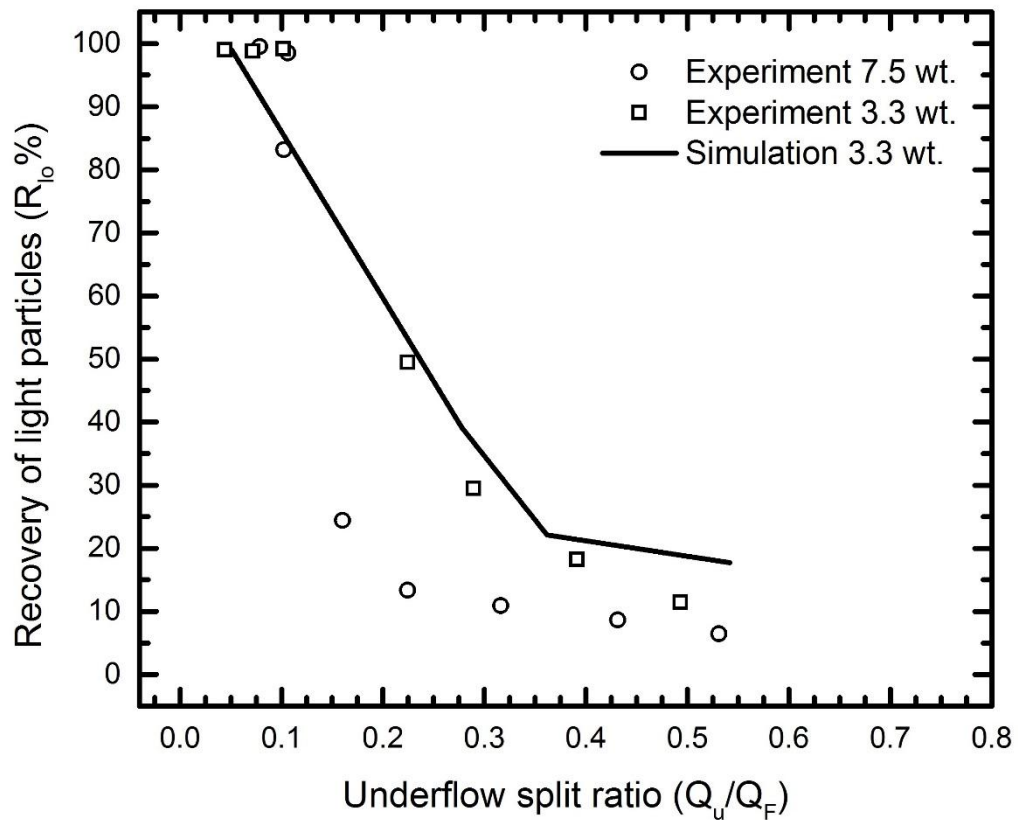


Figure 4.8-Effect of feed solid concentration on light particles recovery in over flow $\alpha_f=1.4\%$; $\alpha_{hf}=1.9\%$; $d_{50}=460\mu\text{m}$;

The recovery of the heavy particles in the underflow stream was not affected by increasing the feed total solids concentration. The recovery of heavy particles in the underflow was nearly 99 % at all underflow split ratios and both feed solid concentrations.

Vortex finder diameter

The most important design parameter on the velocity profile of the hydrocyclone is the vortex finder diameter. In other words the overflow to underflow diameter ratio (D_O/D_U) is the most important design variable affecting the performance and classification of hydrocyclones, such as capacity, cut size, sharpness of classification, split ratio, recovery and air core diameter. (Lynch and Rao, 1975; Plitt, 1976; Nageswararao, 1978). To analyze the effect of the overflow to underflow diameter ratio on the separation of light particles a set of experiments and simulations were conducted using two different ratios. The D_O/D_U ratio was decreased from 2.7 to 0.8 by changing the overflow diameter from 27 mm to 8 mm.

The results in Figure 4.9 shows that the recovery of light particles in the overflow stream is inversely proportional to D_O/D_U ratio. As discussed by Mukherjee et al. (2003) at higher underflow split ratio, the pressure drop between the overflow and feed stream was higher and the residence time was increased for the smaller diameter ratio due to larger volume available inside the hydrocyclone.

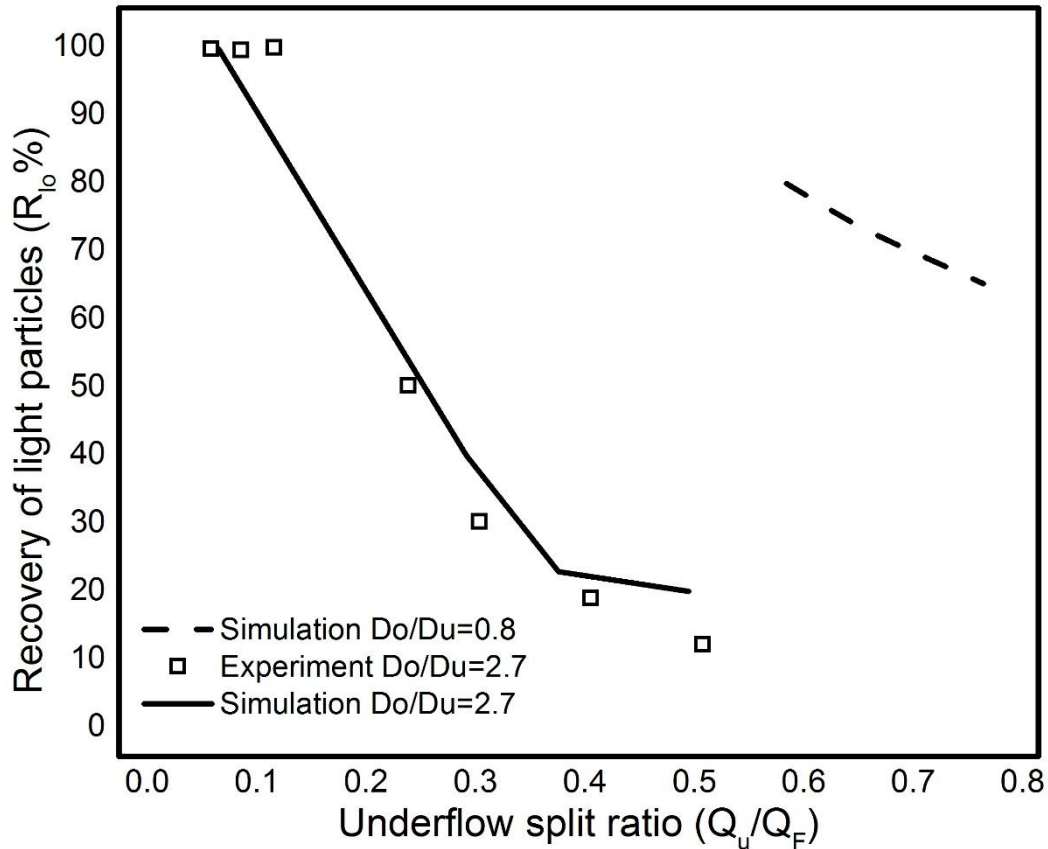


Figure 4.9- Recovery of light particles to the overflow at different overflow to underflow diameter ratio

At low underflow split ratio, the recovery was higher for the larger diameter ratio. Increasing the diameter ratio by increasing the vortex finder diameter increased the air core diameter from top to bottom, increased the upward axial velocity and decreased the radial velocity. Increasing the diameter ratio also results in an increase of the water recovery in the overflow stream and a dense underflow stream. The predicted values in Figure 4.9 for the smaller diameter ratio are not compared against experimental value from Mahmood (2007) since the smaller diameter ratio case was studied under a higher particle concentration and it was

already shown in this study that the concentration effect cannot be considered in this model due to the particle-particle interactions.

The diameter ratio of vortex finder to apex showed a strong effect on the hydrocyclone performance and the operating zone of each hydrocyclone in terms of the underflow split ratio. This phenomenon justifies a deeper analysis of the flow fields of the different ratio. Figures 4.10 and 4.11 show the locus of zero vertical velocity (LZVV) and the air core location for the situation of high recovery of light particles to the overflow.

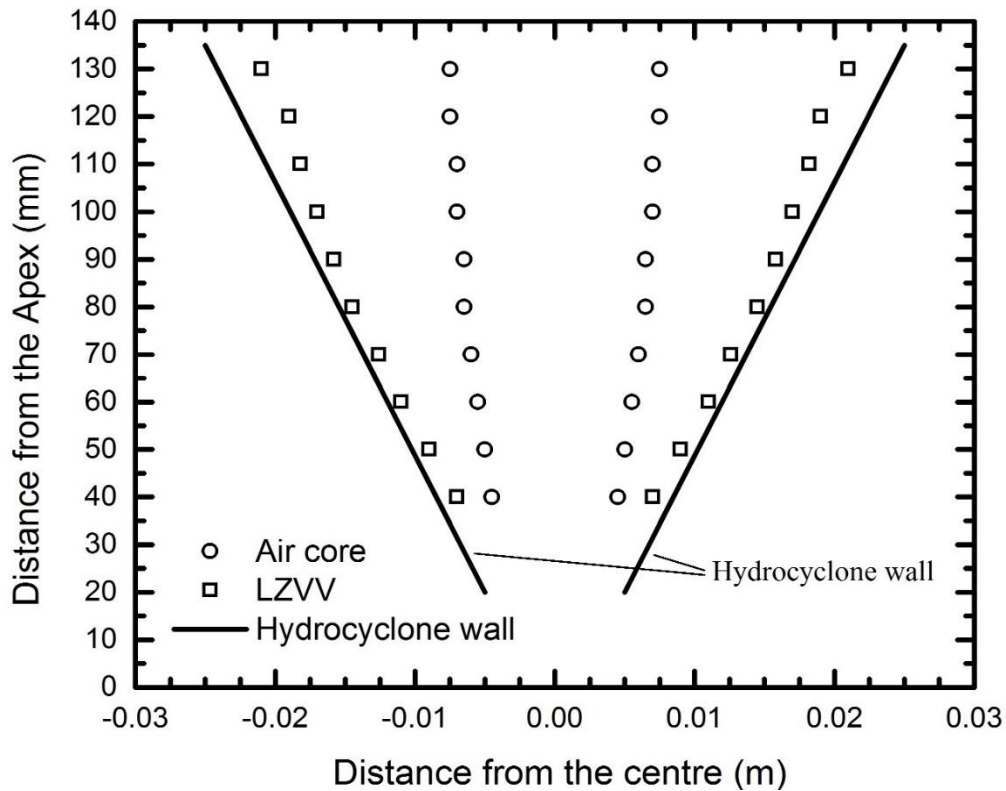


Figure 4.10-The air core location and LZVV for the hydrocyclone with a large vortex finder

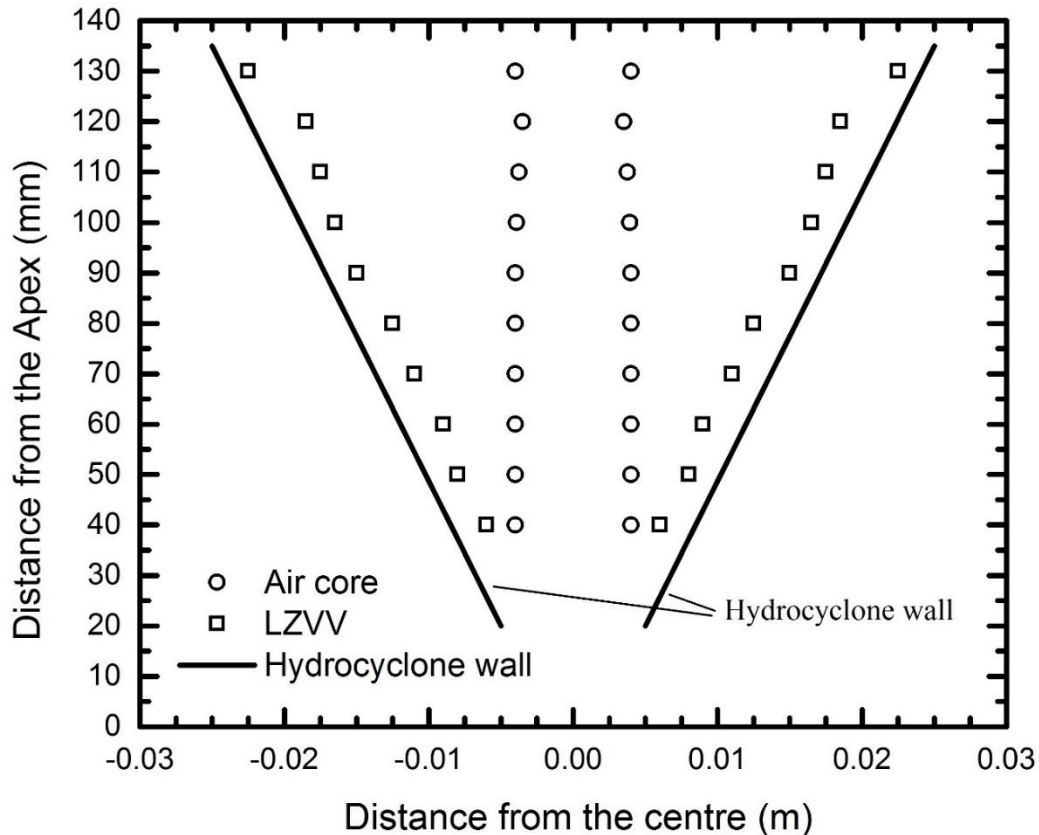


Figure 4.11-The air core location and LZVV for the hydrocyclone with the small vortex finder

Each figure presents an inside look of the flow behaviour under each condition. Comparing these two figures provide some insights of the change of behaviour under different overflow to underflow diameter ratio.

Figures 4.10 and 4.11 belong to the same hydrocyclone with different vortex finder diameters from which we have the same high recovery of light particles in the overflow in spite of the change in the vortex finder diameter. The overflow to underflow diameter ratio change was compensated in the larger vortex finder hydrocyclone. The larger diameter vortex finder hydrocyclone has a higher light particle recovery in the overflow stream at low underflow split ratio while having

a really lower recovery of light particles in the overflow stream at high underflow split ratio. The smaller vortex finder hydrocyclone has a high recovery of light particles in the overflow stream at any underflow split ratio but the recovery decreases as the underflow split ratio decreases. The reason behind the phenomena is hidden in Figures 4.10 and 4.11. Figure 4.10 shows the air core and LZVV (locus of zero vertical velocity) location for a hydrocyclone with a larger vortex finder at a low underflow split ratio. At this underflow split ratio the hydrocyclone has a high recovery of light particles in the overflow. That leaves more space for particles in the upward direction stream to leave the hydrocyclone. Figure 4.10 shows a noticeably larger air core portion inside this hydrocyclone with the larger vortex finder diameter, but on the other hand the LZVV is closer to the wall as such that the upward direction stream which is between these two lines is sufficiently large enough to take the particles to the vortex finder. Figure 4.11 shows the air core and LZVV location for the hydrocyclone with the smaller vortex finder diameter at the same level of recovery of light particles in the overflow stream as the other hydrocyclone with a lower underflow split ratio. The recoveries between these two hydrocyclones are the same. Therefore, air core diameter is noticeably smaller than the other hydrocyclone there should be the same area of upward stream for light particles. As shown in Figure 4.11 the LZVV line is closer to the air core line making the area about the same as the other hydrocyclone. It should also be noted that even though these two cases have close enough upward stream area but the intensity of axial velocity is another important factor which should be considered.

It is also worth mentioning that the end of both air cores has the same diameter and the only difference between these two air cores is the top part. For the larger diameter vortex finder hydrocyclone there is a bigger air core at the top while for the other hydrocyclone the air core looks more like a cylinder at the centre. The air core formation at the centre of the hydrocyclone has shown its importance in the simulations. The air core stability in the larger vortex finder hydrocyclone becomes weaker and the air core becomes less stable and starts to fade away at low underflow split ratio while there is a strong and stable air core at that underflow split ratio in the smaller vortex finder diameter hydrocyclone. The stability of the hydrocyclone plays an important role in particle separation in a hydrocyclone and the decrease in the hydrocyclone efficiency in the larger vortex finder diameter hydrocyclone could be due to its unstable air core at high underflow split ratio.

5 Conclusions and future work

In the modelling development and validation part of the study a procedures for the consistent and reliable simulation of a hydrocyclone was investigated. The focus was on the methodology necessary to produce such simulations. Two important factors were delineated as being critical for the accurate prediction of hydrocyclone performance. The first point relates to the domain discretization. It was found that not only the mesh size, but also the type used, strongly influenced the solution. Hexahedral elements aligned with the flow direction gave the best results, compared to experimental data and other literature simulations. The second point concerns the solution algorithm. The most stable solution was obtained when the pressure and velocity profiles were initialized correctly. This procedure required that a solution was first generated using single phase simulations, starting with the steady state solution and being followed by a period of transient operation. Secondly, the air core must be established using a transient two phase simulation, with the results of the single phase runs as the starting point. The existence of a stable air core is absolutely critical for useful results to be obtained. Finally, simulations involving particles were successfully performed. In addition to these two key aspects, we also noted that the use of the LES turbulence model is essential. Using this solution procedure enabled the modelling of two hydrocyclones, with superior agreement being found between simulated and experimental results.

In the last part of this study, the separation of light and heavy particles in liquid slurry by use of a hydrocyclone was investigated. The effects of overflow pressure, feed flow rate, particle size, vortex finder length and diameter and particle concentration on hydrocyclone separation efficiency were investigated.

Future work

There are many aspects of the hydrocyclone that can be studied for a future work, including the separation of flocculated particles, shear stress investigation inside the hydrocyclone and particle-particle interaction study with specific subjects being listed below:

a) Study the effect of flocculation inside hydrocyclone for different floc sizes and densities

It is worth studying the effect of flocculation on the particle separation efficiency inside the hydrocyclone. Flocs have a larger diameter and a lower density than regular particles within the hydrocyclone. By calculating the fabricated floc sizes and densities these data can be employed for simulating the flocs behavior and consequently the floc separation efficiency under the assumption of no breakage inside the hydrocyclone

b) Study shear field for different geometries and velocity profiles

It is feasible to apply the velocity fields to generate a shear stress field within the hydrocyclone to study the floc breakage. In spite of floc breakage inside the

hydrocyclone a shear study can help us understand the continuous phase behaviour and shear stress distribution inside a hydrocyclone.

c) Particle/particle interaction and particle concentration inside the hydrocyclone

Particle/particle interaction plays an important role at higher concentration of particles. As shown in this study at low solid concentration the particle/particle interactions are negligible but at higher concentrations due to higher interactions between particles this effect should be considered to obtain better agreements with experimental data. Considering particle interactions in modelling a hydrocyclone will increase the cost of simulation.

References

- Ali, S. and Petty, C.A., Deoiling hydrocyclones, International Petroleum Environmental Conference, Houston, TX, March 2-4, 1994.
- Ahmed, M. M., Galal A. Ibrahim, Mohamed G. Farghaly. Performance of a three-product hydrocyclone, International Journal of Mineral Processing, 91, 34–40, 2009.
- Bhaskar, K. U., Murthy, Y. R., Raju, M. R., Tiwari, S., Srivastava, J. K., Ramakrishnan, N., CFD simulation and experimental validation studies on hydrocyclone, Minerals Engineering, 20, 60-71, 2007.
- Bohnet, M., Separation of two liquids in the hydrocyclones, Chemical Engineering Technology, 41, No 5 and 6, 1969.
- Bradley, D., The Hydrocyclone, Pergamon Press, New York, 1965.
- Braun, T. and Bohnet, M., Influence of feed solids concentration on the performance of hydrocyclones. Chemical Engineering Technology, 13, 15-20, 1990.
- Brennan, CFD simulations of hydrocyclones with an air core: comparison between large eddy simulations and a second moment closure, Chemical Engineering Research and Design, 84A, 495–505, 2006.
- Brennan, M.S., Narasimha, M. And Holtham, P.N., Multiphase modelling of hydrocyclones prediction of cut-size, Minerals Engineering, 20, 395-406, 2007.
- Brooks, G. F., Miles, N. J. and J. S. Clayton, Hydrocyclone performance related to velocity parameters, 2nd international conference on hydrocyclones, Oxford, England, C1:67, 1984.

Chen, W., Zydek, N., Parma, F., Evaluation of hydrocyclone models for practical applications. *Chemical Engineering Journal* 80, 295–303, 2000.

Chu, L.Y., Chen, W.M. and X.Z. Lee, Effects of geometric and operating parameters and feed characters on the motion of the solid particles in hydrocyclones, *Separation and Purification Technology*, 26: 237,2002.

Cullivan, J. C., Williams, R. A. Dyakowski, T., Cross, C. R., New understanding of a hydrocyclone flow field and separation mechanism from computational fluid dynamics, *Minerals Engineering*, 17, 651–660, 2004.

Dahlstrom, D.A. *Trans. Amer. Inst. Min. (Metall.) Engrs.*, 184, 331, 1949.

Dahlstrom, D. A. *Chem. Engineering Symposium, Series No. 15, Mineral Engineering Techniques*, 50, 41, 1954.

Dale, G.W. and A.P. Charles, Process engineering of produced water treatment facility based on hydrocyclone technology, *Proceedings of the international Petroleum Environmental Conference*, Houston, Texas, March 2-4, 1994.

Delgadillo, J. A., and Rajamani, R. K., A comparative study of three turbulence-closure models for the hydrocyclone problem. *International Journal of Mineral Processing*, 77(4), 217-230, 2005.

Delgadillo, J.A., Modeling of 75- and 250-mm hydrocyclones and exploration of novel designs using computational fluid dynamics. PhD Thesis, University of Utah, USA, 2006.

Delgadillo, J. A., and Rajamani, R. K., Exploration of hydrocyclone designs using computational fluid dynamics. *International Journal of Mineral Processing*, 84(1-4), 252-261, 2007.

Dyakowski, T., and Williams, R., Prediction of air-core size and shape in a hydrocyclone. *International Journal of Mineral Processing*, 43(1-2), 1-14, 1995.

Flinthoff, B.C., Plitt, L.R., Turak, A.A., Cyclone modelling: a review of present Technology. CIM Bulletin 80 (905), 39-50, 1987.

Gupta, R., Kaulaskar, M., Kumar, V., Sripriya, R., Meikap, B., and Chakraborty, S. , Studies on the understanding mechanism of air core and vortex formation in a hydrocyclone. Chemical Engineering Journal, 144(2), 153-166, 2008.

Ghadirian, M., Hayes, R.E., Mmbaga, J., Afacan, A. and Xu, Z., On the simulation of hydrocyclones using CFD. Can. J. Chem. Eng. in press DOI: 10.1002/cjce.21705, 2013.

He, P., M. Salcudean and I.S. Gartshore, A Numerical Simulation of Hydrocyclones, Chem. Eng. Res. Des. 77, 429-441, 1999.

Hsieh, K.T., Rajamani, R.K., Mathematical model of the hydrocyclone based on physics of fluid flow, American journal of chemical engineering, 37, 735-746, 1991.

Hsieh, K.T., A phenomenological model of the hydrocyclone. PhD Thesis, University of Utah, USA, 1988.

Kelsall, D.F., A study of the motion of solids particles in a hydraulic cyclone. Trans. Inst. Chem. Eng. 30, 87-104, 1952.

King, R.P., Technical Notes on MODSIM, University of Utah, 2000.

Leeuwner, M. J., Eksteen, J.J., Computational fluid dynamic modelling of two phase flow in a hydrocyclone, The journal of the southern African institute of mining and metallurgy, 108, 231-236, 2008.

Lim ,E.W.C., Y.R. Chen; C.H. Wang, R.M. Wu, Experimental and Computational Studies of Multiphase Hydrodynamics in a Hydrocyclone Separator System, Chem. Eng. Sci., 65(24), 6415-6424, 2010.

Lynch A.J. and T.C. Rao, Modeling and scale-up of hydrocyclone classifiers, Proceedings XI Int. Min. Proc. Congress, Cagliari, Paper 9, 1975.

Mahmood, T. Study of hydrocyclones for separation of light and heavy particles. Master's Thesis, University of Alberta, Canada, 2007.

Manninen, M., Taivassalo, V., Kallio, S., On the mixture model for multiphase flow, VTT Publications 288, Technical Research Centre of Finland, 1998.

Martinez, L. F., Lavín, A. G., Mahamud, M. M., Julio L. Bueno, Improvements in hydrocyclone design flow lines stabilization, Powder Technology, 176, 1-8, 2007.

Matschke, D.E. and Dahlstrom, D.A. Chemi. Eng. Progr., 55,79, 1959.

Monredon, T.C., Hydrocyclone: investigation of the fluid flow model. Thesis (MS). University of Utah, Salt Lake City, UT, 122, 1990.

Monredon, T.C., Hsieh, K.T., and Rajamani R.K., Fluid flow models of the hydrocyclone: an investigation of device dimensions", International journal of Mineral Processing, 35, 65-83, 1992.

Mukherjee, A. K., Sripriya, R., Rao, P.V.T. and P. Das, Effect of increase in feed inlet pressure on feed rate of dense media cyclone, International Journal of Mineral Processing, 69: 259,2003.

Nageswararao, N., Wisemen, D.M., Napier-Mun, T.J., Two empirical hydrocyclone models revisited, Minerals Engineering, 17, 671-687, 2004.

Narasimha M., A review of CFD modelling for performance predictions of hydrocyclone, Engineering Applications of Computational Fluid Mechanics, 1, 109-125, 2007.

Narasimha, M., Brennan, M., and Holtham, P., Numerical simulation of magnetite segregation in a dense medium cyclone. *Minerals Engineering*, 19(10), 1034-1047, 2006.

Narasimha M, Sripriya R and Banerjee PK, CFD modelling of hydrocyclone-prediction of cut-size. *Int. J. Mineral. Process* 71(1):53–68, 2005.

Neesse, T. and Dueck, J., Air core formation in the hydrocyclone. *Minerals Engineering*, 20, 349–354, 2007.

Nowakowski, A., Cullivan, J., Williams, R., and Dyakowski, T., Application of CFD to modelling of the flow in hydrocyclones. is this a realizable option or still a research challenge, *Minerals Engineering*, 17(5), 661-669, 2004.

Nowakowski, A., Kraipech, W., Williams, R., and Dyakowski, T., The hydrodynamics of a hydrocyclone based on a three-dimensional multi-continuum model. *Chemical Engineering Journal*, 80(1-3), 275-282, 2007.

Plitt, L.R., A mathematical model of the hydrocyclone classifier. *CIM Bulletin* 69 (776), 114–123, 1976.

Rhodes, N., Pericleous, K. and Drake, S., The Prediction of Hydrocyclone Performance with a Mathematical Model. In *3rd International Conference on Hydrocyclones*, Wood, P. (ed), Elsevier, Oxford, England, 51-58, 1987.

Schiller, L., Naumann, Z., *Z Ver. Deutsh. Ing.* 77, 318, 1935.

Schuetz, S., Mayer, G., Bierdel, M., Piesche, M., Investigations on the flow and separation behaviour of hydrocyclones using computational fluid dynamics, *Int. J. Miner. Process.* 73, 229–237, 2004.

Slack, M. D. , Prasad , R. O., A. Bakker and F. Boysan, Advances in cyclone modeling using unstructured grids, *Trans. Inst. Chem. Eng.* 78A, 1098–1104, 2000.

Slack, M., Del Porte, S., and Engelman, M., Designing automated computational fluid dynamics modelling tools for hydrocyclone design. *Minerals Engineering*, 17(5), 705-711, 2004.

Stephens, D.W. And Mohanarangam, K., Turbulence Model Analysis Of Flow Inside A Hydrocyclone, Seventh International Conference On CFD In The Minerals And Process Industries, 2009.

Suasnabar, D.J., Dense Medium Cyclone Performance, enhancements via computational modeling of the physical process. PhD Thesis, University of New South Wales, 2000.

Svarovsky, L., Hydrocyclones, Technomic Publishing Co. Inc New York, 1984.

Svarovsky, L., Performance of hydrocyclone at high feed solids concentrations, Pap. 4 presented at Int. Conf. Hydrocyclones, BHRA Fluid Engineering, Cambridge, 1980.

Wang, B. and Yu, A. B., Numerical study of particle-fluid flow in hydrocyclones with different body dimensions. *Minerals Engineering*, 19, 1022-1033, 2006.

Wang, B., Chu, K. W., and Yu, A. B., Numerical Study of Particle-Fluid Flow in a Hydrocyclone, *Ind. Eng. Chem. Res.*,46, pp 4695-4705, 2007.

Yang, I.H., Shin, C.B., Kim, T.H., Kim, S., A three-dimensional simulation of a hydrocyclone for the sludge separation in water purifying plants and comparison with experimental data. *Minerals Engineering* 17 (5), 637–641, 2004.

Yoshioka, H. and Hotta, Y. *Chem. Eng., Japan*, 19, 632, 1955.

Young, G. A. B., Wakley, W. D., Taggart, D. L., Andrews, S. L. and J. R. Worrel, Oil-water separation using hydrocyclones, An experimental search for optimum dimensions, *Journal of Petroleum science and engineering*, 11:37, 1994.

Zhao, Q.G., Xia, G.D., A theoretical model for calculating pressure drop in the cone area of light dispersion hydrocyclone. *Chemical Engineering Journal* 117, 231-238, 2006.